Experimental and numerical investigation of the tribological properties of water-hydraulic seals

To the Faculty of Mechanical, Process and Energy Engineering
of the Technische Universität Bergakademie Freiberg

is submitted this

DISSERTATION

to attain the academic degree of
Doctor of Engineering
Dr.-Ing.

Submitted

by **M. Eng. Ngo, Xuan Quang**
born on 13 June 1982 in Hai Duong, Viet Nam

Reviewers: Prof. Dr.-Ing. Matthias Kröger, TU Freiberg
Prof. Dr.-Ing. Kristin de Payrebrune, TU Kaiserslautern

Freiberg, December 10, 2021

Declaration

I hereby declare that I completed this work without any improper help from a third party and without using any aids other than those cited. All ideas derived directly or indirectly from other sources are identified as such. In the selection and use of materials and in the writing of the manuscript, I received support from:

Prof. Dr.-Ing. Matthias Kröger.

Persons other than those above did not contribute to the writing of this thesis. I did not seek the help of a professional doctorate consultant. Only those persons identified as having done so received any financial payment from me for any work done for me.

This thesis has not previously been published in the same or a similar form in Germany or abroad.

June 2021 M. Eng. Ngo, Xuan Quang

Acknowledgments

I am very grateful to my supervisor Professor Matthias Kröger for his guidance, advice and immense support throughout my PhD research studies. He provided the initial idea for this dissertation and encouraged and helped me when performing this study work. Without his help, I would not have been able to finish this dissertation.

I would like to thank my colleagues Dr. Robert Szlosarek and Dr. Thomas Falke for their constant support and advice over the years.

I am grateful to my colleagues at the Institute of Machine Elements, Engineering Design and Manufacturing for their help and providing an excellent atmosphere.

Thank you to Dipl. Steffen Sziedat and Herr Rudolf Müller for all the support sample preparation and manufacturing some parts for the experiments.

To the Technische Universität Bergakademie Freiberg, I would like to express my thanks for providing excellent material and perfect living conditions. Furthermore, thanks to the Center of Advanced Study and Research (GraFA), where I obtained useful short courses and supported me to finish my thesis, I would like to thank the International Center, where I obtained language courses.

I would like to express my thanks to my government for the financial support through the Vietnam International Education Development (VIED), Ministry of Education and Training (MOET).

In the end, I would like to thank my family, parents, wife, and two children for their love, support, and encouragement to follow my study.

Abstract

The friction process occurs in most structures, especially in contact between two faces with relative motion. The process of friction and abrasion affects the productivity and performance of equipment and increases the cost of replacing and repairing worn parts. Wear is the factor that determines equipment service life and reliability.

Therefore, an improved understanding of the complex nature of friction and abrasion processes is essential for tribological research.

In this study, the simulations and experimentations are formed to understand the friction and wear properties of hydraulic rubber seals, which are widely used in agriculture, mining, irrigation and mechanical engineering, in different working conditions. The tribometer test rig is developed to investigate rubber samples' friction and abrasion properties with different contact conditions. An observation structure to measure the contact area of the rubber sample also was constructed.

The experiments are performed with different contact conditions (dry contact, wet contact, mud contact), different geometry of sample (half-cylinder, half-sphere), quite different contact directions (sliding direction axial and sliding direction lateral), fillet radius, contact angle or rubber material with different sliding velocities and normal forces.

In addition, the contact process of rubber seals is simulated and equations for seal wear for the specific experimental conditions are formulated.

This study aims to test the friction and abrasion properties of hydraulic rubber seals in different contact environments. Describing the correlation between the contact conditions and the friction and wear behavior will allow both the prediction of the strength of the seal for a particular application and the development of methods to reduce and increase the seal's life.

Table of Contents

Notations

A	mm^2	Contact area
E	MPa	Young's module
G	MPa	Shear modulus
H_A	Shore A	Hardness of rubber
F_n	N	Normal force
F_r	N	Friction force
F_s	N	Static friction force
F_d	N	Dynamic friction force
w	N	Weight of sample
P	N	Apply load
p	MPa	Pressure in fluid
L	mm	Length of sample
D	mm	Outside diameter of steel plate
d	mm	Inside diameter of steel plate
D_s	mm	Outside diameter of sample
d_s	mm	Inside diameter of sample
d_r	mm	Disc diameter at the point of contact.
θ_c	°	Contact angle of sample
θ	°	Inclination angle of surface
α	°	Inclination limited angle of surface
R	mm	Fillet radius of sample
T	$°C$	Room temperature
t	s	Measurement time
R_z	μm	Roughness of disk plate
Δm	g	Mass loss of sample
S	m	Sliding distance
V	mm/s	Sliding velocity
μ	-	Friction coefficient
ν	-	Poisson ratio
ρ	kgm^{-3}	Density of water
H_u	m	Water levels upstream,
H_d	m	Water levels downstream
B	m	Width of the slide gate

CHAPTER 1

Introduction

1.1 Motivation and objectives of the thesis

The friction process occurs in most structures, especially in contact between two faces with relative motion. The process of friction and abrasion affects the productivity and performance of equipment and increases the cost of replacing and repairing worn parts. Under the operating conditions of the equipment, the contact surfaces of the machine parts change over time due to wear, leading to higher failures and higher costs. Wear is the factor that determines equipment service life and reliability. Abrasion damage occurs due to gradual loss of material and changes in contact surface profiles. This results in changes in geometry or residual thickness, surface profile and roughness. In general, the specific nature of the wear failure conditions is an important factor in addressing or avoiding wear.

The abrasion process is a complex process due to its dependence on many parameters and the machine's environment. For detailed design, besides performance and durability requirements, abrasion mechanisms must also be considered. Therefore, an improved understanding of the complex nature of friction and abrasion processes is essential for abrasion research.

Hydraulic rubber seals are widely used in agriculture, mining, irrigation and mechanical engineering. General rubber seals have been studied and experimented by many scientists.

In irrigation works, hydraulic rubber seals play an important role in the water retention efficiency of the building. Hydraulic rubber seals often work in high-pressure and complex working environments depending on the specific application. Therefore, research and experimentation to understand the friction and wear properties of hydraulic rubber seals in different working conditions are necessary to simulate and predict hydraulic rubber seals' friction and wear behavior in different working conditions. Thereby, it can improve the life of seals and improve the performance of equipment and works.

This study aims to test the friction and abrasion properties of hydraulic rubber seals in different contact environments. Describing the correlation between the contact conditions and the friction and wear behavior will allow both the prediction of the strength of the seal for a particular application and the development of methods to reduce wear and increase the seal's life.

The objective of this study focuses on some key tasks as follows:

- Complement and develop a tribometer test rig to investigate the friction and abrasion properties of rubber samples.
- Construct an observation structure to measure the contact area of rubber samples.
- Investigate the friction and abrasion properties of rubber seals with different contact conditions.
- Simulated the contact process of rubber seals and compare the contact area with experimental measurement results.
- Formulate equations for seal wear for the specific experimental conditions.

1.2 Structure of the dissertation

The dissertation contains results of research work, which is subdivided as follows.

The second chapter reviews the concepts and methodologies of previously published research related to this work. The review provides an understanding of important aspects of friction characteristics and wear mechanisms.

The third chapter provides the setup for experimental studies of the friction and wear properties of the rubber blocks in chapter 4 and the watergate rubber seals in chapter 5. Besides, some input parameters for the simulation process are also presented in this chapter.

The fourth chapter presents the experimental process and research results on the friction and wear properties of the rubber block sample. The experimental process is performed under different contact environments (dry contact, wet contact, mud contact), different geometry of sample (half-cylinder, half-sphere), quite different contact directions (sliding direction axial and sliding direction lateral), fillet radius, contact angle or rubber material with different sliding velocities and normal force.

The fifth chapter presents the experimental process and the results of studying the friction and wear properties of water hydraulic seals under different forces, sliding velocity and contact environment.

The sixth chapter provides results of simulations of the contact between rubber and steel surfaces. Further, several formulations for determining the wear of rubber samples are presented corresponding to the experimental results and conditions.

The seventh chapter gives conclusions and recommendations. The main contributions are summarized and recommendations are given.

CHAPTER 2

State of the art

2.1 Water hydraulic seal

Water hydraulic seals are used in various irrigation projects. Depending on each project's features and application requirements, the seals' properties, features and shape will differ. Several types of watergate seals are shown in Figure 2.1.

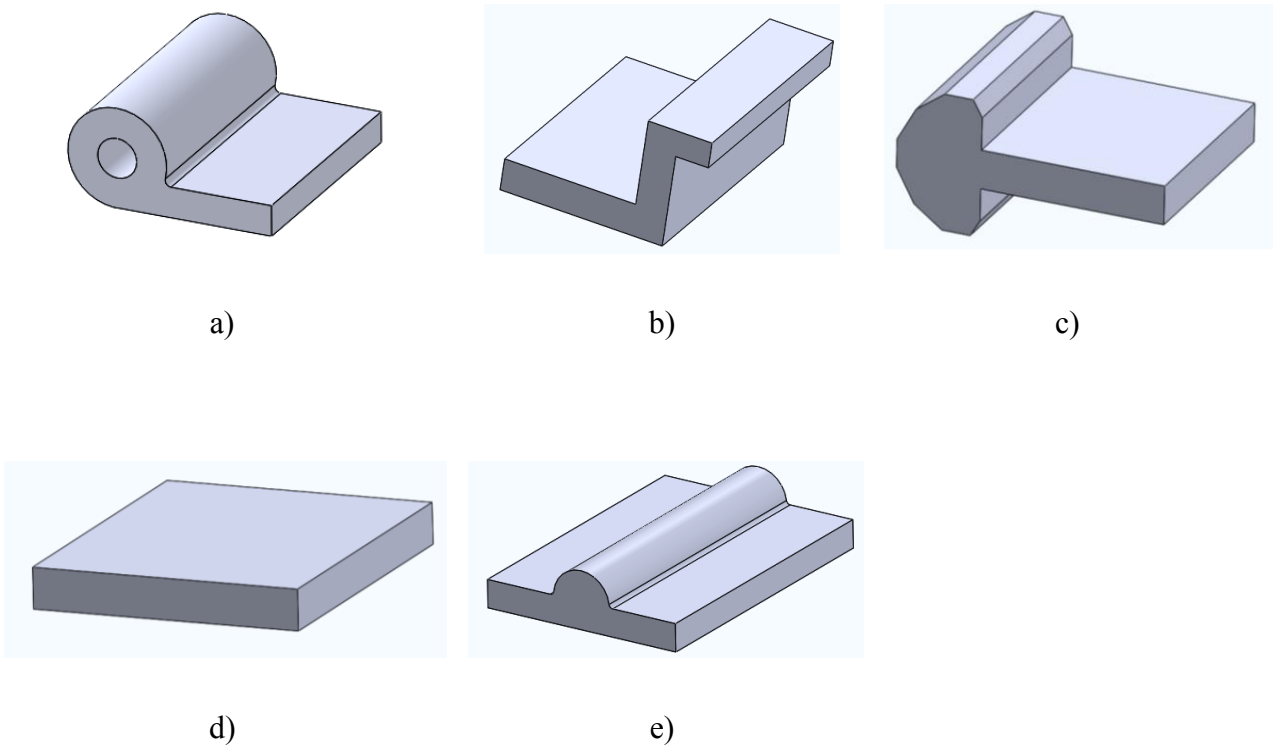

a) b) c)

d) e)

Figure 2.1: Some types of watergate seals: a) Musical note rubber seal, b) Z-type rubber seal, c) Arrow-type rubber seals, d) Flat rubber seal and e) Double stem seals.

Musical note rubber seal: This can also be referred to as a P-type seal or J-type seal. The musical note rubber seal is available with either a solid bulb or Hollow Bulb. Hollow Bulb seals are recommended for gates operated up to 15 m, while solid bulbs are used for heads larger than 15 m.

Z-type rubber seal: These Z-type rubber seals are molded to the required shape and the sealing effect is obtained partly due to initial interference with the embedded

sealing plate and partly due to the deflection under load. This type of seal is used on gates with a high level of water.

Arrow-type rubber seals: These rubber seals are specifically employed for automatic tilting gates. To accommodate different retainer plates, single grooved or double groove designs are available.

Double stem seals: These types of designs are preferred for heads exceeding 30 m. Double stem seals can be used as top seals, side seals as well as bottom seals.

Flat rubber seal: These can be flat type, wedge type, round bottom type. These types of seals are generally employed as bottom seals.

Some types of rubber used for watergate seals:

Ethylene Propylene Rubber (EPDM/EPM): EPM is a copolymer of ethylene and propylene. This type can only be cross-linked with peroxides. If a third monomer, a diene, is added during the copolymerization of ethylene and propylene, the resulting rubber will have unsaturations and can then be vulcanized with sulfur. These rubbers are the so-called EPDM. The main properties of EPDM are its outstanding heat, ozone and weather resistance. The resistance to polar substances and steam is also good. It has excellent electrical insulating properties. The EPDM copolymer can be filled with more than 200 percent of its weight with non-re-inforcing fillers, resulting in reduced cost. For these reasons, this rubber is widely applied in many applications.

Nitrile rubber (NBR): NBR is a family of unsaturated copolymers of acrylonitrile and butadiene monomers. Although its physical and chemical properties vary depending on the polymer's composition of nitrile: The more nitrile within the polymer, the higher is the resistance to oils but the lower the flexibility of the material. This synthetic rubber is generally resistant to oil, fuel, and other chemicals. It is used in the automotive industry to make fuel and oil handling hoses, seals, and grommets. NBR's ability to withstand a range of temperatures from -40 °C to +108 °C makes it an ideal material for automotive applications. Nitrile rubber is more resistant than natural rubber to oils and acids but has less strength and flexibility. Nitrile rubber is generally resistant to aliphatic hydrocarbons. Nitrile, like natural rubber, can be attacked by ozone, aromatic hydrocarbons, ketones, esters and aldehydes.

Natural Rubber (NR): The natural rubber has very high elasticity, high tensile strength and very good abrasion resistance. The material is obtained by coagulation of latex derived from the rubber trees. The rubber is not resistant to aging and oil. For these reasons, NR is rarely used as a seal for technical applications but is mixed with other elastomers compounds like EPDM to improve rubber properties.

Styrene-Butadiene Rubber (SBR): SBR is a synthetic rubber copolymer consisting of styrene and butadiene. It has good abrasion resistance and good aging stability when protected by additives. SBR is widely used in car tires, where it is often blended with natural rubber.

Rubber moulding:

Different manufacturing processes can produce moulded rubber parts. Major techniques are compression moulding, injection moulding and transfer moulding. Rubber block samples used in the experiments of this thesis were created by compression moulding.

Compression moulding is a process in which the rubber is squeezed into a preheated mould, then performing curing due to heat and pressure applied to the rubber.

The compression moulding process involves the following steps:

- A weighed amount of the rubber is placed into the lower half of the mould.

- The upper half of the mould moves downwards, pressing on the rubber and forcing it to fill the mould cavity. The mould, equipped with a heating system, provides curing of the rubber.

- The mould is opened and the part is removed for the next operations.

2.2 Fundamental tribology

2.2.1 Friction

Tribology is defined as the science and technology of interacting surfaces with relative motion. The main topics in the field of tribology are wear, friction and lubrication, as referred by Kragelsky and Alisin [1], Bowden [2] and Goryacheva [3]. Consequently, it is essential to review the general knowledge of tribological behavior and basic concept, which are helpful to provide a comprehensive understanding of significant aspects of tribology.

Friction is defined as the force resisting the relative motion of solid surfaces, particle layers and fluid layers under an external force's action when one surface moves relative to another. Friction exists in every mechanical system and causes a significant loss of energy. The friction coefficient as the relation of friction force and normal force is commonly used to describe friction characteristics between contacting bodies of tribosystem. In general, the friction between contacting surfaces transforms kinetic energy into heat whenever motion with friction occurs, as referred by Kragelsky and Alisin [1], Fleischer [4] and Menezes et al. [5].

Therefore, the influence of friction on wear behavior reveals that with increased heat, the plastic deformation of the contacting surfaces' asperities increases, increasing the material removal. On the other hand, the increasing heat leads to a degradation of the viscous fluid layer's lubricant properties between the sliding surfaces. This leads to a decrease in performance and an increase in damage to elements. Additionally, the friction characteristics influence the tribosystem's operating conditions because the friction can induce self-excited vibrations. Based on the topics above, friction represents significant aspects of the tribological behavior of materials.

Coefficient of friction

Friction is resistance to motion experienced when one surface is sliding over another. The first studies on friction are dated to the fifteenth century and belong to Leonardo da Vinci (1452-1519).

His observations became two hundred years later two of the well-known laws of sliding friction introduced by Guillaume Amontons (1663-1705): The friction force is directly proportional to the applied load. The apparent area of contact has not effect on the friction force.

Leonardo da Vinci also introduced the concept of coefficient of friction (μ) as the ratio of the friction force F_r to normal load F_n :

$$\mu = \frac{F_r}{F_n} \tag{2.1}$$

Johann Andreas von Segner (1704-1777) was the first who made a distinction between static and dynamic friction. The easiest set-up to understand static friction consists of a body placed on an inclined plane proposed by Leonhard Euler (1707-1783), see Figure 2.2.

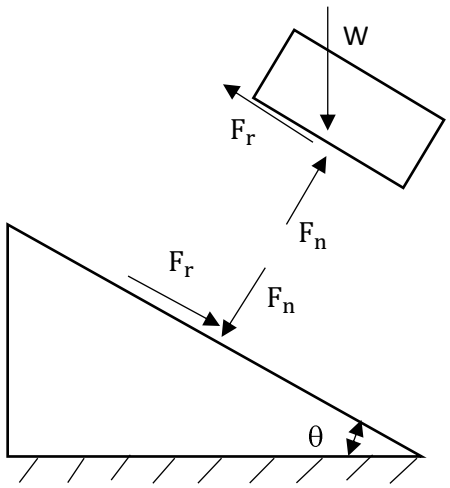

Figure 2.2: Forces acting on a body in sliding motion

The force which maintains the body in rest on the tilted plane is the static friction force. The force needed to initiate sliding is the maximum static friction force F_s. The dynamic friction force F_d is the force required to sustain motion. The coefficient of friction can also be defined as the tangent of the angle of the inclined plane. The body will remain at rest for an angle θ less than a certain value α and start sliding down if the inclination angle exceeds α. Writing the load balance equations for the body from Figure 2.2, the coefficient of static friction is given by:

$$\mu_s = \frac{F_s}{F_n} = \frac{W\sin\alpha}{W\cos\alpha} = \tan\alpha \tag{2.2}.$$

The coefficient of static friction is usually larger than the dynamic one, but it can also be equal to dynamic friction.

Charles - Augustin Coulomb (1736-1806) studied more details on friction. He completed the laws of friction with the third law: The dynamic friction force is

independent of the sliding velocity. These laws of friction have been commonly used to describe friction phenomena because of their simplicity and generality. These empirical laws have been proved to be valid under certain conditions for many material couples. However, these laws are not valid for all materials.

Although the laws mentioned above are generally called laws of friction, they were obtained empirically using dynamic friction data.

Physical rubber friction is mainly caused by adhesion and deformation and can be written as:

$$F_r = F_{Adhesion} + F_{\text{Deformation}} \tag{2.3}.$$

Depending on the materials in contact, different mechanisms can cause these two parts. According to Tabor and McFarlane [6], dry friction between metals can be attributed to adhesion and deformation. The adhesion component of friction occurs while shear local "welded" areas between contacting asperities (Figure 2.3). The adhesion term is regarded as a surface effect and occurs during the making and breaking of bonds on a molecular level. Adhesion is not the only resistance encountered during the motion of one body over another. If one of the surfaces in contact is harder than the other one and rough, the hard one plows through the soft surface giving rise to the deformation term of friction. The force's magnitude is strongly dependent on the plowing body's geometry and the hardness of the softer body. The energy is dissipated in this way by deformation. The deformation component also called hysteresis friction, is caused by the deformed rubber's delayed recovery, see Figure 2.3. The energy is dissipated through the rubber bulk's internal damping. Therefore it is considered a bulk property. Nevertheless, it is experienced as a resisting force to one body's movement relative to the other body at the interface.

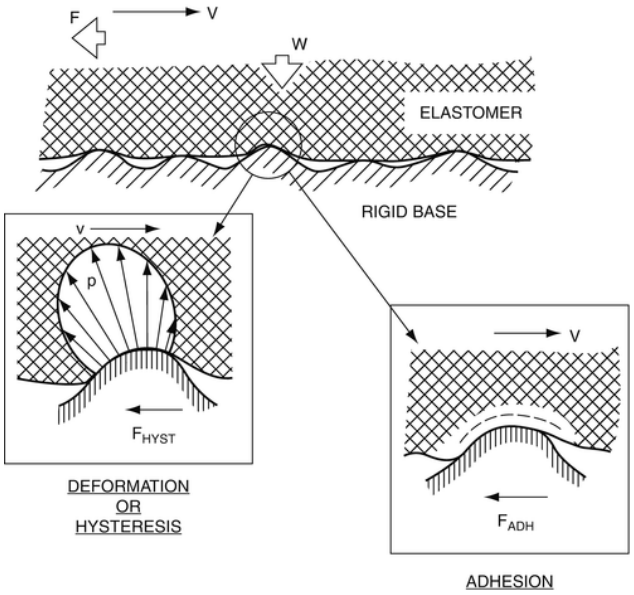

Figure 2.3: Adhesion and hysteresis friction [7]

The dependency of friction on velocity and temperature is researched by R. Stribeck and K. Grosch.

In 1902 R. Stribeck published his work on lubricated friction [8] depending on velocity. Named after him, the Stribeck curve (Figure 2.4) splits up into several velocity intervals:

- Without any movement, only static friction appears.
- For minimal velocity, the lubrication film is too thin to show a significant effect, leading to boundary friction similar to dry friction.
- Moderate velocities cause sufficient lubrication. A film separates most parts of the sliding partners. In this "mixed friction", the friction coefficient and wear decrease with velocity.
- After reaching a minimum, friction rises with velocity when the interface is completely covered with lubricant and hydrodynamic effects become relevant.

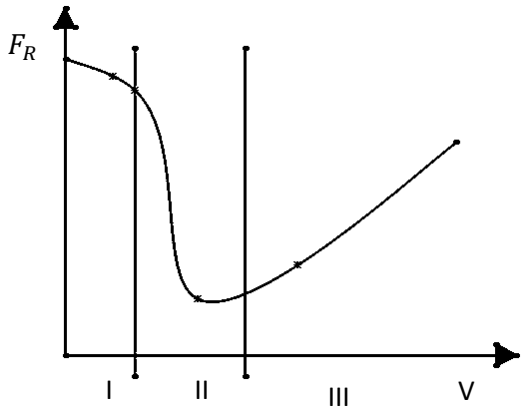

Figure 2.4: Stribeck curve with boundary friction (I), mixed friction (II) and fluid friction (III) [28]

According to viscoelastic properties, the relationship between friction coefficient and its change with temperature was first presented in 1963 by K. Grosch [9] for rubber systems. His investigations show that velocity-dependent friction at different temperatures can be merged into master curves. Thus, shifting the friction curves taken at different temperatures horizontally to the velocity axis results empirically in a continuous curve. His results also reveal a maximum of friction, building a plateau for certain systems over a limited velocity and temperature interval before declining. Other combinations of rubber and substrate decline directly after the plateau is reached.

Knowing the effect of surface roughness on the rubber's friction, Barquins and Roberts measured friction on individual glass lenses and a smooth rubber surface. The result differs from the Grosch results and exhibits a slight variation of the friction coefficient over the whole range of velocity [10]. The friction coefficient appeared to be more rate-sensitive by increasing the counterpart's roughness and followed a similar path as the classical Grosch data. This makes clear that an additional factor hinders the increase of friction for smooth surfaces.

Roughness has two opposite effects on rubber friction: First, though the micro-indentation of surfaces asperities into the elastomer, a part of the mechanical energy is dissipated through viscoelastic losses (hysteresis friction). On the other side, reducing the contact area with increasing roughness should decrease the level of adhesion. The level of appearing adhesion depends strongly on the real contact conditions.

2.2.2 Wear

Wear is generally defined as a process of mechanical actions due to relative motion between the contacting surfaces, resulting in progressive loss of material due to its fracture from these surfaces, as mentioned by Czichos and Habig [11], Hutchings et al. [12], Goryacheva [3], Popov [13] and Kragelsky and Alisin [1].

Some common types of wear, classified by specific wear mechanisms or processes, comprise abrasive wear, adhesive wear, fatigue wear, and corrosive wear. In this section, several different abrasive concepts are presented to provide an overview of wear behavior.

Abrasive wear is commonly defined as a process. It occurs if two solid surfaces are pressed together and move along each other, causing material removal from the contacting surfaces.

In general, abrasive wear is classified by the type of mechanical interaction between solid bodies, which are known as two-body and three-body contact, as mentioned by Rabinowicz and Mutis [14], Bayer [15], Czichos [16] and Misra and Finnie [17]. These typical modes of abrasive wear are distinguished by the presence or absence of hard particles and their motion behavior in the contact region.

The effects of counterparts material hardness, hardness and size of particles on wear were also studied. In particular, the abrasive process involves lubricants in the contact area. The contact pair is copper on copper. The wear rates corresponding to large abrasive sizes are greater in the lubricants. The wear value obtained for unlubricated copper surfaces is high with the small particles (12 μ).

Adhesion wear is generally described as two solid bodies which are pressed together and slide over each other. Under the applied load, the asperities of two contacting surfaces are subjected to localized pressure causing the high temperature in the contact region, so they deform and stick to each other. If the surfaces move relative to each other, the material is transferred from one surface to the other during sliding process. Therefore, adhesive wear results are a growing roughness and development of undulating on the interacting surfaces, as mentioned by Czichos and Habig [11] and Mang et al. [18]. The main influential factors causing the decrease of adhesive wear include low applied load, hard abrading materials, and lubrication.

Fatigue wear is defined as a process by which the surface layer is subjected to cyclic loading during friction, so microcracks are created on or inside the surface. Consequently, these microcracks are developed and propagated, which results in pieces of the surface material being removed or delaminated if the stresses are higher than the fatigue strength of the material, as referred by Menezes et al. [19]. Because two solid bodies are pressed by cyclic loading, asperities in contact are subjected to high local stress which is repeated during sliding or rolling with or without lubrication. The result of repeated stress leads to increases in fatigue wear.

Erosive wear is the loss of material from a solid surface which is in contact and relative motion with the fluid that contains solid particles. Erosive wear is studied by Mang et al. [18], Czichos and Habig [11].

2.2.3 Lubrication

Lubrication is the improvement of friction and wear by the introduction of a friction-reducing film between moving surfaces in contact. The lubricant presence at the interface can prevent the rubber from directly contacting the counter surface. This is especially true if the sliding velocity is very high or if the lubricant's viscosity is very high. The conditions of appearance of such films have been expressed in the frame of the theory of hydrodynamic lubrication [20]. If the load is increased, the lubricant film, though enhanced viscosity, is even less likely to be drained out of the contact area and the related theory is elastohydrodynamic lubrication. By using optical interferometry, the thickness of the lubricant film has been measured during dynamic contact between a rubber hemisphere and a glass plate [21]. Also, in water, the friction coefficient's high level at very low sliding speeds indicates a film breakdown. There is a general tendency towards film breakdown at low sliding velocity. But a notable exception occurs if the water contains a small amount of soap. In this case, the friction values are very low, suggesting that the soap film is stabilized and direct contact is hindered at the interface [21].

Many different lubricants can be used to lubricate surfaces, e.g., solid, liquid, mixed solid-liquid, or even gas, as mentioned by Mang, Bobzin and Bartels [18] and Czichos and Habig [11]. In general, there are three distinct regimes of lubrication

that are determined by the thickness of the fluid film such as fluid film lubrication, mixed lubrication, and boundary lubrication, see Figure 2.5.

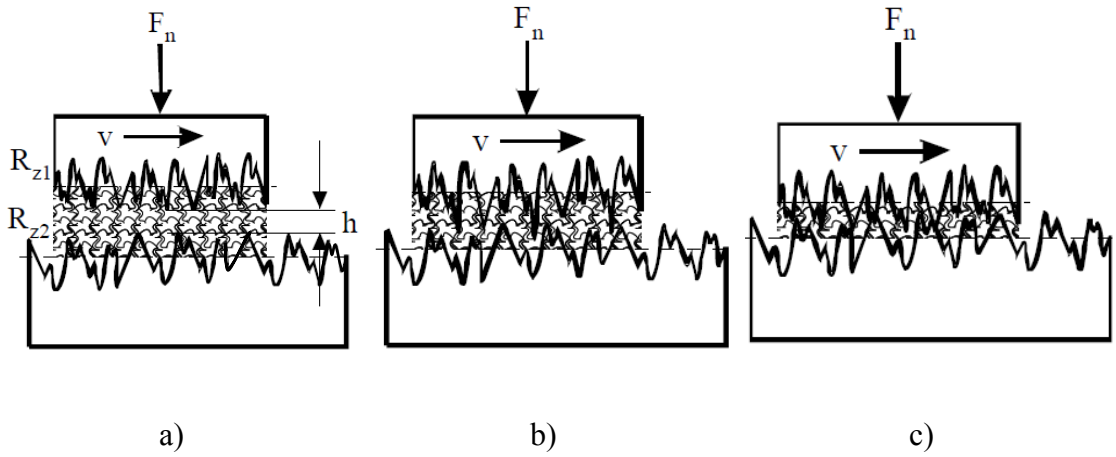

a) b) c)

Figure 2.5: Regimes of fluid film lubrication a), mixed lubrication b) and boundary lubrication c) [22].

Fluid film lubrication is the lubrication regime if a lubricant film layer completely separates two contacting surfaces. Therefore, the lubricant film's thickness h is thicker than the total surface roughness of two contacting surfaces.

Boundary lubrication occurs if the highest asperities of surfaces contact each other. This regime is characterized by a high coefficient of friction, high heat and strong wear due to localized pressure peaks.

Mixed lubrication is the intermediate regime between boundary lubrication and fluid film lubrication. In this regime, intermittent contact between the friction surfaces at the few highest surface asperities occurs.

2.3 Experimental Investigation

2.3.1 Friction characteristic

Friction represents one key factor of the tribological behavior of materials, which affects the wear process causing different wear mechanisms. Therefore, friction characteristic of the tribosystem is an area of great interest to scientists over past decades, as done by Stevenson and Hutchings [23], Dube and Hutchings [24] and Chowdhury et al. [25]. The published research has mainly focused on investigations of relations between friction coefficient and process parameters as well as material properties. The friction coefficient of the tribosystem often decreases slightly with increasing sliding velocity.

Besides the normal friction process between two surfaces, many scientists are also interested in the friction with particles in the contact area.

Doan, de Payrebrune and Kröger [26, 27] studied the dependency of friction coefficient on the process parameter. A series of experiments for two-body contact between the aluminum sample and steel disc and three-body contact with sand particles in the contact area was conducted on the tribometer test rig with the applied load up to 1500 N and the velocity up to 700 mm/s. The friction coefficient for two-body contact is approximately 0.5. The friction coefficient of two-body contact is higher than that of three-body contact and the friction coefficient decreases if the velocity increases.

Abdul Hamid et al. [28] and Ostermeyer [29] investigated hard particles' effect on the braking system's friction characteristics. The abrasion tests were performed on a brake test rig under test conditions of two-body contact without hard particles and three-body contact with mixed particles and the wear debris. The significant results showed that if the particles are present in the contact zone between the brake pad and the rotating disc, the friction coefficient is reduced compared to the case without the particles. The hard particles decrease the original effective contact area at the sliding interface due to particles' presence and wear debris. Therefore, the abrasive particles cause a decrease in friction coefficient due to various motions of the abrasive particles. The friction coefficient depends on applied load and velocity.

In the friction of rubber, the adhesive force is one part affecting the friction process's characteristics. Experimental observations have shown that friction is both

load and velocity-dependent [30–32]. Furthermore, one of the common observations in friction experiments is the drop in the friction force from a maximum value, commonly referred to as static friction, to a steady-state value, commonly referred to as dynamic friction, changing the contact from pre-sliding to full sliding. It is well established that adhesion forces are developed within the contact area if two surfaces are brought into contact due to physical and chemical interactions between the surfaces. If the contacting surfaces are clean, then strong adhesion occurs, and as a result, a large force is required to shear these interfacial junctions. Thus, adhesion is an additional source of energy dissipation [33]. It has been shown that the adhesion forces of rubber are time-dependent and increase with rest time before reaching a stable value [34, 35].

2.3.2 Wear behavior

The seal is an important and common component in mechanical equipment. The basic function of the seal is to prevent leakage of lubricant. Leakage occurs after a period of operation due to the wear of the elastomeric seal. The failure of the seal often has serious consequences. Therefore, understanding and controlling the principal factors that govers the wear process is critical to seals life. Accordingly, the improvement of seal design is very focused. There have been some important basic empirical studies that have advanced the understanding of seals.

Hirabayashi et al. [36] optimized the seals used in automotive cooling systems after studying how salt is used in anti-freeze agents which crystallize and damage seals. They point out that seals made from harder materials resist better wear at low contact pressures, while softer materials perform better at higher loads. Golubiev and Gordeev [37] improved the seal design of water pumps that operate in liquids with a high concentration of abrasive particles. The new designs incorporate anti-wear materials, change in sealing shape and change the sealing mechanism.

In the study of Ravindra Verma et al. [38], rubber specimens' abrasive wear behavior is experimentally investigated with the help of a ‘Two-body abrasion tester’ machine and the wear results are compared with different load & speeds. The wear rate is calculated from experiments. From the observation about rubber's wear behavior, it is found that the abrasive wear rate is increasing with load & speed.

In an experimental study on the influence of sliding velocity and sliding angle on wear rate of the tread rubber wheel. J. Wu al el. [39] showed that the wear rate increases when the velocity increases and there is little wear when the angle is zero. The growth in velocity results in strong growth in excitation frequency, and thus, its effect on the wear rate is large. In addition, the contact profile is changed obviously during the wear process of the rubber wheel, and the contact pressure distribution is changed significantly. Generally, the larger the sliding angle is, the bigger the nonuniformity of contact pressure. Therefore, the wear rate is larger when there is a greater sliding angle.

2.3.3 Contact area

The contact area is an important parameter in tribology and contact mechanics. To describe the contact area, H. Hertz [40] approximated the surface 1882 with a model of half-sphere. Greenwood and Williams (GW) [41] enhanced Hertz's idea to approximate surface asperities with spheres of Gaussian distributed heights (Figure 2.6). From there, they determined the actual contact area relative to the nominal contact area. The spheres' real contact area is significantly smaller than the nominal contact area.

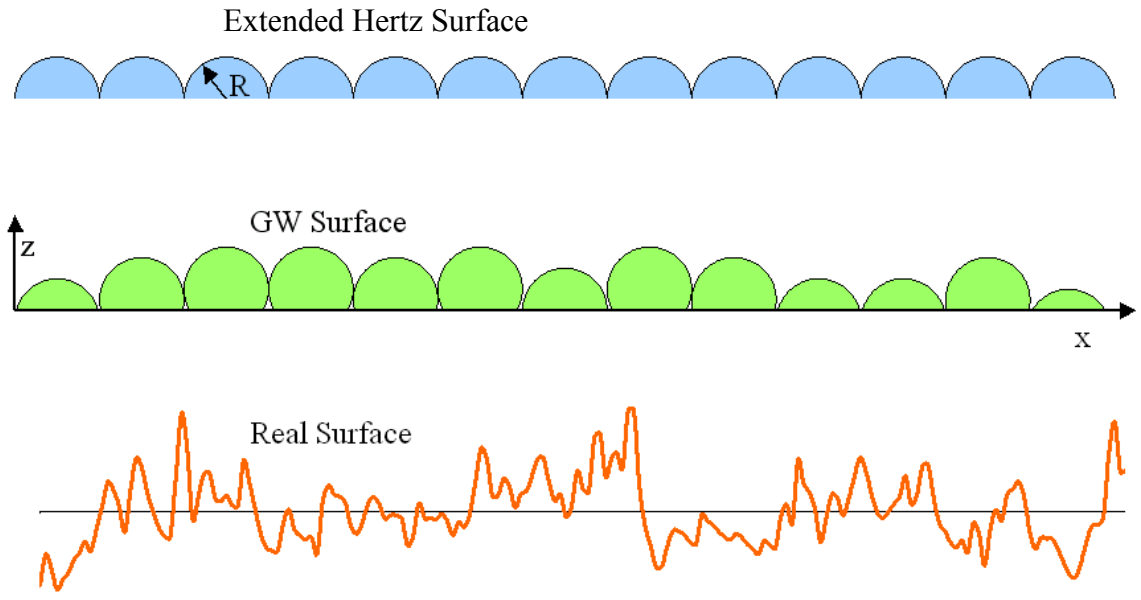

Figure 2.6: Extended Hertz and Greenwood-Williams description of surface geometry [15]

In general, the real area of contact is often smaller than the nominal area of contact. So it was proposed that the adhesional friction force is proportional to the real area of contact [42].

Tabor's [43] assessment of friction is if surfaces are brought in contact with each other by a normal force, the contact initiates at the asperity tips. The total real area of contact is proportional to the applied load which was also shown by the GW model.

Tambe and Bhushan [44] indicated the dependence of adhesion on Young's modulus, where low Young's modulus materials have higher adhesion than high Young's modulus materials. For the same applied normal load, materials with low Young's modulus will have higher contact area and penetration depth and, consequently, larger adhesion force than materials with high Young's modulus [45].

Several methods have been developed to accurately determine the actual contact area for in situ studies of the contact area between surfaces. In situ examination of the real contact area has been done by contact resistance measurements [42, 46], laser profilometry measurements [47], and optical measurements [48, 49]. The optical method is a widely used technique to measure the contact area due to the simplicity in the experimental setup and the ability to obtain discrete or continuous measurements. Krick et al. [49] developed an optical in situ apparatus to investigate a rough rubber half sphere's tribological behavior sliding against a glass window. They observed a strong hysteresis in the contact area versus applied force during loading/unloading. The change in the contact geometry and an increase in contact area for the rubber half-sphere were observed during sliding on glass. They also calculated the relative contact area and found it very nearly linearly with the applied load even when adhesion was included.

2.4 Simulation

The friction of rubber tread is related to both normal pressure and slip velocity. The contact area between the rubber wheel and road is simulated and measured by J. Wu et al. [39] under the load of 40 N. The contact area was measured and calculated by using image processing. J. Wu et al. showed that the rubber wheel specimen's contact area increases linearly with the corresponding load level.

To design elastomer parts for tribological applications, modeling friction is necessary to determine the part's functionality's contact conditions. In most cases, the reason for the elastomer parts to be replaced is the wear. The wear can change its geometry and the contact nature if the lubrication is not ideal. Therefore, wear modeling is needed to estimate the product life. Wear simulation techniques were developed more and more and became more common. Wear simulation methods incorporate various numerical methods, such as the boundary element method [50] or the discrete element method [51]. The most successful and popular is the finite element method since it is a general method for mechanical stress analysis.

Moldenhauer and Kröger [52] simulated the tread block's local wear in contact with the rough road surface. The tread block model was described by point contact elements representing non-linear springs with their initial lengths. The tread block model's wear process was defined as decreasing the length of the non-linear springs at each discretized point contact element. The wear equation describing the tread block's wear behavior was established based on Fleischer’s wear law, which describes wear rate proportional to friction power. According to this law, the wear rate depends on the local pressure, velocity and friction coefficient.

Ostermeyer and Müller [53] and Ostermeyer [54] studied the principal wear mechanism in brake systems' contact zone, leading to the friction layer's characteristic structure on the brake pad. Results showed that the friction coefficient's actual value depends on the patches' actual state on the pad, which changes over time due to wear particles' flow in the contact area. With increasing wear, the number of particles increases as well, and consequently, the number of patches increases. The sliding resistance in brake systems is shown as the number and the size of the patches. The dependency of the friction coefficient and temperature on normal load and relative velocity was presented with a decreasing value of μ corresponding to an increasing friction power. Additionally, if velocity or the normal load increases, the

temperature increases as well. The effect of velocity on friction coefficient shows that friction and wear increase if the velocity increases, whereas friction and wear decrease if the velocity decreases.

Ludwig [55] and Ludwig and Kuna [56] studied the distribution of wear affected by the contact pressure distribution on the silicon wafer surface during chemical mechanical polishing. The polishing process is implemented by pressing a silicon wafer against a moving polymer pad with a continuous slurry presence containing abrasives and chemicals. An analytical study and numerical simulation were performed to calculate the distribution of contact pressure between the wafer and pad. The finite element method (FEM) was implemented. Furthermore, the results of experimental investigations were compared with the FEM results. The analytical model produces an error of approximately 10%.

The popular FE-based wear simulation method was developed by Pödra and Andersson [57]. In this iterative method, the contact pressure distribution is determined by FEM and the wear equation of Archard [58] is used to calculate wear increments of the nodal. Then the contacting nodes are moved concerning the nodal wear values. Finally, the FE contact calculation is carried out again with the modified mesh and the cycle is repeated according to the simulated wear process. Several researchers [59,60] have improved this method for various applications, different geometries and materials, such as metals, ceramics, polymers and composites. Kónya and Váradi in [61] improved the method to consider heat generation and time-dependent material properties in the wear simulation.

CHAPTER 3

Test setup

3.1 Tribometer test rig

3.1.1 Operating principle of the tribometer test rig

Investigations of the friction characteristic and the wear behavior in contact between steel plate and rubber sample are performed by a tribometer test rig, as shown in Figure 3.1.

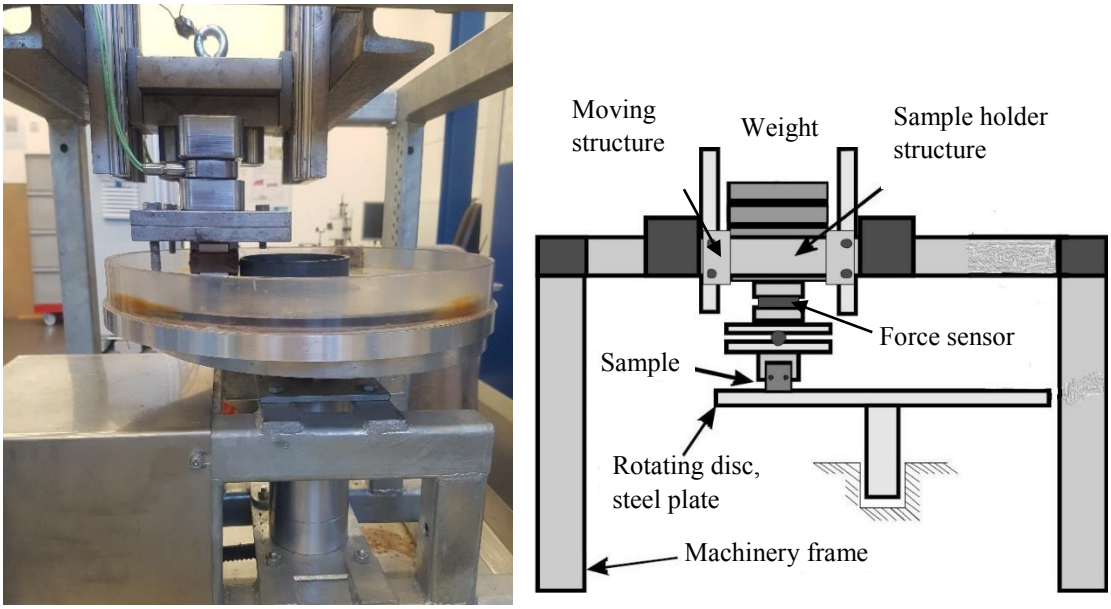

a) b)

Figure 3.1: a) Tribometer test rig and b) schematic structure of the tribometer test rig

The tribometer test rig operates with a relative motion between the rotating disc and the sample. The friction coefficient was measured by friction force and normal force, and the wear rate was calculated based on the material removed. The friction coefficient and wear rate depend on the input parameters, such as material, geometry, load, sliding velocity and testing time. Figure 3.1 b) shows a schematic of the tribometer test rig and a sample sliding on a rotating disc. The rubber sample contacts consecutive on the disc. The friction coefficient and wear rate are measured and analyzed by measured forces and mass loss.

3.1.2 Structure of the tribometer test rig

The main structure of the tribometer test rig consists of a rotating disc, a motor, the machinery frame, a sample holder structure and a control system of the rotating speed. An extra disc is designed to expand the range of the contact environment. This disc can hold sand, mud, or water during the test, see Figure 3.2 a).

Under the force sensor, a sample clamping is fixed on which the sample can be mounted or dismounted. The rubber samples were mounted with the sample clamping by L-corners, which were cut from the L-profile of aluminum or made from steel. The rubber samples are glued on the L corners with a dimension of 45x40 mm or 45x25 mm, see Figure 3.2 b).

a)

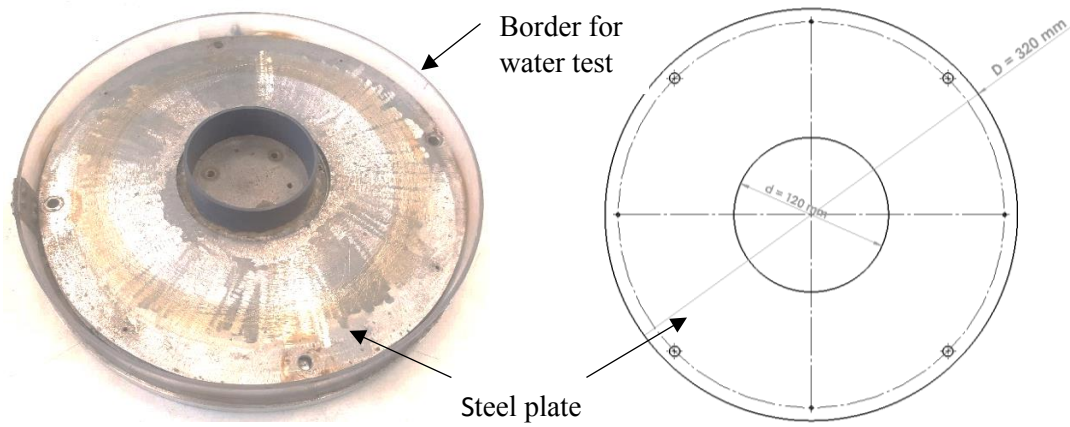

b)

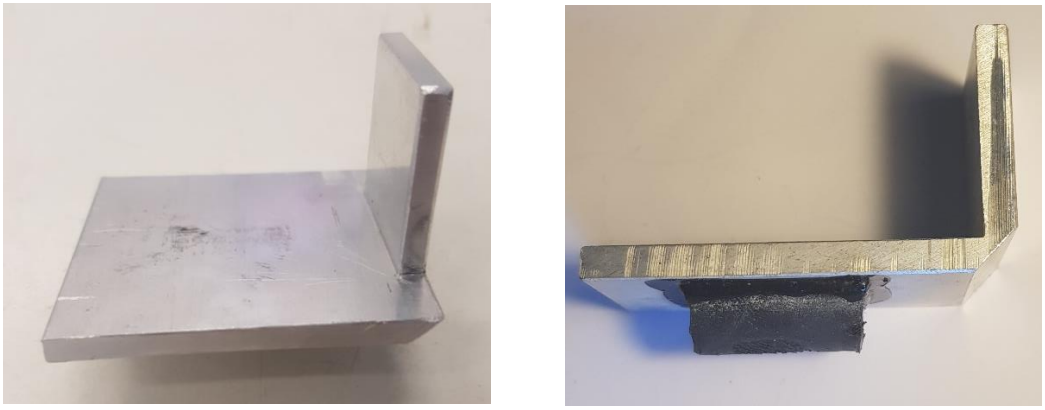

Figure 3.2: a) Steel plate and disc plate with a border for the water tests and b) the L-profiles of aluminum with glued rubber sample 45x40 mm and 45x20 mm

The normal force F_n and friction force F_r are measured by a three-axial force sensor, Kistler 9047C. The force sensor is mounted between the moving structure and the plate where the sample holder is mounted. The sample holder structure consists of two supporting plates on which four rollers are fixed, rolling on four guiding bars. The sample holder structure is easy to move perpendicular to the movement of the rotating disc. It has a high stiffness to avoid vibrations of the system during the tests, as shown in Figure 3.3 a).

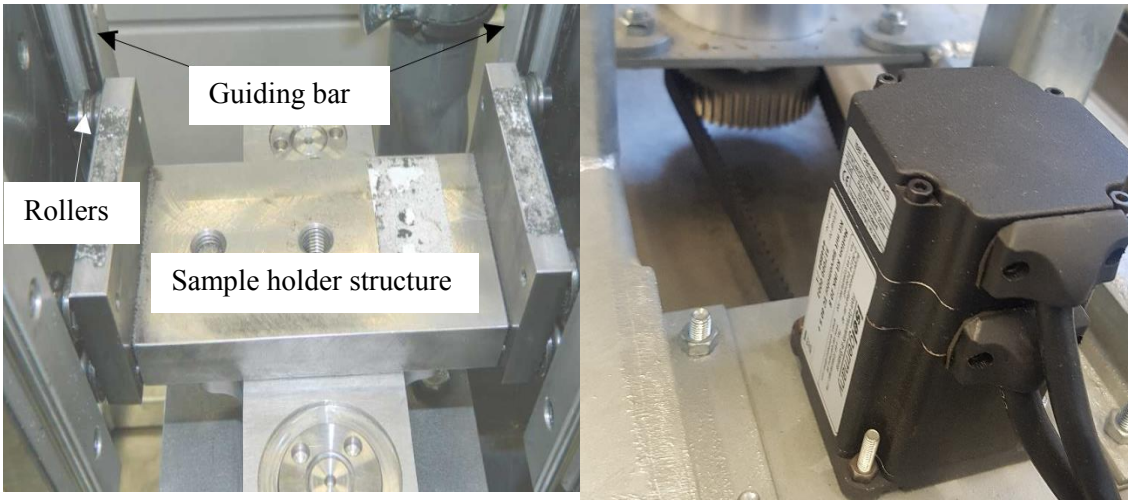

a) b)

Figure 3.3: a) Sample holder structure with a three-axial force sensor and b) the servo motor EC 60S and harmonic drive gearbox

The rotation of the disc creates the relative sliding movement between the contact surfaces. The rotation of the servo motor EC 60S is transmitted to the rotation axis of the disc via a harmonic drive gearbox, Figure 3.3 b).

Additionally, a signal processing box and a computer with Labview software are used to control the rotating speed, collect data and show the results.

The investigation with different parameters uses this tribometer test rig to collect the friction coefficient and wear rate. The friction characteristics and wear behavior of rubber can be analyzed by the influence of parameters on friction coefficient and wear rate. In the next section, the settings to test the influence of parameters on friction coefficient and wear rate are applied.

3.2 Setup for experimental investigation with rubber block

The investigation uses rubber blocks and steel plates. The steel plates have a roughness of R_a = 0.04 µm, outside diameter D = 320 mm, inside diameter d = 120 mm, see Figure 3.2. The samples are vulcanized from raw rubber compounds of ethylene propylene diene monomer (EPDM) or natural rubber (NR).

Rubber samples with different geometries, fillet radius and contact angles were created and tested to see the different influences of the contact between rubber and steel plate. The molds with different designs corresponding to the rubber samples are created and combined with the rubber molding machine to create the samples. The molds and the rubber molding machine are shown in Figure 3.4.

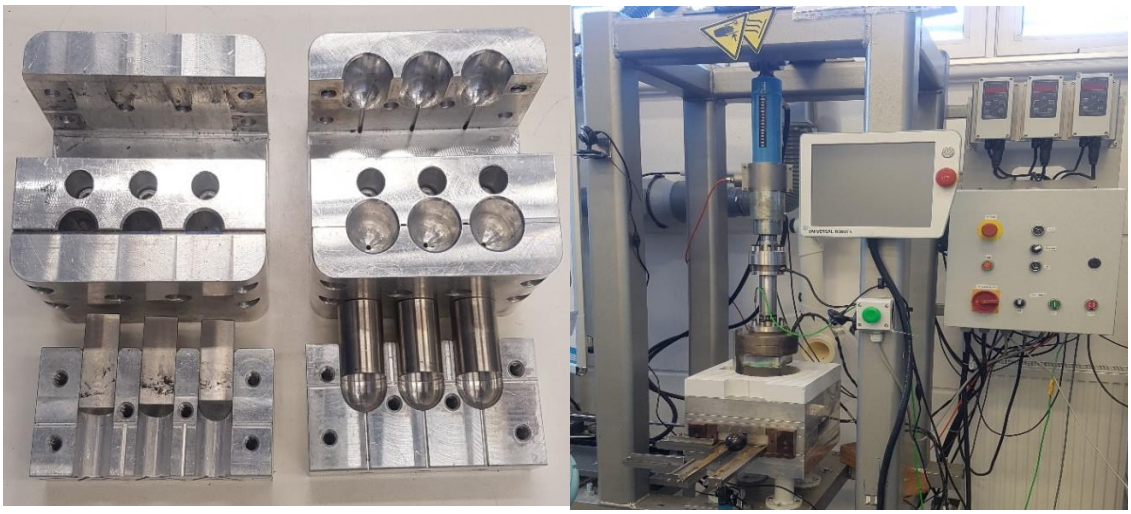

a) b)

Figure 3.4: a) The molds for the samples and b) the rubber molding machine

The molding sample process is carried out as follows:

- Design the samples and the molds on Solidwork software
- Manufacture the molds
- Prepare raw material, calculate the weight of raw material need for the sample
- The samples are made with the rubber molding machine

Some parameters used for the molding sample process are shown in Table 3.1.

Table 3.1: Parameters used for the molding sample process

Parameters	**Range**
Raw material rubber	EPDM, NR
Hardness [shore A]	60
Molding temperature [°C]	160
Molding time [min]	24
Molding pressure [bar]	16

Experimental determination of rubber block's tribogical properties is tested in three different contact conditions: dry contact, water contact and mud contact. Three contact conditions are shown in Figure 3.5 (a), b), c)).

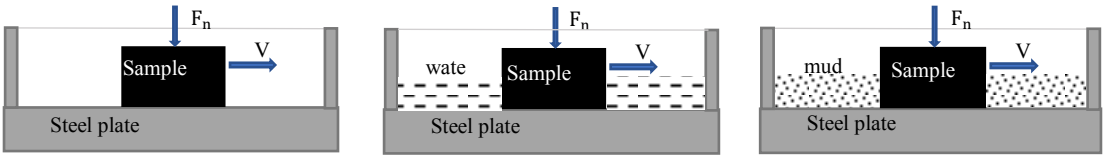

a) b) c)

Figure 3.5: The different contact environments: a) dry contact, b) wet contact and c) mud contact.

Table 3.2: Particle size of dry mud analysis - Particle group [%]

Particle group [%] by mass										
Gravel			Sand					Silt		Clay
From 20.0 to 10.0 mm	From 10.0 to 5.0 mm	From 5.0 to 2.0 mm	From 2.0 to 1.0 mm	From 1.0 to 0.5 mm	From 0.5 to 0.25 mm	From 0.25 to 0.1 mm	From 0.1 to 0.05 mm	From 0.05 to 0.01 mm	From 0.01 to 0.005 mm	< 0.005 mm
0.00	0.00	1.05	0.25	0.78	0.88	10.83	38.07	22.03	10.74	15.38

The mud used in the tests is a mixture of dry mud (60%) and water (40%). The percentage by mass of the particles in the dry mud is analyzed and shown in Table 3.2. When testing contact in mud, it should ensure that the mud always has in the contact area. So a structure to push the mud into the contact area has been added.

3.2.1 Setup for the experiment: The influence of geometry and sliding direction of the sample on the friction coefficient

In this section, experiments were performed with half-cylinder and half-sphere samples (spherical samples). Half-cylinder samples are tested in two sliding directions: sliding direction axial (axial cylindrical sample) and sliding direction lateral (lateral cylindrical sample). Figure 3.6 shows the geometry and the sliding direction of the sample in the contact.

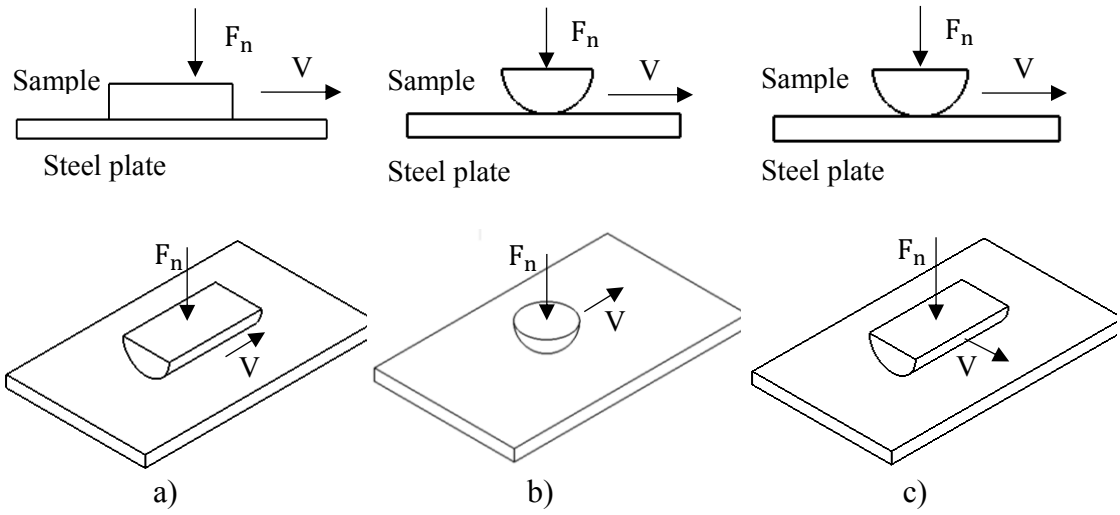

Figure 3.6: Geometry of sample and sliding direction: a) Axial cylindrical sample, b) half-sphere sample and c) lateral cylindrical sample

The samples were made from EPDM rubber, shore A 60. The samples have a contact angle θ_c = 90° and without fillet radius R = 0 (compare Figure 3.7). The tests were performed with a normal force of 90 N, velocities of 50 mm/s and 100 mm/s. The room temperature is from 20°C to 23°C and the testing time for all tests is 180 s. The parameters of the tests are shown in Table 3.3. With different samples, different parameters and different contact conditions, the results are different. These results are analyzed and presented in section 4.3.1.

Table 3.3: Parameters of the experiment: The influence of geometry and sliding direction of the sample on the friction coefficient

Parameters	**Range**
Steel plate	Stainless steel, R_a = 0.4 µm, D = 320 mm, d = 120 mm
Rubber sample	EPDM rubber, Shore A 60
Geometry of sample	Axial cylindrical, spherical and lateral cylindrical sample
Contact angle θ_c [°]	90°
Fillet radius R [mm]	0
Sliding velocity V [mm/s]	50, 100
Normal force F_n [N]	90
Contact condition	Dry contact, mud contact, water contact
Room temperature T [°C]	20 – 23
Testing time t [s]	180

3.2.2 Setup for the experiment: The influence of the fillet radius and contact angle on the friction coefficient

To study the influence of the sample´s geometry, the contact angle and fillet radius of the sample have been varied. Samples with fillet radius of R = 1 mm and 2 mm, contact angles of 105°, 120° and 135° have been manufactured and experimental tested, see Figure 3.7.

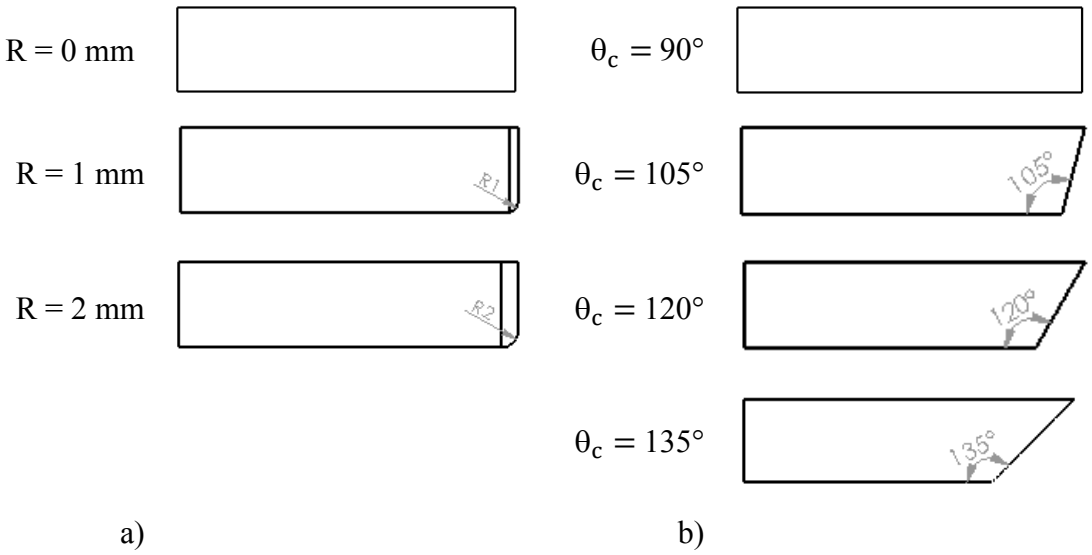

Figure 3.7: a) Samples with fillet radius R = 0 mm, 1 mm and 2 mm, b) samples with contact angle $\theta_c = 90°$, 105°, 120 ° and 135°.

The experimental process was performed at sliding velocities of 10 mm/s, 50 mm/s, 100 mm/s and 200 mm/s and normal forces of 60 N and 90 N.

Preliminary tests show that samples with fillet radius and contact angle larger than 90° limit the phenomena of lip contact and increase particles' penetration into the contact area, changing the contact properties. With dry contact, no effects of the fillet radius nor the contact angle are observed. Water easily penetrates the contact area, so it is very little affected by the fillet radius and contact angle. Experiments performed in mud contact will show the difference of samples stronger than in dry and water contact. Therefore in this experimental part, all samples were tested in mud contact. The parameters of the test are summarized in Table 3.4. The tests are carried out in 180 seconds at room temperature of 20°C - 23°C. The results are analyzed and presented in section 4.3.2.

Table 3.4: Parameters of the experiment: the influence of fillet radius and contact angle

Parameters	**Range**
Steel plate	Stainless steel, R_a = 0. 4 µm, D = 320 mm, d = 120 mm
Rubber sample	EPDM rubber, Shore A 60
Geometry of sample	Semi-cylindrical sample
Contact angle θ_c [°]	90°, 105°, 120°, 135°
Fillet radius R [mm]	0, 1, 2
Sliding velocity V [mm/s]	10, 50, 100, 200
Normal force F_n [N]	60, 90
Contact condition	Contact in mud
Room temperature T [°C]	20 - 23
Testing time t [s]	180

3.2.3 Setup for the experiment: The influence of sliding velocity on the friction coefficient

In some cases, velocity does not significantly affect the coefficient of friction. However, for each pair of materials in contact and under different contact conditions, the effect of velocity on friction can be different.

In this study's scope, friction experiments are done between rubber samples and steel plates under different contact conditions (dry, mud, water). In contact, the mud and water partly act as a lubricant. Therefore, the sliding velocity is one of the factors affecting the friction coefficient of the contact process. The setting parameters for this experiment are presented in Table 3.5.

Table 3.5: Parameters of the experiment: The influence of sliding velocity on the friction coefficient

Parameters	**Range**
Steel plate	Stainless steel, R_a = 0.4 µm, D = 320 mm, d = 120 mm
Rubber sample	EPDM rubber, Shore A 60
Geometry of sample	Semi-cylindrical sample
Contact angle θ_c [°]	90°
Fillet radius R [mm]	0
Sliding velocity V [mm/s]	10, 50, 100, 200
Normal force F_n [N]	90
Contact condition	Dry contact, mud contact, water contact
Room temperature T [°C]	20 - 23
Measurement time t [s]	180

The friction tests in different contact environments are compared at sliding velocity of 10 mm/s, 50 mm/s, 100 mm/s and 200 mm/s. The results presented in section 4.3.3 show the sliding velocity's influence on this pair of materials' friction properties. Thereby, it is possible to use the appropriate velocity to have suitable friction properties in the respective practical application conditions.

3.2.4 Setup for the experiment: The influence of the contact condition on the friction coefficient

In friction, coolant and lubricant are important parameters to reduce the friction coefficient between the two contact surfaces. Different contact environments will have a strong impact on the frictional properties. Depending on the contact environment, the reduction in the friction coefficient is different. Mud and water present in the contact area will also act as lubricants and coolants. Therefore, water is an important factor that affects the rubber's friction properties a lot. In this experimental part, the friction coefficient is measured in three different contact

conditions: dry contact, mud contact and water contact. The setting parameters for this experiment are presented in Table 3.5.

3.2.5 Setup for the experiment: The influence of normal force on the friction coefficient

Normal force acting on the sample is created by adding or removing masses placed on a moving mechanism carrying a force sensor. In this experiment, the normal force changes with three values of 30 N, 60 N and 90 N. Other parameters are similar to the experiment of the influence of sliding velocity, see Figure 3.5.

3.2.6 Setup for the experiment: The influence of material of the sample on the friction coefficient

In this investigation, the samples are made from two kinds of material: rubber EPDM and rubber NR. Rubber EPDM and NR are materials used to manufacture hydraulic water gate seals. Other parameters used for this experiment are shown in Table 3.5.

3.3 Setup for experimental investigation with a hydraulic seal

3.3.1 Pressure effects on the hydraulic seal

The pressure of water effects on the rubber seal by different water levels between upstream and downstream is illustrated in Figure 3.8.

The mean pressure is determined to follow the equation

$$\sigma = \frac{P}{A} \tag{3.1}$$

where P is apply load by different water levels between upstream and downstream, A is the contact area. The contact area A corresponds to the applied load P is determined from the simulation.

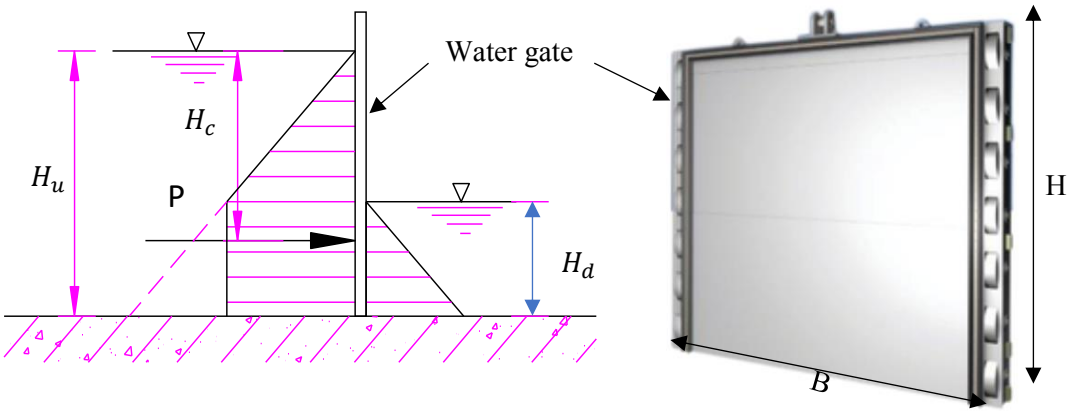

a) b)

Figure 3.8: a) Apply load effects on the water gate and b) slide water gate with rubber seal

Pressure in fluid effect on the surface of water gate is determined to follow the equation

$$p = \rho\, g\, h \tag{3.2}$$

where ρ is density of water ($\rho = 1000\ kgm^{-3}$), g is gravity acceleration ($g = 9.81\ ms^{-2}$) and h is the height of the water level.

Applyed load P is the total pressure in fluid effect on the surface of the water gate. P is determined to follow the equation

$$P = \frac{1}{2}\ \rho\ g\ (H_u^2 - H_d^2)\ B \tag{3.3}$$

where H_u is water levels at upstream, H_d is water levels at downstream and B is the width of the slide gate.

The application cases of different water gate sizes, different seal sizes and different water levels are calculated based on equations (3.1) and (3.3). The results are presented in Table 3.6.

Table 3.6: Results of calculated application cases

Size of the water gate H, B [m]	Size of hydraulic seal D_s, d_s [mm]	H_u [m]	H_d [m]	ΔH [m] $(H_u - H_d)$	Applied load P [kN]	Contact area A [m^2]	Mean Pressure p [MPa]
H = 4 B = 3	D_s = 40 d_s = 16	3.5	2.5	1	90	0.22	0.41
H = 4 B = 3	D_s = 40 d_s = 16	3.5	0.5	3	180	0.33	0.55
H = 2 B = 2	D_s = 20 d_s = 6	1.5	1	0.5	12.5	0.048	0.26
H = 2 B = 2	D_s = 20 d_s = 6	1.5	0	1.5	22.5	0.072	0.31

The investigation uses a real rubber seal and a mild stainless steel plates. The steel plates have a high roughness of R_a = 1.5 µm, outside diameter D = 320 mm, inside diameter d = 120 mm, see Figure 3.2. The samples are cut from a small hydraulic seal, L = 40 mm, D_s = 20 mm and d_s = 6 mm, see Figure 3.9.

In the experiments in the laboratory with the small rubber seal, the normal force is selected to be 45 N, 65 N and 95 N. Corresponding to the normal forces, the contact area A is determined from the simulation and the mean pressure values are determined to follow the equation (3.1) and presented in Table 3.7.

Thus, the experimental stress values are close to the stress values in the application.

Table 3.7: Values are determined for experiments

Size of the Rubber sample			Apply load P [N]	Contact area A [m^2]	Pressure p [MPa]
L [mm]	D_s [mm]	d_s [mm]			
40	20	6	45	0.00016	0.28
			65	0.00020	0.33
			95	0.00024	0.40

3.3.2 Measurement of friction coefficient

Experimental tests to determine the friction properties of rubber seal were performed with sliding velocities of 50 mm/s, 100 mm/s and 150 mm/s. Normal forces of 45 N, 65 N and 95 N. Other parameters are shown in Table 3.5.

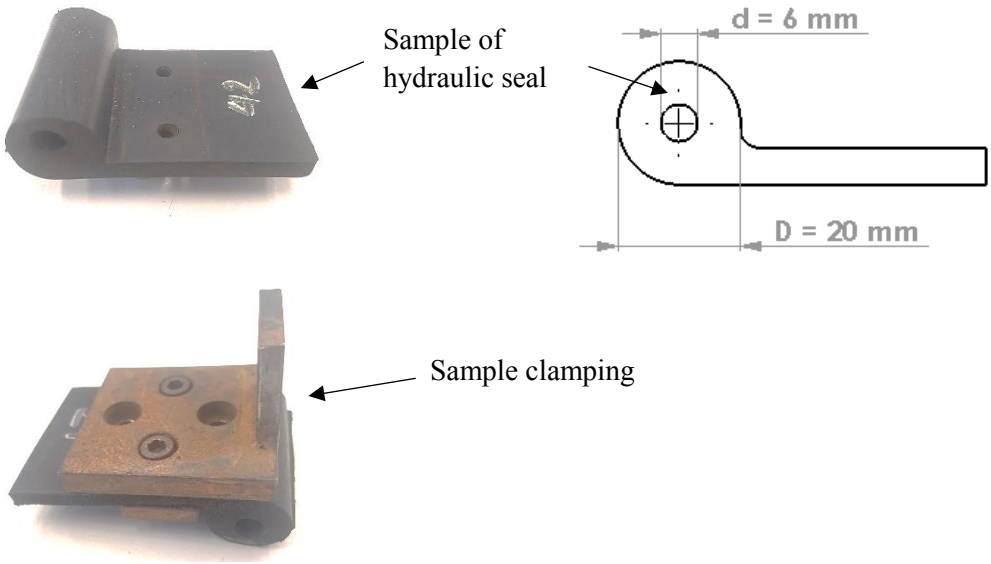

Figure 3.9: Sample of real hydraulic seal and sample clamping

3.3.3 Measurement of wear

Measurement tests to determine the wear behavior of real rubber seal were performed with normal forces of 45 N and 95 N and sliding velocities of 50 mm/s and 100 mm/s. Other parameters are shown in Table 3.5.

In dry contact, with sliding velocity of 50 mm/s, the mass loss is measured in 2 minutes, 4 minutes, 6 minutes, 8 minutes, 10 minutes and 12 minutes. With sliding velocity of 100 mm/s, the mass loss is measured in measurement times of 1 minute, 2 minutes, 3 minutes, 4 minutes, 5 minutes and 6 minutes. The sliding distances corresponding to the sliding velocity and measurement time are 60 m, 120 m, 180 m, 240 m, 300 m and 360 m.

Due to smaller wear rates, in mud and water contact, the mass loss is measured in 24 hours, 48 hours, 72 hours and 96 hours with sliding velocity of 100 mm/s. The sliding distances corresponding to the sliding velocity and measurement time are 8640 m, 17280 m, 25920 m and 34560 m.

Rubber absorbs water if it sinks in water for a long time. Therefore, after testing in mud and water environment, it is necessary to clean and dry to return to its original dry sample without water penetration. The time it takes for the sample to return to its original dry state depends on how long it was in the water.

3.3.4 Measurement of the contact area

The contact area performed on the measuring system includes contact pair of a rubber sample and a transparent plastic plate. The contact area measuring system is shown in Figure 3.10. Friction force and normal force are measured by a force sensor Kistler 9047C and are displayed. Light, mirror and digital camera were used to observe and determine the contact area between both surfaces.

The contact areas are measured at the normal forces of 28 N, 35 N, 42 N, 49 N, 56 N, 63 N and 70 N when friction force is zero. In other cases, the contact area is measured at a normal force of 70 N and the friction forcea are 0 N, 8 N, 16 N, 24 N, 32 N, 40 N and 48 N.

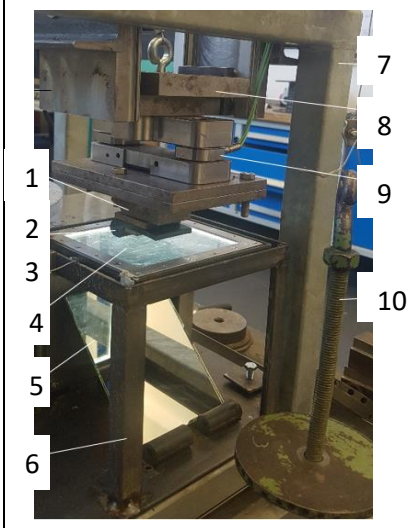

Some components of the measurement setup for contact area	
1	Sample holder
2	Sample
3	Structure to control friction force
4	Transparent plastic plate
5	Mirror
6	Frame of the contact area measuring system
7	Frame of tribometer
8	Vertical moving structure
9	Force sensor
10	Weight to control normal force

Figure 3.10: Contact area measurement system

Measurement of the contact area is performed following some steps:

- Applied load to the sample:
  - The normal force is controlled by weight.
  - The friction force is controlled by creating a small movement of the counterpart of seal. When the displacement of the place increasing, the friction force increases. The displacement was increased until the friction force reaches the desired value. Contact area is measured at the different friction force values. Take photos of the contact area with a camera.
- Using image processing software to calculate the value of contact area.

3.4 Setup for Simulation

The simulation of the friction process is performed on HyperWorks software. Geometric data of contact pairs are imported from SolidWorks. The elastic modulus E (Young's modulus) of EPDM rubber with hardness Shore A 60 is determined by equation [62]

$$E = 2\,G\,(1 + \nu) \tag{3.4}$$

where ν Poisson's ratio (ν of rubber is 0.5) and G is Shear modulus, calculated by

$$G = \frac{0.07515\ H_A + 0.549}{(4.1 + 3.9\ e^{-1.397\ h})(0.395\ h + 0.315\ h^2)} \quad \text{(MPa)} \tag{3.5}$$

with $h = 0.025\ (100 - H_A)$ and H_A is the hardness of EPDM rubber seal. The hardness of the used rubber is $H_A = 60$ Shore A. Filling the values into equations (3.4) and (3.5), G is 1.4 MPa and E is 4.2 MPa. Parameters set up for simulation with the software are given in Table 3.8.

Table 3.8: Parameters setup for the simulation

Parameters	**Value**
Steel plate	$E = 2.1*10^5$ MPa
Rubber sample	E = 4.2 MPa
Normal force	50 N, 70 N, 90 N
Friction force	20 N, 40 N, 60 N
Poisson's ratio	0.5

This chapter calculated and described the experimental and simulation process parameters. The results are presented in chapters 4, 5 and 6.

CHAPTER 4

Friction characteristics of the rubber block

In tribology, friction and wear are two main factors that play a significant role in researching the contact process's behavior. This chapter studies the influence of different parameters on friction characteristics.

The coefficient of friction μ is a measure of friction existing between two surfaces. A low value of the friction coefficient indicates that the force required for sliding is smaller than the force required if the coefficient of friction is high. The value of the coefficient of friction is given by

$$\mu = \frac{Friction\ force\ (F_r)}{Normal\ force\ (F_n)} \tag{4.1}$$

The direction of the forces given in this equation is shown in Figure 4.1. The coefficient of friction is the ratio of a force to a force and hence has no units.

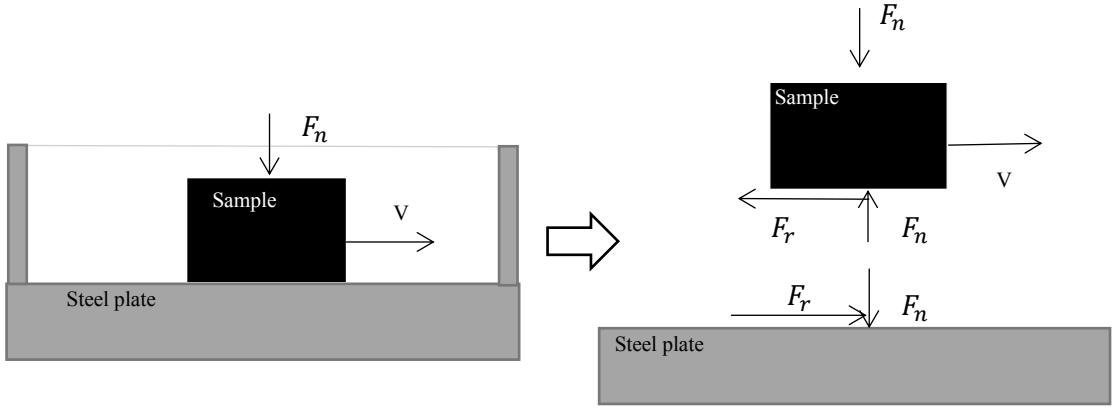

Figure 4.1: The direction of the forces in friction contact

In previous researches [63-71], the variation of friction depends on interfacial conditions, e.g., normal force, geometry, sliding velocity, the surface roughness of the rubbing surfaces, surface cleanliness, type of material, system rigidity, temperature, stick-slip, relative humidity, lubrication, vibration and contact condition. Section 4.1 presented some fundamental factors that effect on the coefficient of friction between two contact surfaces.

4.1 Influences on friction characteristic

Influence of the out of roundness of the disc

During the experiment, the sample is in contact with the metal disc surface. The rotation of the disc produces the relative sliding velocity between the sample and the disc. Because the disc has an out of roundness, the vertical displacement of the sample differs over one evolution. The value of the displacement depends on the inclination angle of the disc. Therefore, the motion of the sample is cyclic reciprocating in each revolution of the disc. Figure 4.2 described the displacement of both the disc and the sample. Influence of the out of roundness of the disc on The normal force F_n and friction force F_r can be seen in Figure 4.4.

Besides, in the structure of the measuring system, the sample holder structure's vertical moving ability with the force sensor also directly affects determining the coefficient of friction.

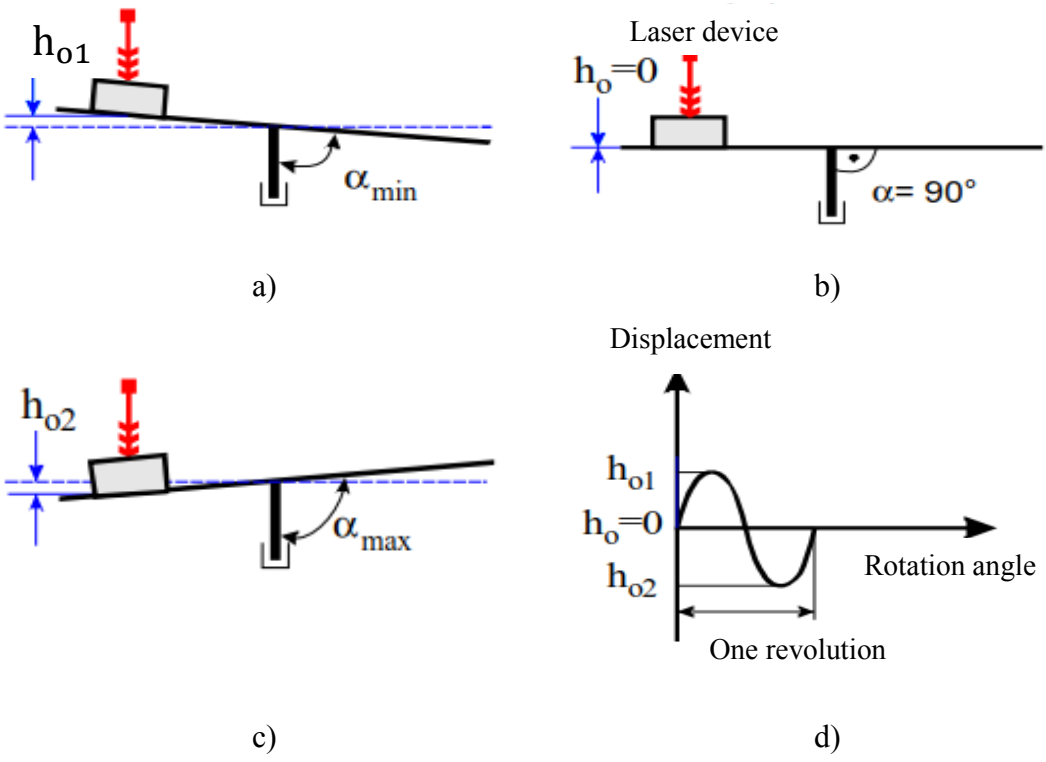

Figure 4.2: Scheme of displacement of the sample for the inclination angle of the disc [11]: a) α_{min}, b) $\alpha = 90°$, c) α_{max} and d) displacement of sample vs. one revolution

Influence of friction between rollers and guiding bar

Because the disc has an out of roundness, there is a change of the disc's absolute vertical position covering one revolution, so the sample moves up and down slightly. The sample holder structure has to move up and down sensitively correlating to the contact behavior between the sample and the disc to avoid changing normal force. For this reason, the moving mechanism of the sample holder structure is designed with eight rollers moving along the guiding bars, as shown in Figure 4.3.

It is necessary to adjust the rollers before performing experiments. If the gap between rollers and the guiding bar is large, the loading structure can perform horizontal vibrations. These horizontal vibrations lead to errors, especially when measuring the displacement of the sample. Besides, if the gap is too small, the loading structure's motion is not sensitive, and the normal force is substantially variating.

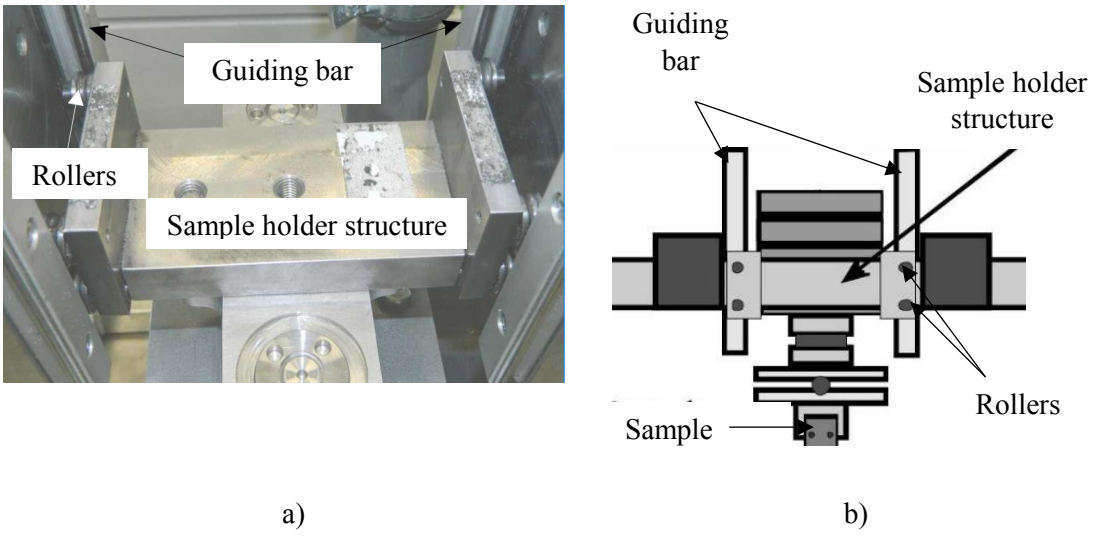

Figure 4.3: a) Photo of the sample holder structure and b) schematic principle of the sample holder structure

The out of roundness of the disc and friction between rollers and guiding bars are two system parameters that affect friction coefficient. Therefore, it is necessary to ensure accuracy and adjustable capabilities while manufacturing and assembling

Influence of contact angle and geometry of the sample

The geometry of the sample affects the deformability of sample. In sliding friction with sliding velocity V, the sample's geometry affects the tendency to squeeze out the liquid. When the samples have a contact angle bigger than 90 ° or a fillet radius, liquid or small particles may penetrate the contact area easily and altering the contact properties. In the samples with different geometries, when the normal force is applied, the contact area can change, leading to changes in the contact pressure and affecting the contact process's properties. The contact properties at the starting point can be affect by contact angles. The samples with angles of contact less than 90° have a lip at contact because the starting point of contact of the sample is easy to deformation resulting in a contact only at the site of deformation. This phenomenon usually occurs with soft materials, and the contact angle is small especially under dry contact conditions.

Influence of contact conditions

In friction, the contact environment is one of the important factors that directly affect friction properties. Depending on the contact conditions, the coefficient of friction may change more or less. In dry contact conditions, the friction coefficient is usually higher than that under contact conditions with lubricants. Dry exposure can rapidly increase the temperature in the contact area, which changes the properties of the exposed material. Conventional lubricant exposure reduces the coefficient of friction. Lubricants reduce heat generated by friction and transport debris material out of the contact area. Under the right conditions of speed, the lubricant can form a lubricating film between the two contact surfaces.

4.2 Test configuration and analysis of measured data

Test configuration

In this chapter, experiments are used to analyze the rubber's friction properties by studying the effect of basic parameters on the friction coefficient between the rubber sample and steel plate. Rubber samples were tested with different shapes and different contact angles for friction in different velocities, normal forces, and contact environments. Each experiment was repeated three times.

After experimenting, the obtained results are analyzed to assess the influence of different factors on the rubber's friction properties. Specific settings for this experimental process are presented in section 3.2. Table 4.1 presents some basic parameters for the experimental process.

Table 4.1 Parameters of investigations

Investigations	**Influence of sample geometry**	**Influence of fillet radius and contact angle**	**Influence of velocity and contact condition**	**Influence of normal force**	**Influence of sample material**
Steel plate	Stainless steel	Stainless steel	Stainless steel	Stainless steel	Stainless steel
Rubber sample	EPDM-60	EPDM-60	EPDM-60	EPDM-60	EPDM-60, NR-60
Geometry of sample	Half cylinder, half sphere, horizontal cylinder	Half cylinder	Half cylinder	Half cylinder	Half cylinder
Contact angle θ_c [°]	90°	90°, 105°, 120°, 135°	90°	90°	90°
Fillet radius R [mm]	R = 0	R = 0, 1, 2	R = 0	R = 0	R = 0
Sliding velocity V [mm/s]	50, 100	10, 50, 100, 200	10, 50, 100, 200	10, 50, 100, 200	10, 50, 100, 200
Normal force F_n [N]	90	60, 90	90	30, 60, 90	90
Contact condition	Dry, mud and water contact	Dry, mud and water contact	Dry, mud and water contact	Dry, mud and water contact	Dry, mud and water contact
Room temperature T [$°C$]	20 - 23	20 - 23	20 - 23	20 - 23	20 - 23
Measurement time t [s]	180	180	180	180	180
Repeat of experiment	Three times	Three times	Three times	Three times	Three times

Analysis of measured data

In this section, the influence of different parameters on the friction characteristics is studied. The values of the normal force F_n and friction force F_r are measured together during the test time. During one experiment's testing time, the normal force and friction force are displayed as an example in Figure 4.4.

The analysis of measured data is implemented for all experiments as follows. The friction coefficient μ is calculated by the mean values of F_n and F_r with $\mu = F_r/F_n$. The friction coefficient μ is determined over the same measurement time of 180 s for all experiments.

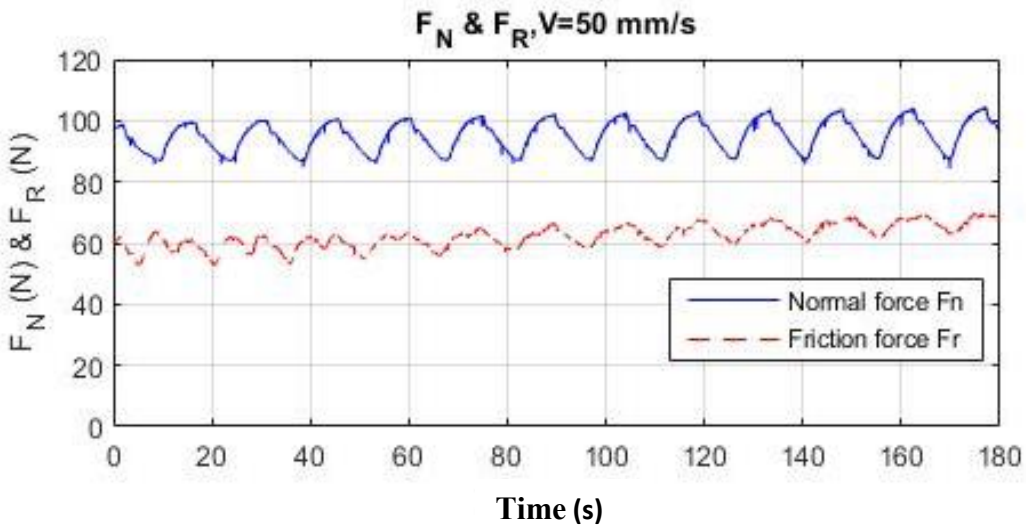

Figure 4.4: The normal force F_n, friction force F_r during the testing time of one experiment, nominal normal force F_n = 90 N, V = 50 mm/s, in dry contact

During the experiment, if the setting parameters changed, the values of F_n and F_r are different. With the friction coefficient values obtained from F_n and F_r, those factors' influence can be evaluated. These results are presented in section 4.3.

4.3 Results of experiments

4.3.1 Influence of contact direction and geometry of the sample

In this experiment, the friction coefficients of the semi-cylindrical and hemispherical samples were compared. The semi-cylindrical sample was tested in two different sliding directions: sliding direction lateral (lateral cylindrical samples) and sliding direction axial (cylindrical samples), see Figure 3.6. The friction coefficient of three geometries of samples in dry contact is presented in Figure 4.5.

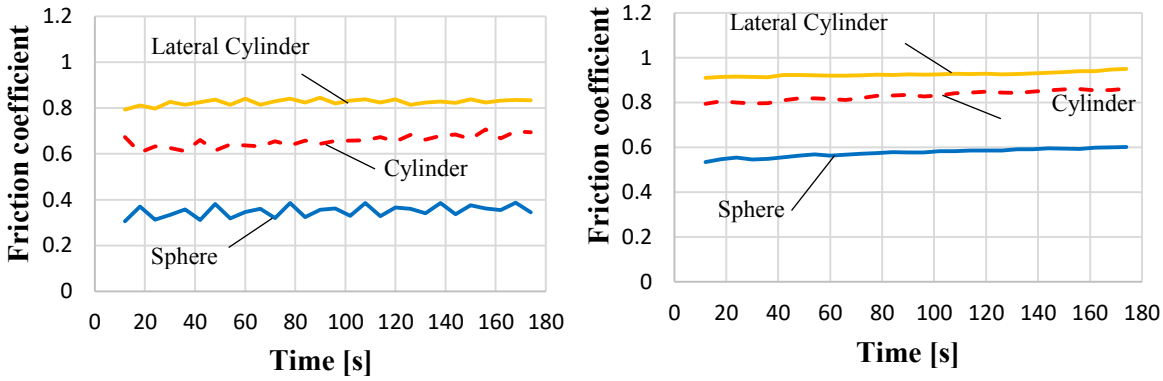

a) b)

Figure 4.5: Influence of sample geometry on the friction coefficient in dry contact: a) F_n = 90 N, V = 50 mm/s and b) F_n = 90 N , V = 100 mm/s

Under dry contact conditions at both 50 mm/s and 100 mm/s, it is found that the friction coefficient of the sphere sample is smaller than that of the lateral cylindrical sample and cylindrical sample. The lateral cylindrical sample gives the highest coefficient of friction.

Thus, with the same sliding velocity and normal force, different sample geometries give different friction coefficients.

Under wet contact conditions, Figure 4.6, all three cases of the geometry of samples have a small coefficient of friction. Friction coefficients of both the spherical and lateral cylindrical samples are smaller than those of the cylindrical samples. In the sliding direction, contact angles of spherical and lateral cylindrical

samples are larger than 90 degrees. Thus, water easily penetrates the contact area in the moving process, so heat and abrasive materials in the contact area are smaller than in the dry friction process. For the cylindrical sample the contact length in sliding distance is the sample's length. The friction coefficient with water is smaller than in dry contact, but it is larger than the spherical and lateral cylindrical samples. The cylindrical sample's contact angle is 90 degrees in the sliding direction, so it is more difficult for water to penetrate the contact area than for the two other samples. Figure 4.6 also shows that the friction coefficients of both sphere, cylindrical and lateral cylindrical samples in water contact decrease when increasing sliding velocity from 50 mm/s to 100 mm/s.

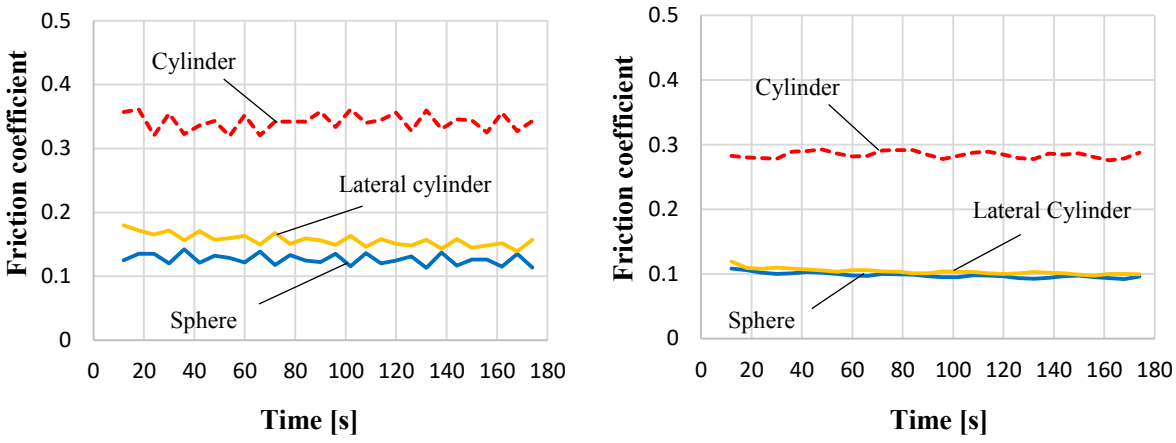

Figure 4.6: Influence of sample geometry on the friction coefficient in water contact: a) F_n = 90 N, V = 50 mm/s and b) F_n = 90 N , V = 100 mm/s

Figure 4.7 shows the coefficient of friction of sample geometries in mud contact. Unlike dry contact, in mud contact, the lateral cylindrical sample has the smallest coefficient of friction. Similar to water contact, the mud mixture penetrates more easily into the contact area of the lateral cylindrical sample. Thus the lubrication is better and the friction coefficient is smaller.

Thus, in dry contact, the lateral cylindrical sample has a higher coefficient of friction than the cylindrical sample. In the mud contact and water contact, the lateral cylindrical sample's friction coefficient is smaller than the friction coefficient of the

cylindrical sample. The spherical sample's friction coefficient is smaller than the friction coefficient of the cylindrical sample in dry and wet contact.

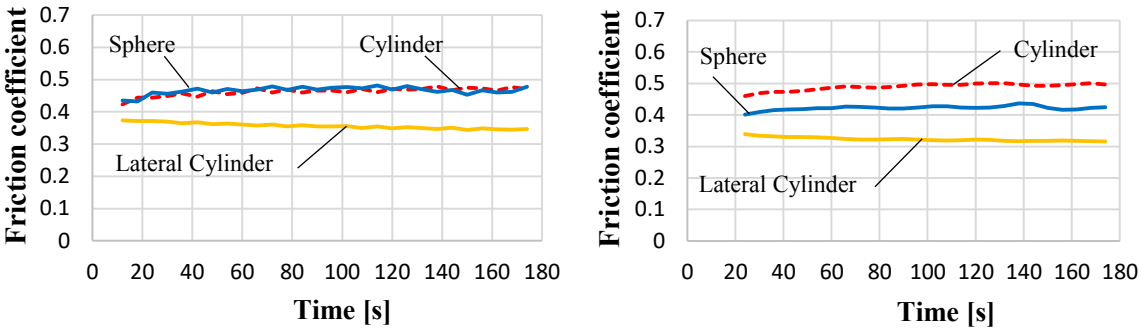

a) b)

Figure 4.7: Influence of sample geometry on the friction coefficient in mud contact: a) F_n = 90 N, V = 50 mm/s and b) F_n = 90 N , V = 100 mm/s

The spherical sample's friction coefficient is smaller than the friction coefficient of the cylindrical sample in dry and wet contact. The friction coefficient of sphere and lateral samples in mud contact decrease when increasing sliding velocity from 50 mm/s to 100 mm/s. But influence of velocity on friction coefficient in mud contact is smaller than in water contact.

4.3.2 Influence of contact angle and fillet radius

Test results on the influence of radius and contact angle on friction properties are shown in Figure 4.8 and Figure 4.9. Experimental samples are tested in mud contact with three values of radius R = 0 mm, 1 mm and 2 mm and four values of contact angles θ_c = 90 °, 105 °, 120 ° and 135 °, see Figure 3.7.

In both cases, the normal force is 60 N, see Figure 4.8 a) and 90 N, see Figure 4.8 b). It is found that the sample with a fillet radius (R =1 mm or 2 mm) has a friction coefficient smaller than that of a normal sample without fillet radius (R = 0). When the fillet radius increases, the coefficient of friction decreases. However, the difference is small. The average coefficient of friction corresponding to the radius

R = 0 mm, 1 mm and 2 mm are 0.51, 0.43 and 0.41 when F_n = 60 N and 0.46, 0.41 and 0.39 when F_n = 90 N.

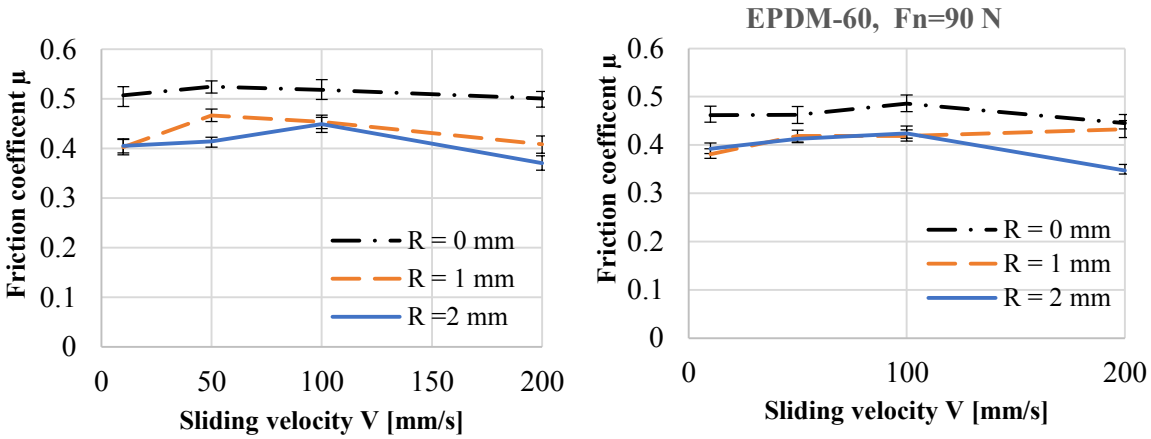

a) b)

Figure 4.8: Influence of fillet radius on the friction coefficient: a) Normal force 60 N and b) normal force 90 N

Changing the sample's fillet radius at the starting position of contact will change the penetration of water or small particles into the contact area. This changes the contact process's properties. Normally, when the radius increases, water and particles easily enter the contact area to create a lubricating film or partially convert from sliding contact to rolling contact particles, thereby reducing the coefficient of friction.

Figure 4.9 shows the influence of the contact angle on the coefficient of friction. The friction coefficient changes when the contact angle changes, but the change does not follow certain rules. The mean coefficient of friction for samples with contact angles greater than 90° will be less than that of samples with contact angles of 90°. Corresponding to the normal force of 60 N and 90 N, the friction coefficient variation with sliding velocity. The influence of contact angle is small.

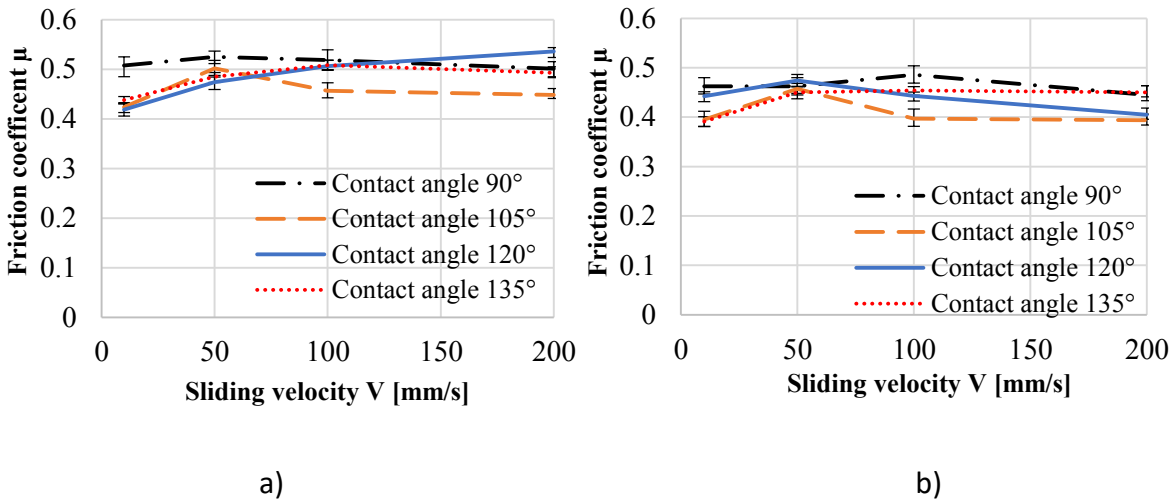

Figure 4.9: Influence of contact angle on friction coefficient with variable sliding velocity: a) Normal force 60 N and b) normal force 90 N

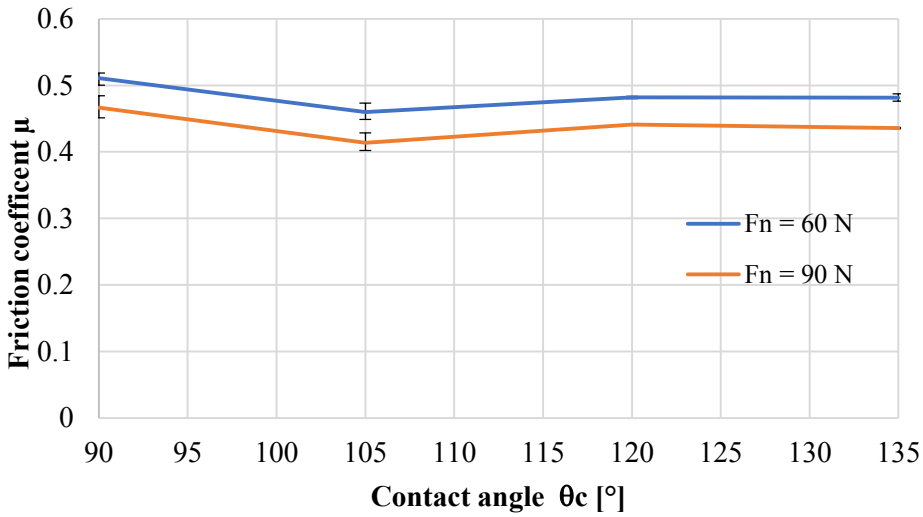

Figure 4.10: Relation of mean friction coefficient and contact angle

Figure 4.10 shows the influence of the contact angle and normal force on the mean coefficient of friction. Corresponding to the larger normal force, the coefficient of friction is smaller. When the contact angle changes, the variation of the friction coefficient is small. If the contact angle increases, the mean coefficient of friction is a little bit smaller than the mean coefficient of friction of samples with contact angles of 90°.

4.3.3 Influence of sliding velocity

In this section, friction tests between rubber and steel are performed with different sliding velocity values. Depending on contact conditions, the dependence of friction coefficient on sliding velocity is large or small. The dependence of the friction coefficient on velocity is shown in Figure 4.11.

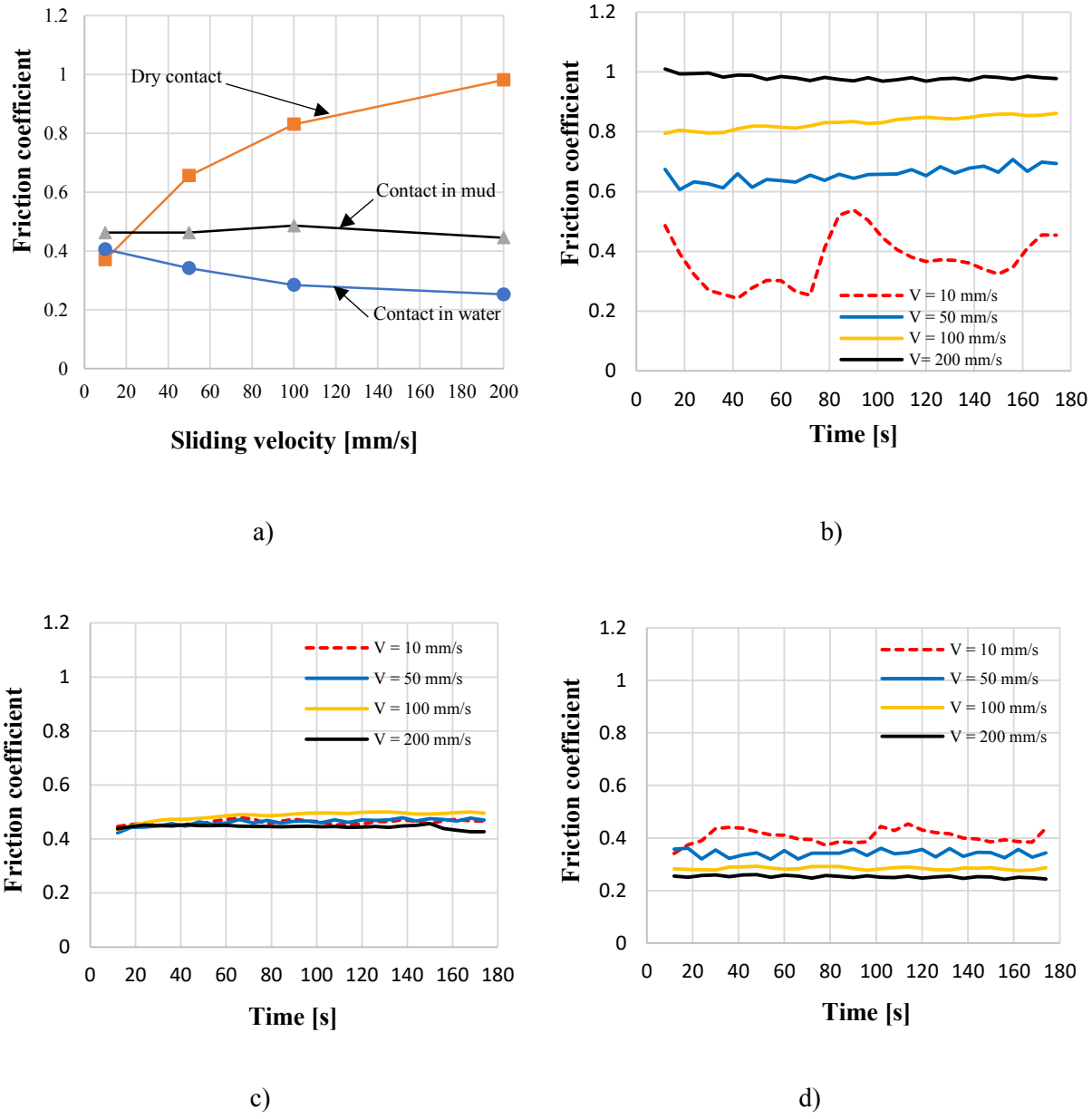

Figure 4.11: Influence of sliding velocity on the friction coefficient with normal force F_n = 90 N, sliding velocities are 10 mm/s, 50 mm/s, 100 mm/s and 200 mm/s: a) Comparison of contact conditions, b) dry contact, c) contact in mud and d) contact in water

In Figure 4.11 a) and b), with constant initial normal force F_n = 90 N, in dry contact, it can be seen that the coefficient of friction increases a lot with increasing sliding velocity from 10 mm/s to 50 mm/s, 100 mm/s and 200 mm/s. If the sliding velocity increases, the coefficient of friction increases.

Under mud contact conditions, Figure 4.11 a) and c), the friction coefficient is almost constant with increasing sliding velocity at low values of 10 mm/s, 50 mm/s, 100 mm/s and 200 mm/s. Thus it can be seen that in the mud contact, the coefficient of friction is independent from the sliding velocity.

Figure 4.11 a) and d) show the change in friction coefficient depending on sliding velocity in water contact. Unlike dry contact, if sliding velocity increases, the coefficient of friction decreases. The coefficient of friction in water contact is the smallest. However, the variation of the coefficient of friction in water contact is higher than in mud contact. The water lubricates the contact area, reduces the temperature and removes debris material from the contact area. The higher velocity, the more effective the lubricating film is created and reduces the coefficient of friction.

Besides, velocity increases the measuring system's vibration frequency due to the influence of the steel plate's out of roundness. The vibration system causes the applied load to change, which affects the normal and friction force and a little bit the coefficient of friction. The variation of the applied load according to the variation of velocity with the normal force F_n = 90 N is illustrated in Figure 4.12.

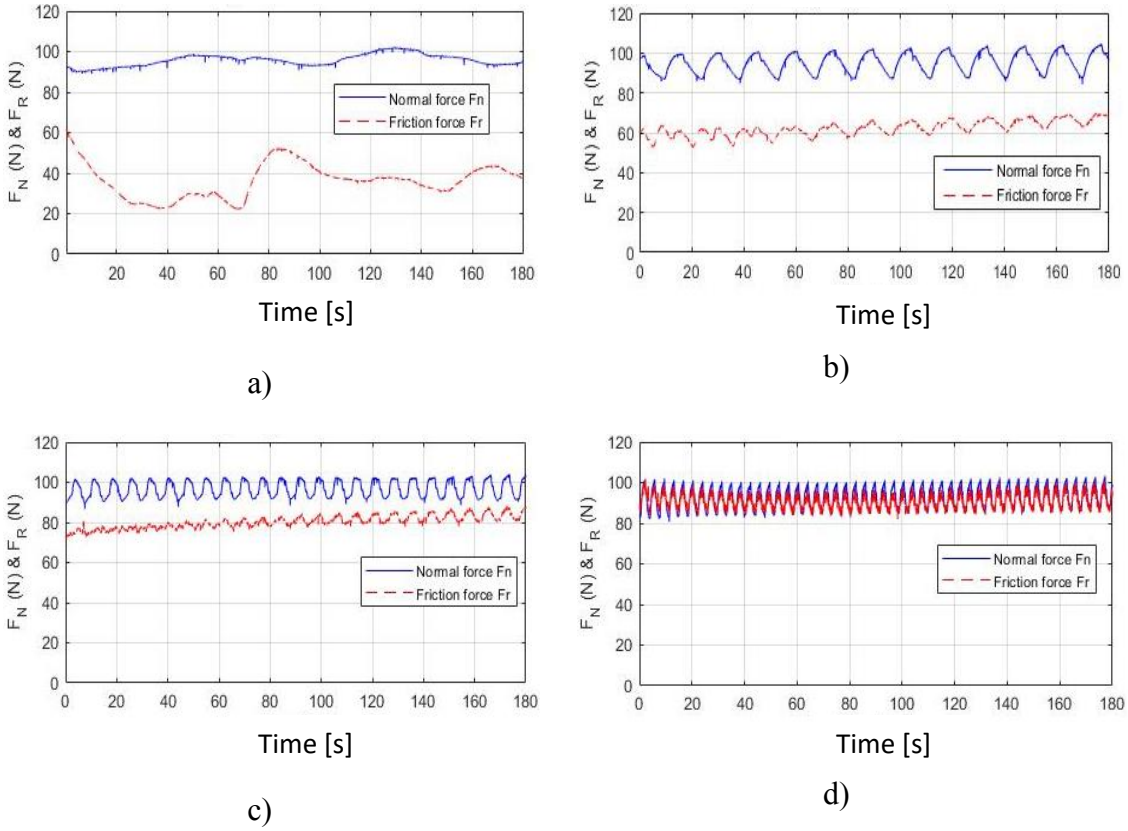

Figure 4.12: Influence of sliding velocity on normal force and friction force in dry contact with nominal normal force F_n = 90 N: a) Velocity 10 mm/s, b) velocity 50 mm/s, c) velocity 100 mm/s and d) velocity 200 mm/s

When the sliding velocity increases, the normal force has a high frequency and variates around the nominal value of 90 N. The friction force increases as the sliding velocity increases.

At a low sliding velocity of 10 mm/s Figure 4.12 a), the applied loads' vibration frequency is small and the mean value of friction force is not stable. At the sliding velocity of 200 mm/s, Figure 4.12 d), the applied loads' vibration frequency is higher and the mean values of both forces are stable. The excitation frequency can be calculated by:

$$f = \frac{V}{\pi d_r} \tag{4.2}$$

where V is sliding velocity and d_r = 200 mm is disc diameter at the point of contact.

4.3.4 Influence of normal force

The effect of normal force under different contact conditions on the friction coefficient is shown in Figure 4.13. The coefficient of friction is measured with normal forces of 30 N, 60 N and 90 N.

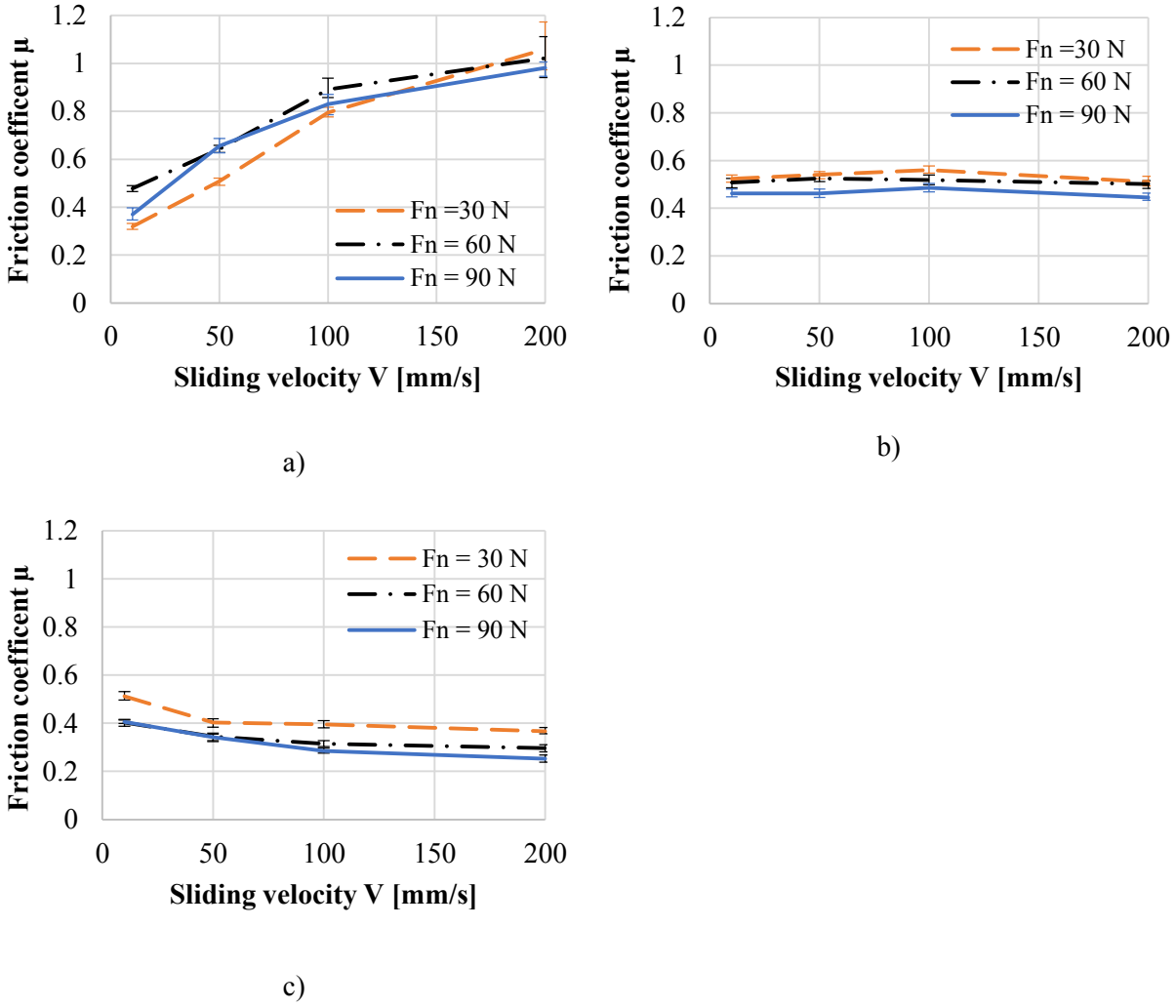

Figure 4.13: Influence of normal force on the friction coefficient with a) dry contact, b) contact in mud and c) contact in water

Figure 4.13 shows that the influence of normal force F_n on the coefficient of friction is not great. In different contact conditions, the influence of normal force F_n on the coefficient of friction is different. In the dry contact, Figure 4.13 a), it is found that the dependence of the friction coefficient on the normal force is not clear. However, the coefficient of friction for all three values of normal force F_n increases as the sliding velocity increases.

In the mud contact and water contact, Figures 4.13 b) and c), the coefficient of friction decreases with increasing normal force F_n value.

4.3.5 Influence of contact condition

The friction coefficients are measured under three contact conditions: dry contact, mud contact and water contact, see Figure 3.5. The result of the influence of the contact condition on the friction coefficient is shown in Figure 4.14.

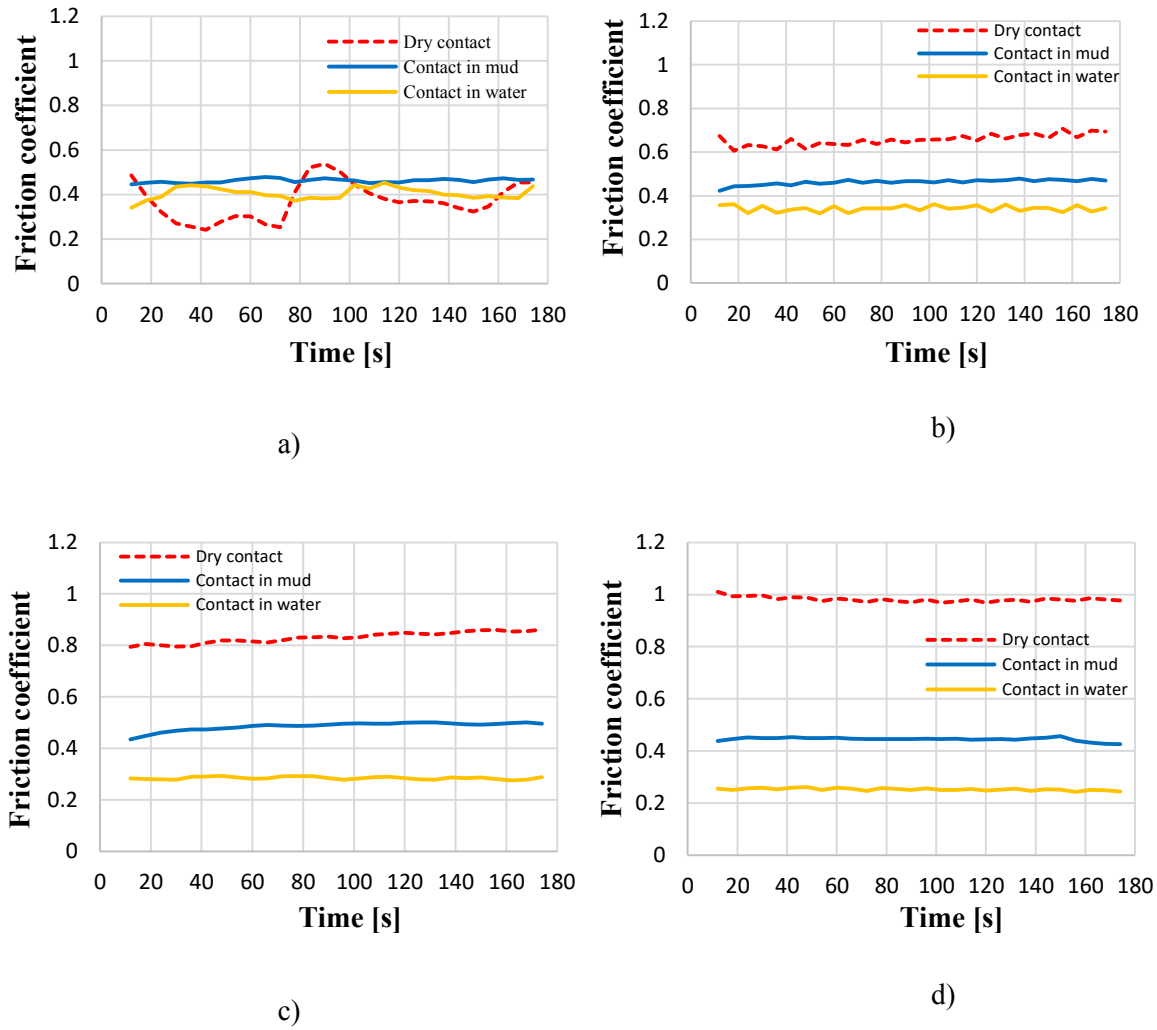

Figure 4.14: Influence of contact condition on the friction coefficient with normal force F_n = 90 N: a) V = 10 mm/s, b) V = 50 mm/s, c) V = 100 mm/s and d) V = 200 mm/s

At the sliding velocity of 10 mm/s, it is found that the coefficient of friction in mud contact is more stable than in water contact and in dry contact. The mean

value of the friction coefficient is not much different (dry contact 0.37, mud contact 0.46, water contact 0.41).

In the different contact conditions, for larger sliding velocity, the differences of friction coefficient are larger. In dry contact, the coefficient of friction increases when the sliding velocity increases. However, in water contact, the coefficient of friction decreases when the sliding velocity increases. So, at the sliding velocity of 200 mm/s, the friction coefficient of the rubber in dry contact is much higher than in water contact. The mean value of the friction coefficient at the sliding velocity of 200 mm/s in dry contact is 0.98 and in water contact is 0.25. The friction coefficient in mud contact does not change with the velocity.

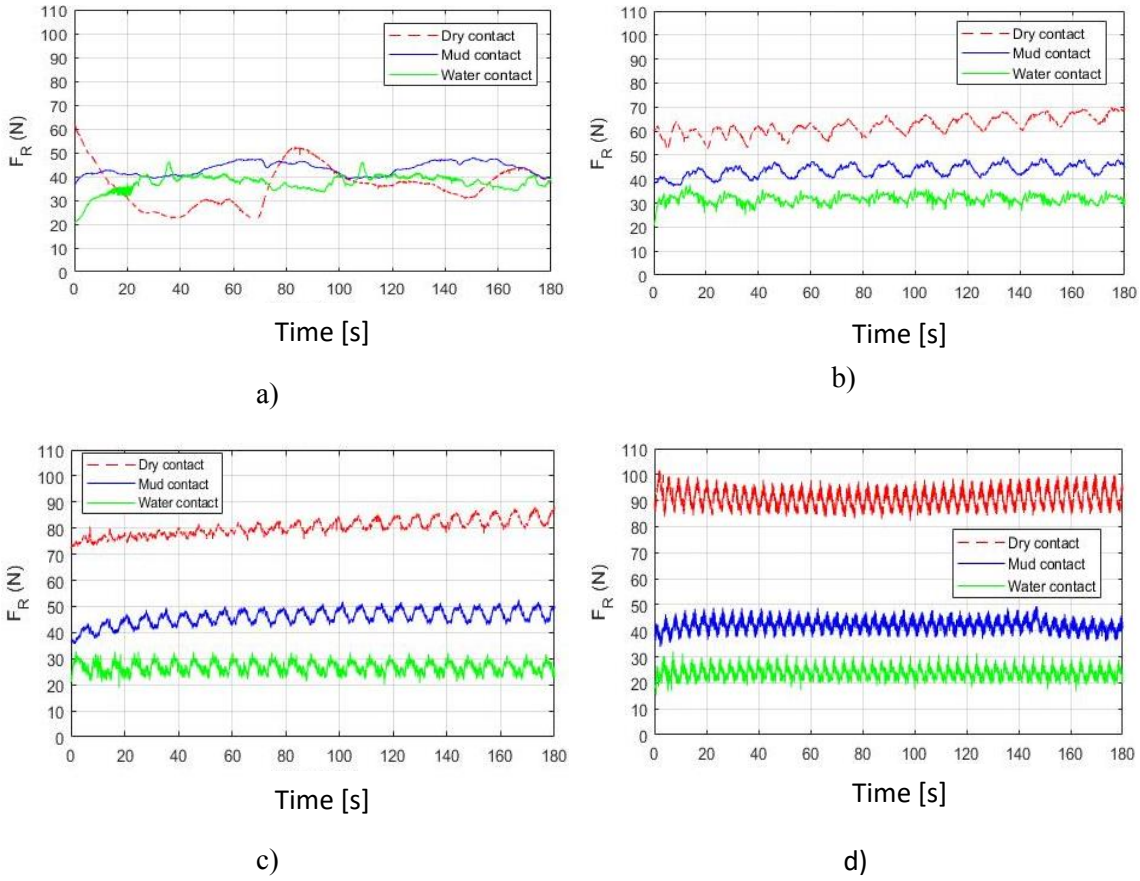

Figure 4.15: Influence of the contact condition on friction force with nominal normal force F_n = 90 N: : a) V = 10 mm/s, b) V = 50 mm/s, c) V = 100 mm/s and d) V = 200 mm/s

Mud is a mixture of water and particles of different size shapes and hardness. The mud contact process has both dry contact and a part of water contact properties. The small particles in mud can penetrate the contact area. In the contact area with

these small particles, the contact property changes from two-body contact to three-body contact [22]. Some particles slide and some roll. Rolling particles reduce the friction coefficient because the rolling friction coefficient is smaller than the sliding friction coefficient.

Figure 4.15 shows the change in the time of friction force depending on contact conditions. At the high value of sliding velocity (200 mm/s), the vibration frequency of force is large and the difference of friction force is quite large for all contact conditions.

Thus, it can be seen that the coefficient of friction between the rubber sample and steel plate depends a lot on contact conditions. The coefficient of friction decreases when changing from dry contact to mud contact and water contact.

4.3.6 Influence of material of the sample

During the friction process, the rubber material of the sample will affect the coefficient of friction. Figure 4.16 shows the experimental results comparing the friction coefficient of two rubber materials, EPDM and NR rubber. These two materials are used to produce the hydraulic rubber seal type – P.

In dry contact, Figure 4.16 a), EPDM and NR have very different friction coefficients. The friction coefficient of NR (1.65) is much larger than EPDM's friction coefficient (0.8).

The friction coefficients of both NR and EPDM in mud contact, Figure 4.16 b) are small and the difference in the friction coefficient of them is small. However, the friction coefficient of NR is smaller than that of EPDM.

Figure 4.16 c) shows that both EPDM and NR have a small coefficient of friction in water contact. The difference in the friction coefficient is not large NR (0.4) and EPDM (0.3).

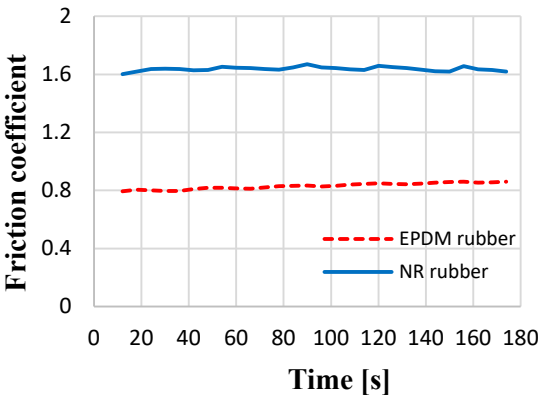

a)

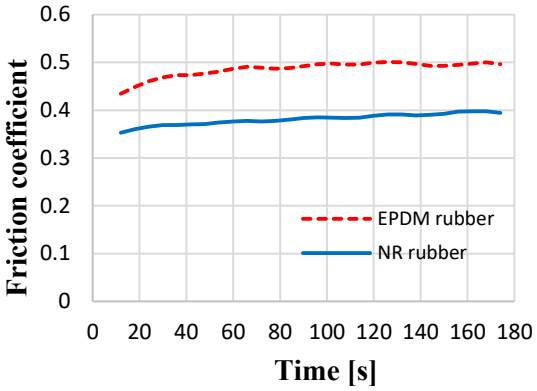

b)

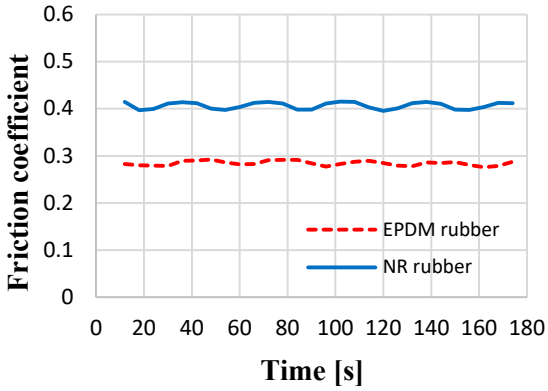

c)

Figure 4.16: Influence of material on friction coefficient over time with V = 100 mm/s and F_n = 90 N: a) Dry contact, b) contact in mud and c) contact in water

Although there is a difference in the coefficient of friction in dependence of sliding velocity observing Figure 4.17. It is found that the trend of influence of two materials on the friction coefficient is relatively similar. In the dry contact, Figure 4.17 a), both materials' friction coefficient increases if sliding velocity increases. In mud contact, Figure 4.17 b), the coefficient of friction is not influenced by sliding velocity. The coefficient of friction changes only a small amount with increasing sliding velocity.

The influence of sliding velocity in water contact is opposed to dry contact. When the sliding velocity increases, the coefficient of friction of both materials decreases.

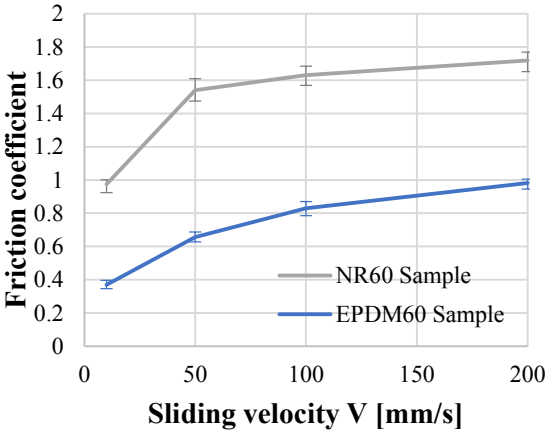

a)

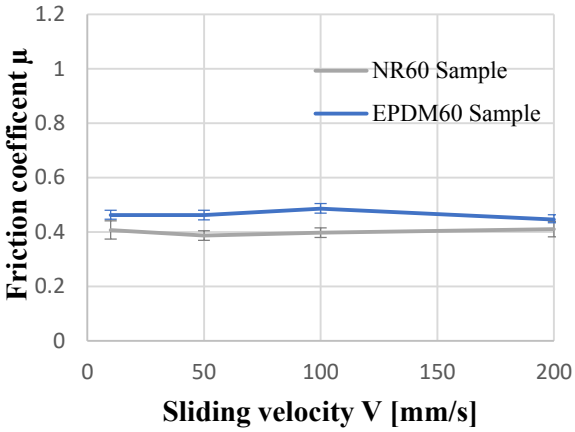

b)

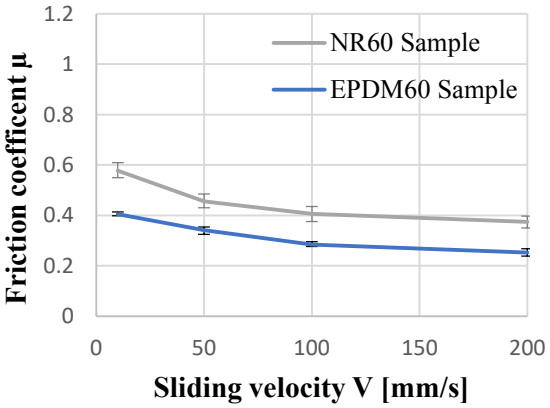

c)

Figure 4.17: Influence of rubber material on the friction coefficient with normal force F_n = 90 N and varied sliding velocity: a) Dry contact, b) contact in mud and c) contact in water

4.4 Summary

Many factors influence the frictional properties of the contact between two bodies. This section presents the experimental results of the study of frictional properties between rubber and stainless steel. Under different contact conditions (dry contact, wet contact, mud contact), different geometry of sample (half-cylinder, half-sphere), quite different contact direction (sliding direction axial and sliding direction lateral), fillet radius, contact angle or rubber material with different sliding velocity and normal force, the sample have a different coefficient of friction. Some results on the influence of the above factors on the friction coefficient are summarized as follows:

- In dry contact, the lateral cylindrical sample has a higher coefficient of friction than the cylindrical sample. In the mud contact and water contact, the friction coefficient of the lateral cylindrical sample is smaller than the friction coefficient of the cylindrical sample.
- The friction coefficient of the spherical sample is smaller than the friction coefficient of the cylindrical sample in both dry and wet contact.
- The friction coefficients of samples with fillet radius R = 1 mm and R = 2 mm are smaller than the sample's friction coefficient without fillet radius R = 0.
- The friction coefficients of samples that have contact angles θ_c = 105 °, 120 ° and 135 ° are a little bit smaller than the friction coefficient of the sample which has a contact angle θ_c = 90 °.
- In water contact, the friction coefficient decreases when sliding velocity increases. In dry contact, the friction coefficient increases when sliding velocity increases. The friction coefficient is nearly not effected on sliding velocity in mud contact.
- If sliding velocity increases, the applied load's vibration frequency increases.
- In fluence of normal force on the friction coefficient is small. If normal force increases, the friction coefficient has a small change in dry contact and the friction coefficient decreases slidly in mud contact and in water contact.
- The contact condition is one of the parameters that affect a lot on the friction coefficient. The friction coefficient in water contact is much smaller than that in dry contact. In dry contact, the friction coefficient depends a lot on sliding

velocity. The depending of friction coefficient on sliding is smaller in water contact. All three contact conditions result in almost the same friction coefficient for small sliding velocities.

- With different sample materials, the friction coefficient is different. The friction coefficient of the EPDM rubber is smaller than the friction coefficient of NR rubber in dry contact and water contact and higher in mud contact. With different contact conditions, the trend of influence of sliding velocity on the friction coefficient is relatively similar for both materials.

The results of this work are very valuable to understand the friction characteristic of rubber. In each application with different conditions, the friction coefficient can be adjusted by adjusting the parameters of the contact process. Additionally, this work's results can be used to analyze the friction characteristic of hydraulic rubber seals in chapter 5.

CHAPTER 5

Experimental investigation with hydraulic seals

5.1 Test configuration

Measurement of friction coefficient

Characteristics of the contact process between the rubber seal and stainless steel are shown first by the contact pair's frictional properties. Therefore, it is necessary to determine the friction characteristics of the rubber seal against stainless steel.

The investigation of the friction coefficient between the hydraulic seal and steel plates is performed on the tribometer of IMKF. The rubber seal is a P-type hydraulic seal used in irrigation work. The hydraulic seal is cut into the sample with a length L = 40 mm, D_s = 20 mm and d_s = 6 mm. The hardness of the rubber seal is Shore A 62. Stainless steel plates are manufactured with the roughness of surface $R_a = 1.5$ µm and D = 320 mm. The seal and steel plate are shown in Figure 3.9 and Figure 3.2.

The friction coefficient between the rubber sample and steel plate is measured in three different contact environments: dry contact, wet contact and mud contact, see Figure 3.5. The coefficient of friction µ is tested in dependents of normal load F_n, sliding velocity V and environment E_n.

$$\mu = f(F_n , E_n) \tag{5.1}$$

The coefficient of friction is determined by determining the friction force corresponding to the normal force:

$$\mu = \frac{F_r}{F_n} \tag{5.2}$$

The forces' values are measured, recorded and saved by a three-axial force sensor, Kistler 9047C and LabVIEW software.

The input parameters values of the experiment are shown in Table 5.1.

Table 5.1: The input parameter values of the experiment measuring the friction coefficient

Rubber seal	Rubber EPDM, Shore A 62, D_s = 20mm, d_s = 6 mm, L = 40 mm
Steel plate	Stainless steel, R_a = 1.5 µm, E = 2.1*10^5 Mpa
Normal forces	45 N, 65 N, 95 N
Sliding velocities	50 mm/s, 100 mm/s, 150 mm/s
Contact conditions	Dry contact, water contact and mud contact
Measurement time	180 s
Room temperature	20 ^oC - 23 ^oC

The measurement process is performed according to some basic steps as follows:

- Step one: Determine the normal force on the measuring system according to the input parameters by adding or subtracting masses on the system connected to the sample and the contact via the three-axis force measuring sensor of the system.
- Step two: The sliding velocity between the sample and the stainless steel disc is controlled by the rotation speed of the disc with the engine speed control software. Before the measuring system works and before the rubber sample comes into contact with the steel disc, the normal force and friction force is set to zero.
- Step three: Normal force and friction force values are measured for 180 seconds.

When measuring the friction characteristics in mud contact, a wiper system is supplemented to ensure there is always mud and liquid in the contact area.

Measurement of wear

To study the characteristics of the contact between rubber seal and steel plate, apart from the importance of friction, wear is also an important feature that needs to be reviewed and studied to see the essence of the contact process.

Similar to the friction test, wear characteristics were also tested on the Tribometer test rig of IMKF. Moreover, wear characteristics are also determined in

three cases of dry, wet, and mud contact. The different contact environments are shown in Figure 3.5. Wear properties are determined by the mass of the sample lost over time. The amount of material lost Δm depends on contact time t, sliding velocity V, normal force F_n and contact environment E_n.

$$\Delta m = f(t, F_n, V, E_n) \tag{5.3}$$

The mass of material removed during dry contact is determined after the sliding distance is 60 m, 120 m, 180 m, 240 m, 300 m, and 360 m.

Under the same dry contact conditions, varying normal force and sliding velocity will give different wear results.

In wet and mud contact environments, the friction coefficient is small, so the process of material loss also occurs slowly. Experiments with sliding distance higher than the sliding distance in dry contact are performed to observe the wear process.

The amount of material removed in wet and mud contact is determined after the sliding distance of 8640 m, 17280 m, 25920 m, and 34560 m. The set values for experimental wear characteristics are the same as experimental friction characteristics, see Table 5.1.

The process of determining the wear properties of rubber seal is carried out according to some basic steps as follows:

- Determine the weight of the sample before testing. Mount the sample on the measuring system.
- Set initial parameters for the measuring system: normal force, sliding velocity, contact environment and sliding distance through measurement time.
- Measure wear at setup intervals. During the measurement process, ensure stable contact conditions, especially that there is always mud and water in the contact area.

After each test, dry, clean the sample and determine the weight loss of the sample. The wear characteristics of the rubber seal can be analyzed and compared in different contact environments by the measurement results.

Measurement of the contact area

The contact area is also one of the key factors related to the contact characteristics of the two surfaces. With the change in the magnitude of normal force and friction force by the movement of the sample, the size of the contact area and the contact area shape also change accordingly.

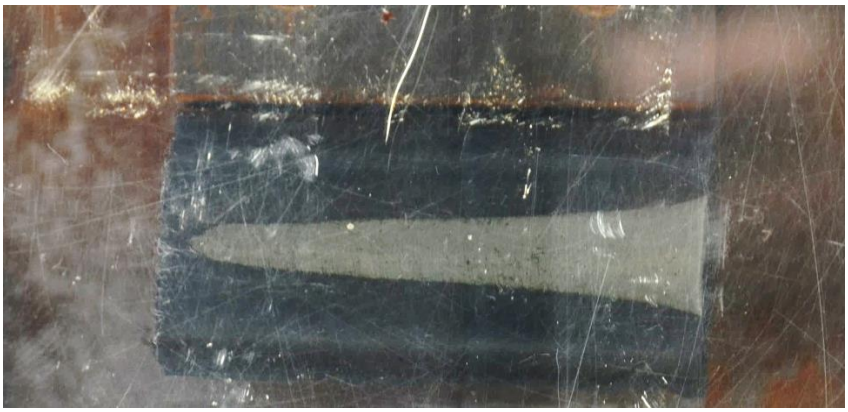

a)

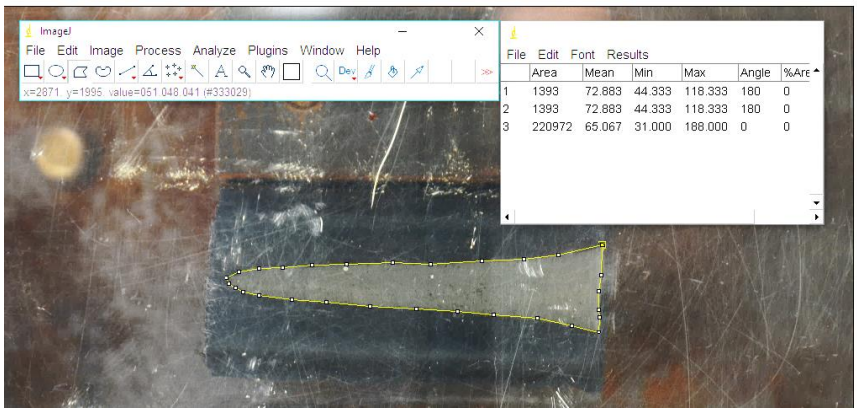

b)

Figure 5.1: Measured contact area: a) Photo of the contact area and b) Measured contact area on software

The measuring system for the contact area is designed and presented in section 3.3. With different normal force values, respectively, images obtain contact areas. Image processing support software is used to calculate the contact area between the rubber sample and the plastic plate. The measured contact area is illustrated in Figure 5.1. With the contact area, the deformation of the sample can be analyzed and evaluated.

5.2 Result of experimental investigation

After setting parameters and conducting experiments, the data from measurement results are collected. In this section, experimental results of friction, wear rate and contact area of hydraulic seal are analyzed and presented.

5.2.1 Friction coefficient

For the experimental determination of rubber seals' friction coefficients, the initial normal force values were 45 N or 65 N and 95 N with changes in the sliding velocity of 50 mm/s, 100 mm/s, and 150 mm/s.

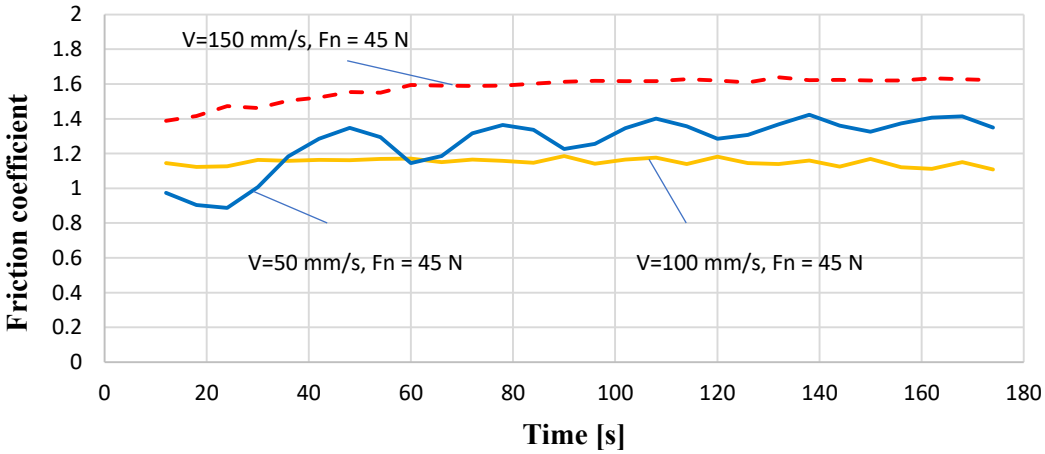

a)

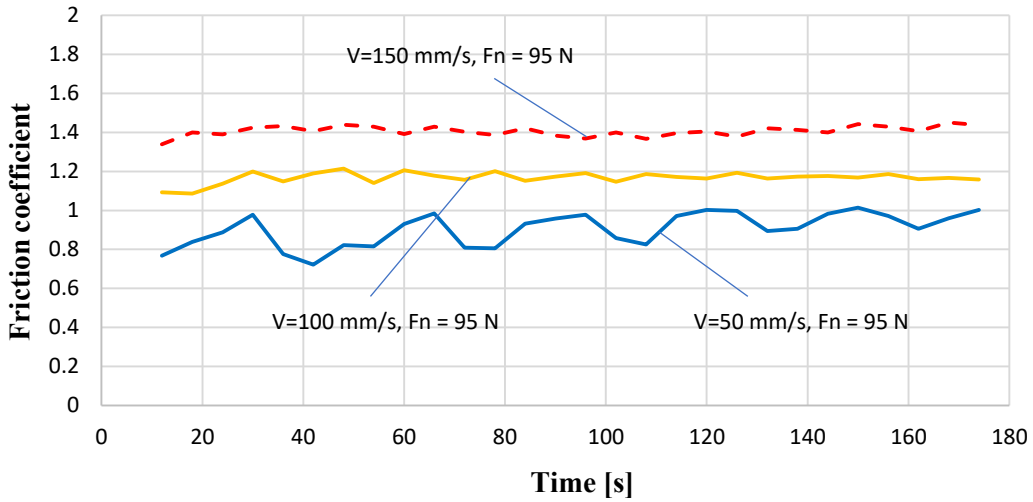

b)

Figure 5.2: The effect of sliding velocity and normal force on the coefficient of friction in dry contact with sliding velocities 50 mm/s, 100 mm/s, and 150 mm/s: a) Normal force 45 N, b) normal force 95 N

The measured values of the normal force F_n and friction force F_r during the whole test, one experiment is displayed in chapter 4. μ is determined over the same measurement time of 180 s for all dry contact experiments.

In dry contact, see the chart in Figure 5.2, it is found that the coefficient of friction at sliding velocities values of 50 mm/s and 150 mm/s are quite different. At the sliding velocity of 150 mm/s, the coefficient of friction is the largest. This is the same for normal force of 45 N and 95 N.

It is found that coefficient of friction decreases when increasing the normal force. However, with different normal force values, the corresponding friction coefficient will increase much more if increasing the sliding velocity.

With different normal force values, the friction coefficient corresponding to the sliding velocity of 100 mm/s has a relatively stable value (1.1 - 1.2).

a) b) c)

Figure 5.3: Contact surface of the sample after the test: a) After dry contact, b) after contact in mud and c) after contact in water

In dry contact conditions, the sliding velocity increases the temperature at the contact area. Besides, it is difficult to remove abrasive particles from the contact area. These particles scratch and rub contact surfaces (see Figure 5.3), thus increasing the friction coefficient.

Friction tests were carried out according to the experimental procedure presented in section 5.1. In the following, wet conditions mean that the rough plate was completely covered by water or mud.

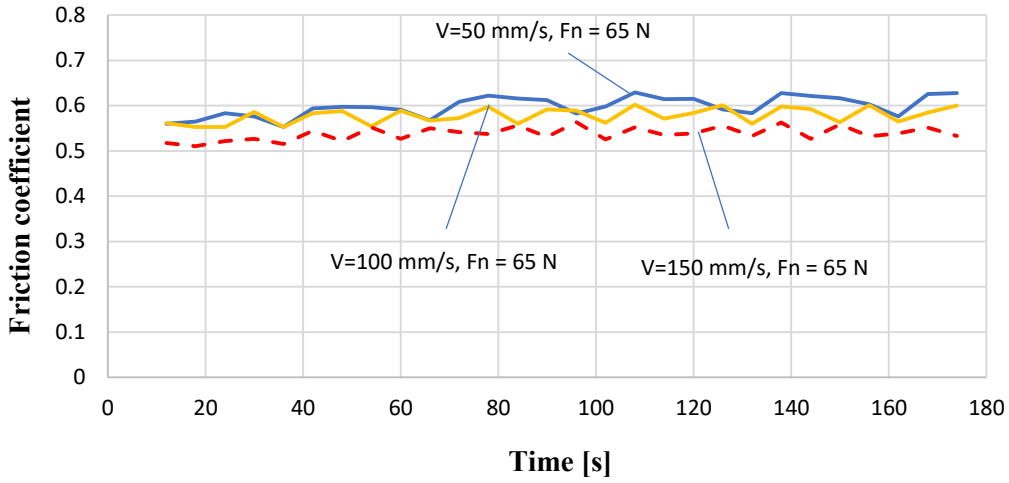

a)

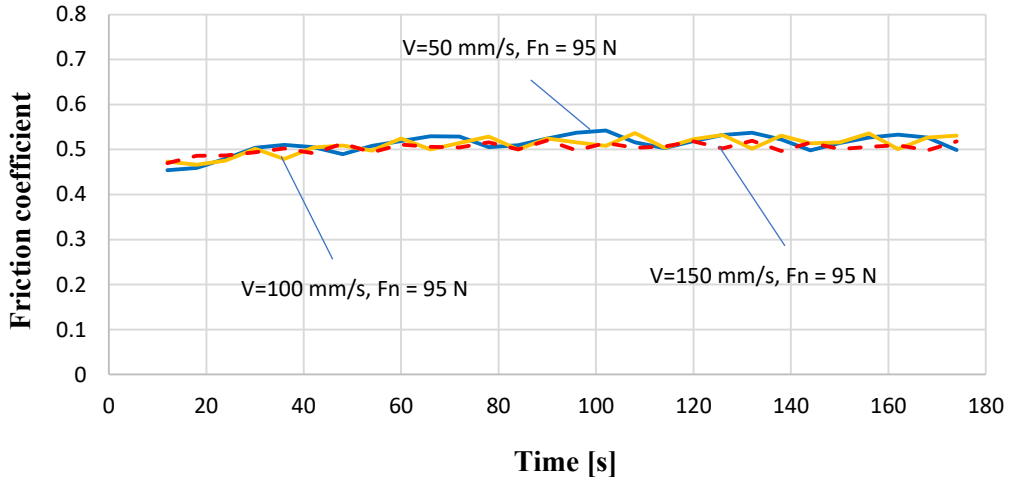

b)

Figure 5.4: The effect of sliding velocity and normal force on the coefficient of friction in mud contact with sliding velocities 50 mm/s, 100 mm/s, and 150 mm/s: a) Normal force 65 N and b) normal force 95 N

In mud contact conditions, it is observable that if the normal force increases, the friction coefficient decreases; compare Fig 5.4 a) and b). This observation is the same as in the dry contact. However, if increasing the sliding velocity, the corresponding friction coefficient decreases slidly. This observation is the opposite of the dry contact, see especially Figure 5.4 a).

In the condition of mud contact, the friction coefficient does not change much when changing the sliding velocity, which means that the friction coefficient depends only little on the sliding velocity, see especially Figure 5.4 b).

In water contact condition, Fig 5.5, it observes that the trend of the coefficient of friction is the same as in the mud contact conditions. If the sliding velocity is increased, the corresponding friction coefficient decreases. However, the coefficient of friction is nearly independent of the normal force.

When changing the sliding velocity, the changing of the friction coefficient in water contact is more than in mud contact, which means that the friction coefficient depends on the sliding velocity in water contact more than in mud contact.

So the effect of sliding velocity on the coefficient of friction in wet contact and mud contact conditions is the opposite of dry contact.

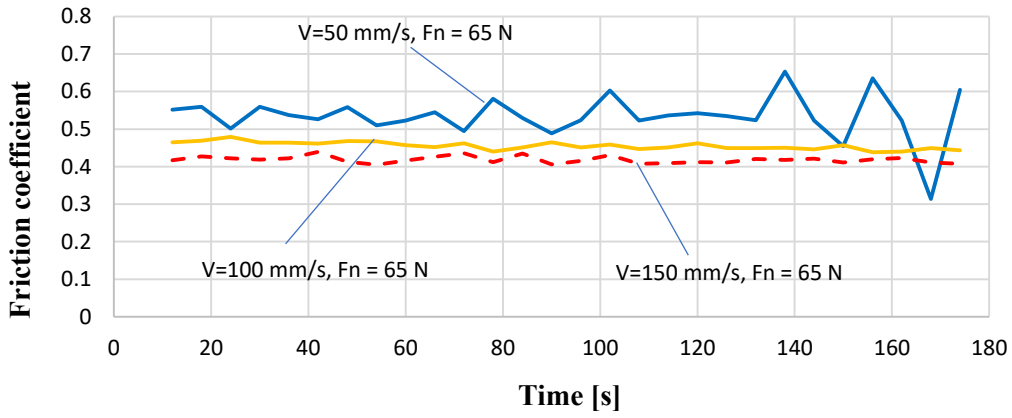

a)

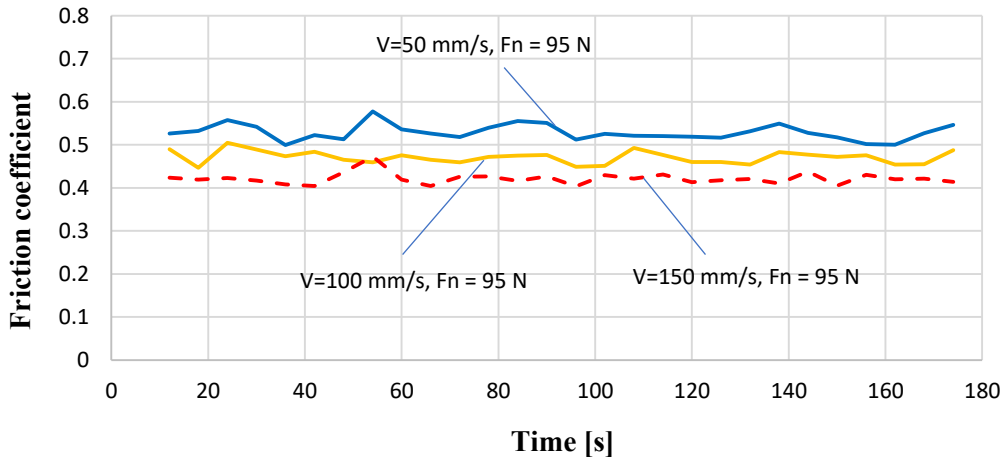

b)

Figure 5.5: The effect of sliding velocity and normal force on the coefficient of friction in water contact with sliding velocities 50 mm/s, 100 mm/s, and 150 mm/s: a) Normal force 65 N and b) normal force 95 N

In addition to the experiment of normal force and sliding velocity influence on the friction coefficient between the rubber seal and steel plate, the experimental results of the investigation on the influence of the contact conditions on the friction coefficient are also presented in this section.

The presence of lubricant is of extreme importance for the level of rubber friction on rough surfaces. As previously observed by Grosch, the friction coefficient is strongly reduced under wet conditions over the whole range of sliding velocities [72].

In the chart of the friction coefficient Fig 5.6, it is found that the friction coefficient in water contact (0.47) and mud contact environments (0.52) is much smaller compared to the friction coefficient in dry contact conditions (1.15).

In wet contact conditions, water penetrates the contact area. When the rubber seal and steel plate have a relative sliding velocity, the debris could be quickly removed at high velocities, and the fluid film can be formed between two contact surfaces.

The mud mixture contains water and various particles of different sizes and hardness are used in the mud contact condition. A mud contact condition is a form of wet contact. However, there are particles in the mud mixture, penetrating the contact area between the rubber seal and the steel plate. Thus causes that some particles change from a sliding friction state to a rolling friction state resulting in a reduction of the friction coefficient [11].

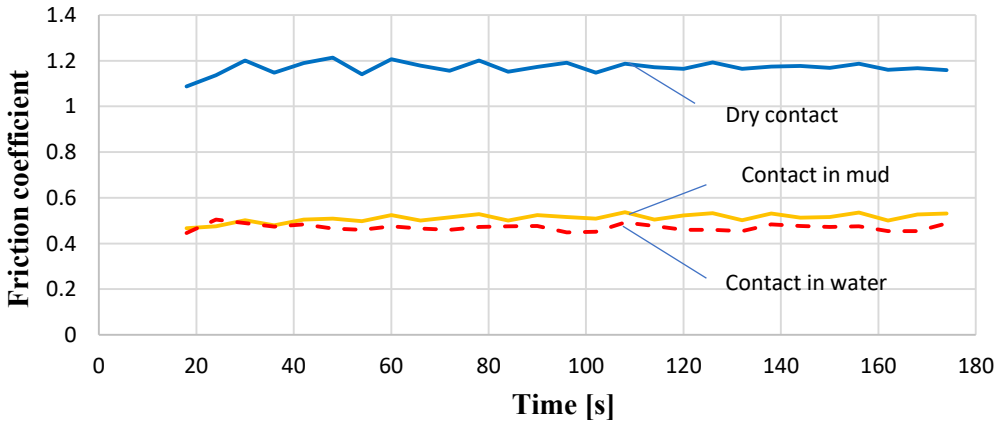

Figure 5.6: The coefficient of friction in dry contact, mud contact and water contact conditions, V = 100 mm/s, F_n = 95 N

5.2.2 Wear behavior

This section presents an experimental investigation of the wear process of a face rubber seal operating in different abrasive conditions. Besides the dry contact process, the processes with water or mud with particles are experimentally investigated and mass loss of each seal is determined. By experimental data quantifying each seal, correlation of wear rate with sliding velocity, normal force and contact conditions were determined.

The rubber samples of these tests correspond to the test configuration listed in Table 5.2. The experimental results were analyzed to study the wear behavior in the contact system between the rubber seal and stainless steel. The wear behavior of a material is represented by the depth of wear and the intensity of wear. Therefore, a procedure for calculating wear is carried out for all experiments to determine wear depth and wear intensity as follows:

First, the mass loss related to the sliding distance is calculated. Second, the depth of wear and the intensity of wear are determined based on the loss of mass, the contact area of the sample, and the density of rubber material. Third, an approximation function is determined by a curve fit for the test results.

Table 5.2: Mass of the samples before the test

Sample	M1	M2	M3	M4	M15	M16	M17	M18
Mass [g]	28.553	29.877	30.359	30.057	29.141	28.718	28.741	28.883
Sample	M19	M36	M37	M38	M39	M40	M41	M42
Mass [g]	28.104	31.326	30.074	29.625	31.115	29.586	31.646	31.465

Influence of sliding velocity and normal force on wear characteristics of rubber seals under dry contact conditions

Many scientists have studied the abrasive properties of rubber in contact with other materials under dry contact conditions by experimental analyzes. Pihtili and Tosun [73] showed that applied load and sliding speed play a significant role in

polymers and composites' wear behavior. They also showed that normal force has more effect on the wear than the sliding velocity for composites.

In this section, the wear characteristics between rubber seals and stainless steel under dry contact conditions are investigated and shown. The effect of normal force on wear characteristics is investigated with the normal forces 45 N and 90 N, sliding velocity 50 mm/s and 100 mm/s and sliding distance 60 m, 120 m, 180 m, 240 m, 300 m, and 360 m, respectively.

The wear rate was determined by the following equation

$$W_s = \frac{\Delta m}{\Delta S} \tag{5.4}$$

where Δm is the mass loss, and S the sliding distance. The weight loss was measured with an electronic balance of 0.001 g accurancy. The results of the mass loss are shown in Table 5.3 and Table 5.4

Table 5.3: Mean of mass loss of the rubber seal in dry contact, sliding velocity of 50 mm/s and 100 mm/s, normal force of 45 N and 95 N

Sliding distance S [m]	**Mean of mass loss Δm [g]**			
	$F_n = 45$ N, V = 50 mm/s	$F_n = 45$ N, V = 100 mm/s	$F_n = 95$ N, V = 50 mm/s	$F_n = 95$ N, V = 100 mm/s
60	0.027	0.060	0.031	0.116
120	0.043	0.112	0.061	0.218
180	0.066	0.163	0.084	0.280
240	0.087	0.203	0.113	0.328
300	0.111	0.237	0.137	0.376

The mass loss versus sliding distance and wear rate versus sliding distance for rubber seal in dry contact environments are shown in Figure 5.7 and Figure 5.8 for normal forces of 45 N and 90 N.

Table 5.4: Mean of mass loss of the rubber seal corresponding to sliding distance ΔS in dry contact, sliding velocity of 50 mm/s and 100 mm/s, normal force of 45 N and 95 N

Sliding distance ΔS =60 m (from…to…)	**Mean of mass loss Δm [g]**			
	F_n = 45 N, V = 50 mm/s	F_n = 45 N, V = 100 mm/s	F_n = 95 N, V = 50 mm/s	F_n = 95 N, V = 100 mm/s
0 - 60	0.027	0.060	0.031	0.116
60 - 120	0.016	0.051	0.030	0.102
120 - 180	0.023	0.051	0.023	0.062
180 - 240	0.021	0.040	0.029	0.048
240 - 300	0.024	0.034	0.024	0.048

With normal force higher, the mass loss is higher. If sliding distance increases, the mass loss increases. The rate of wear at the beginning is higher. Then, the wear rate decreases with the distance of sliding. After 180 m the different of wear rate is quite small between both normal forces. With a significant sliding distance, the wear amount is almost linearly to the sliding distance and the wear rate gets constant to the sliding distance.

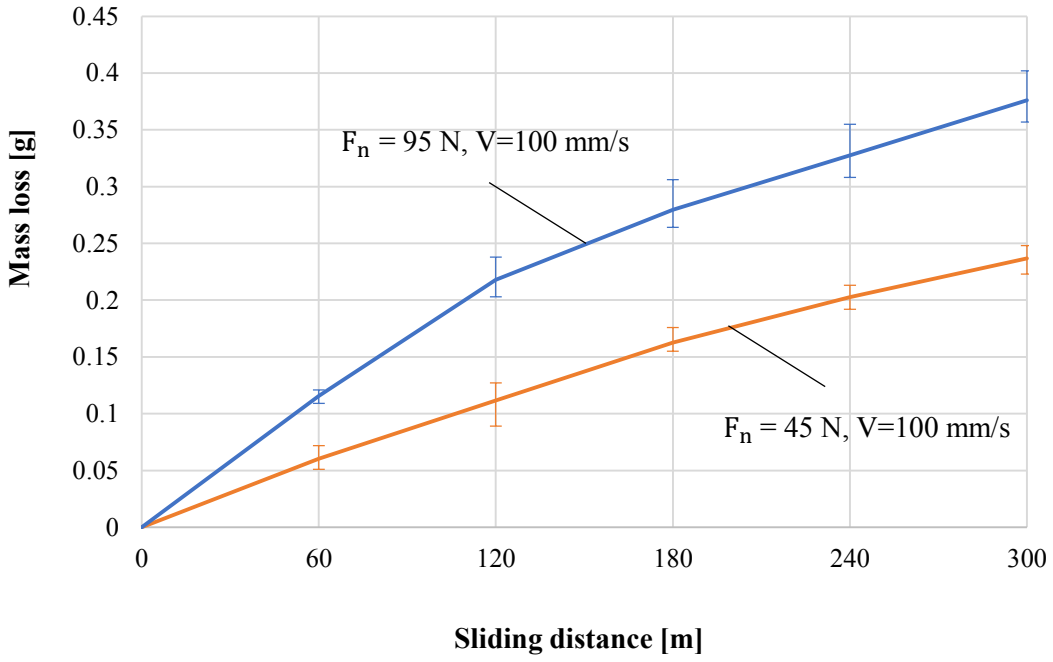

Figure 5.7: Effect of normal force on wear in dry contact

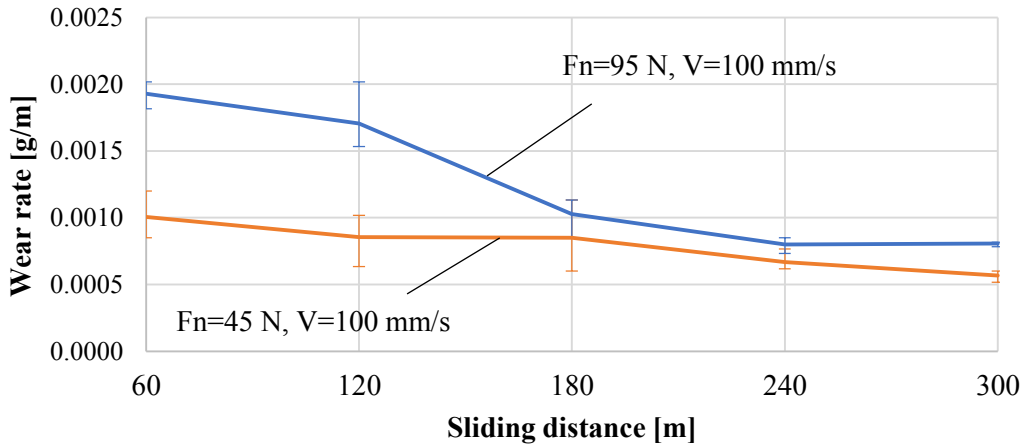

Figure 5.8: Effect of normal force on wear rate in dry contact

Besides the influence of normal force, the sliding speed also affects the wear properties of the rubber seal. If increasing the sliding speed in dry contact conditions, the coefficient of friction increases. At the sliding speed of 100 mm/s, the mass loss is higher than at the sliding speed of 50 mm/s. The wear rate also increases if the sliding velocity increases. The mass loss and the wear rate are shown in Figure 5.9 and Figure 5.10

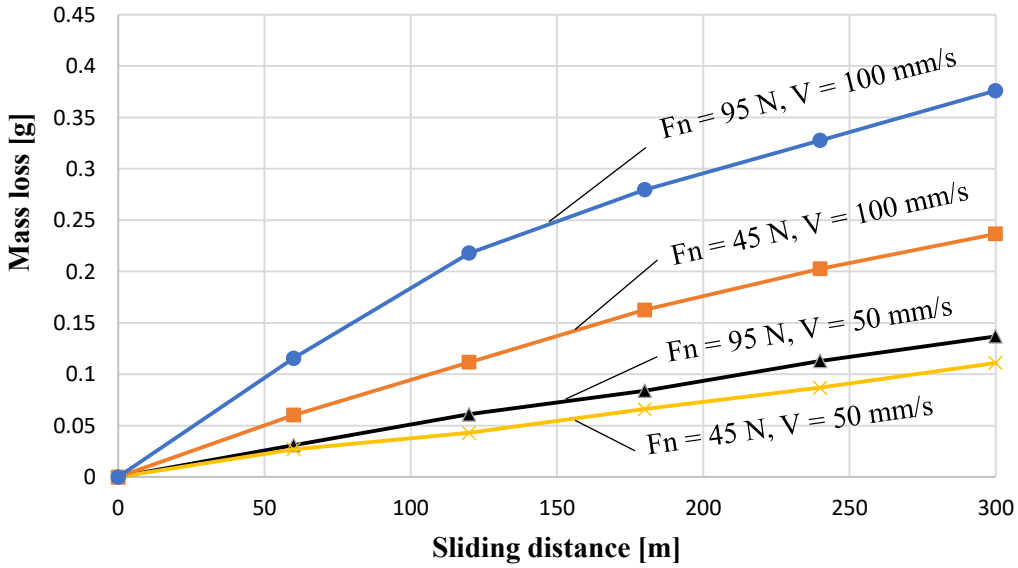

Figure 5.9: Effect of sliding velocity on wear in dry contact

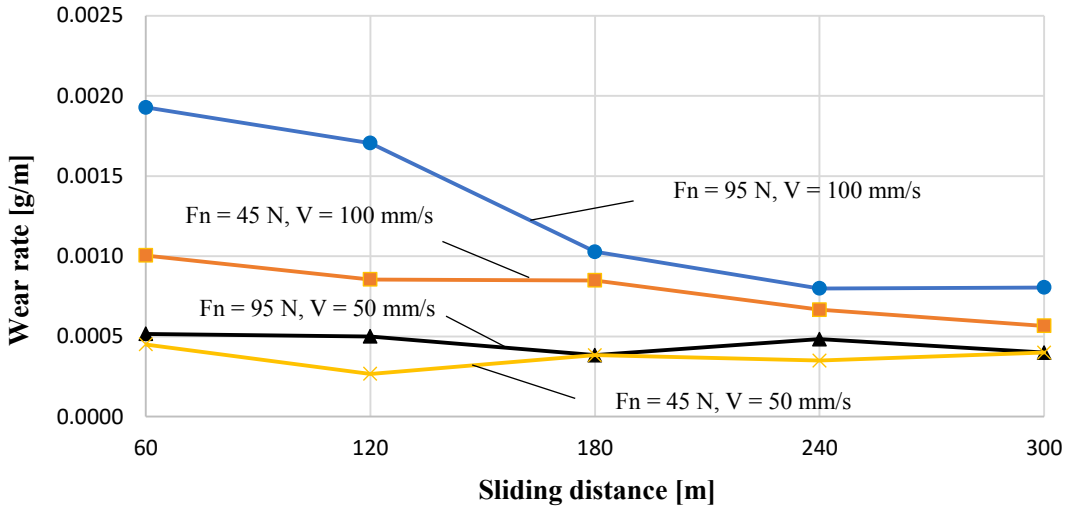

Figure 5.10: Effect of sliding velocity on wear rate in dry contact

The mass loss increases with increasing the sliding distance. However, at the sliding velocity of 100 mm/s, the wear rate decreases with the sliding distance. Initially, the rough surface of the contact layer contains undulating peaks, and the contact only happens at peaks. Thus the surface is fast to wear during sliding contact between the two surfaces. After the undulating peaks are abraded, the wear rate is smaller.

Observing Figure 5.9 and Figure 5.10, it is found that the amount of wear is higher if the sliding velocity is large and the normal force is large. The wear rate is also higher if the normal force is large and the sliding velocity is large. If the sliding distance increases, the wear rate at high sliding velocity and greater normal force will decrease more than the wear rate value at small velocity and normal force. The more the sliding distance increases, the more the wear is linear to the sliding distance so that the wear rate tends to reach a constant value.

Influence of contact conditions on wear characteristics of the rubber seal

The lubricant has an important role in the friction process and significant effects on the contact process's properties. The friction coefficient during dry contact is much higher than the friction coefficient in contact with the lubricant. In experiments with water and mud in the contact area, water and mud act as lubricants. The results of the mass loss are shown in Table 5.5.

If there is water in the contact area, it will reduce friction and transfer heat away from the contact between the two contact partners. Also, worn materials are transported out of the contact area under the effect of water flow, reducing the scratching and adhesive contact of the contact surface, thus limiting the wear process.

In an environment containing mud, the coefficient of friction is low. Also, the amount of wear is relatively small compared to dry contact. The mixture of mud contains water and particles of different sizes and hardness. During friction, this mixture will enter the central area between the two contact surfaces. Therefore, one part will slip, and one part will have the phenomenon of rolling on small particles of the mud (friction in three-body contact) [11]. The amount of wear increases almost linearly with the sliding distance, see Fig 5.11.

Table 5.5: The mass loss of the rubber seal in mud contact and in water contact, normal force 95 N and sliding velocity 100 mm/s

Sliding distance S [m]	Mass loss Δm [g], contact in mud			Mass loss Δm [g], contact in water		
	M15	M16	M17	M18	M19	M42
8640	0.058	0.063	0.053	0.025	0.027	0.017
17280	0.112	0.115	0.119	0.044	0.052	0.037
25920	0.163	0.162	0.172	0.069	0.073	0.056
34560	0.215	0.205	0.227	0.095	0.091	0.083

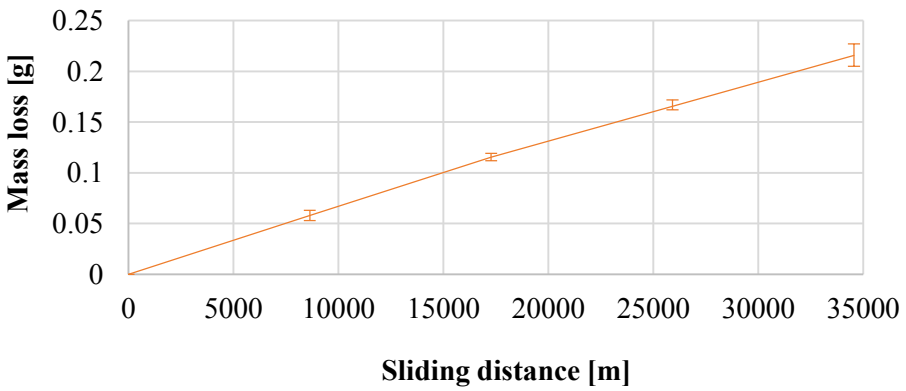

Figure 5.11: The mass loss in mud contact condition with F_n = 95 N, V = 100 mm/s

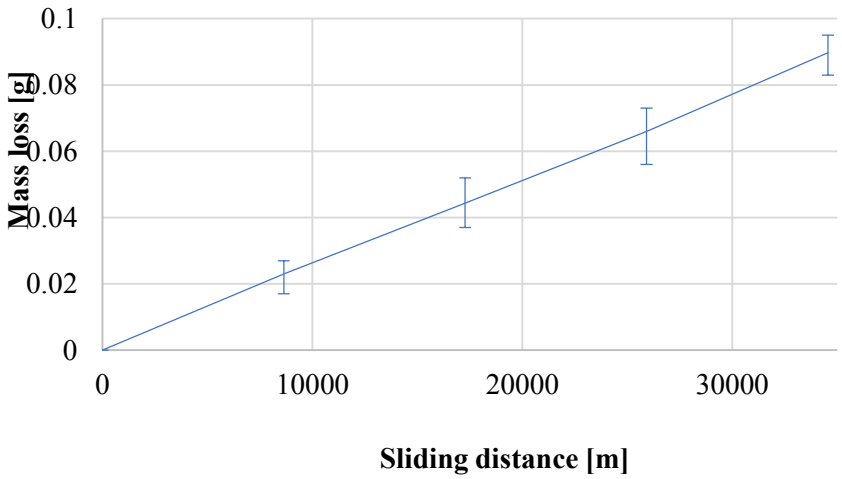

Figure 5.12: The mass loss in water contact condition with F_n = 95 N, V = 100 mm/s

Like contact in mud, contact in water also exhibits much smaller wear and wear rate than dry contact. The amount of wear of samples in water contact is illustrated in Figure 5.12.

The sample's wear properties are compared for contact in water with contact in mud, see Figure.5.13. It can be seen that contact in the mud condition has higher wear than contact in the water condition. Water easily penetrates the contact area between the two surfaces during the contact to remove heat and worm material from the contact area. If the velocity is large enough, a lubricant film is formed between the two surfaces. This limits the abrasion process of the contact surface. Therefore, the amount of wear during contact is relatively small. The amount of wear and wear rate in the mud contact is greater than in the water contact. In both water and mud contact conditions, the wear rate decreases with increasing sliding distance. The wear rates of samples in water and mud contact are shown in Figure 5.14. The wear rate of samples in both water contact and mud contact decreases with increasing sliding distance.

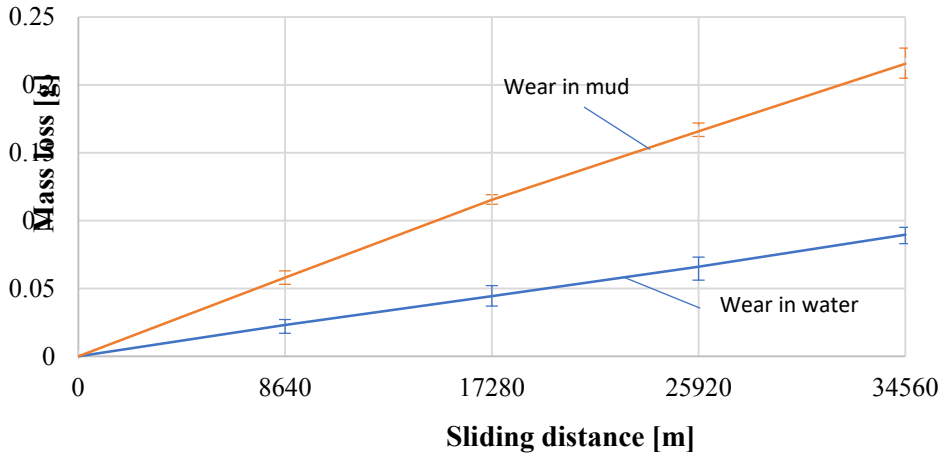

Figure 5.13: Comparing the mass loss between contact in mud and contact in water with F_n = 95 N, V = 100 mm/s

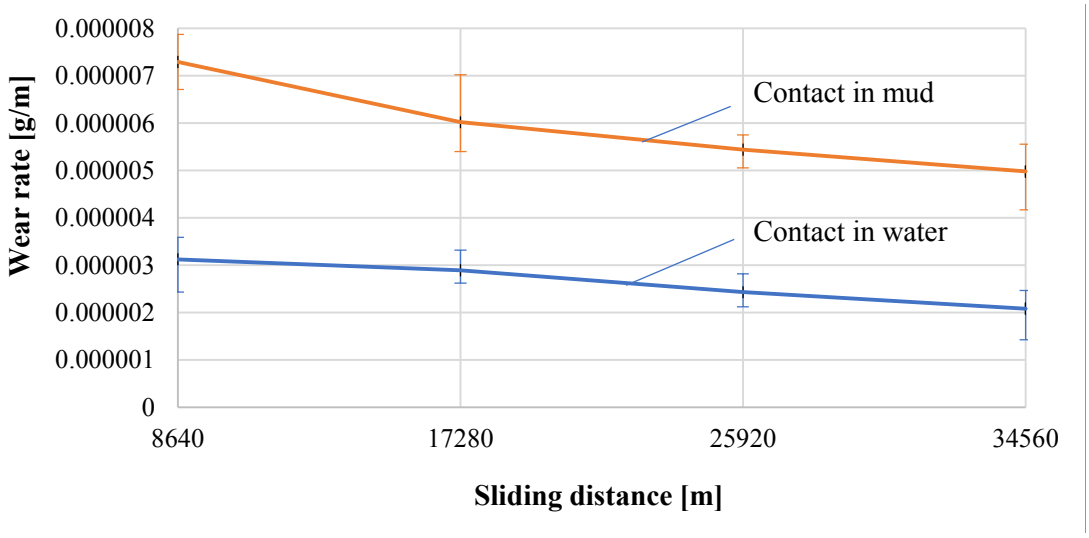

Figure 5.14: Wear rate in mud contact and in water contact conditions with F_n = 95 N, V = 100 mm/s

5.2.3 Contact area

The contact area is measured on the measuring system by recording the photos of contact area between the rubber seals and the transparent acrylic plate. The different images are collected corresponding to the normal and friction forces. The contact area is calculated by image processing software and presented in Table 5.6 and Table 5.7.

Table 5.6: The results of contact area with friction force F_r = 0 N

Normal force F_n (N)	28	35	42	49	56	63	70
Contact area A (mm^2)	107	129	150	167	180	199	210
Contact pressure $\sigma = F_n/A$ (/N/mm^2)	0.26	0.27	0.28	0.29	0.31	0.32	0.33

Table 5.7: The results of contact area with normal force F_n = 70 N

Friction force F_r (N)	0	8	16	24	32	40	48
Contact area A (mm^2)	210	206	209	217	218	221	214
Contact pressure $\sigma = F_n/A$ (/N/mm^2)	0.33	0.34	0.33	0.32	0.32	0.32	0.33

Depending on the shape of the specimen, the contact area between the sample and the plate may constant, change little or greate with increasing normal force. For this experiment the contact area of the rubber seals are measured with cylindrical rubber seals. Therefore, if the normal forces increase, the contact area increases accordingly. For small normal loads, the contact between the sample and the plate is almost a straight line. Because the rubber sample is elastic and easily deformed, the sample deforms and changes the contact area when the force attacks the sample. The change in the contact area is illustrated in Figure 5.15 and Figure 5.16.

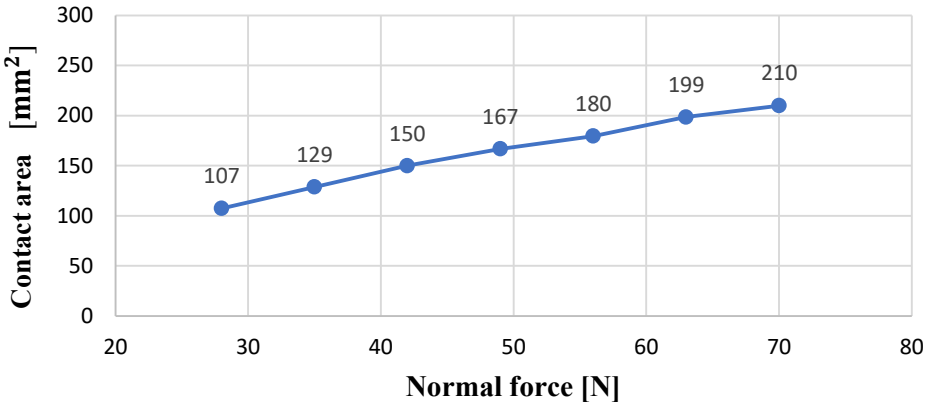

Figure 5.15: Effect of the normal force on the contact area with friction force $F_r = 0$ N

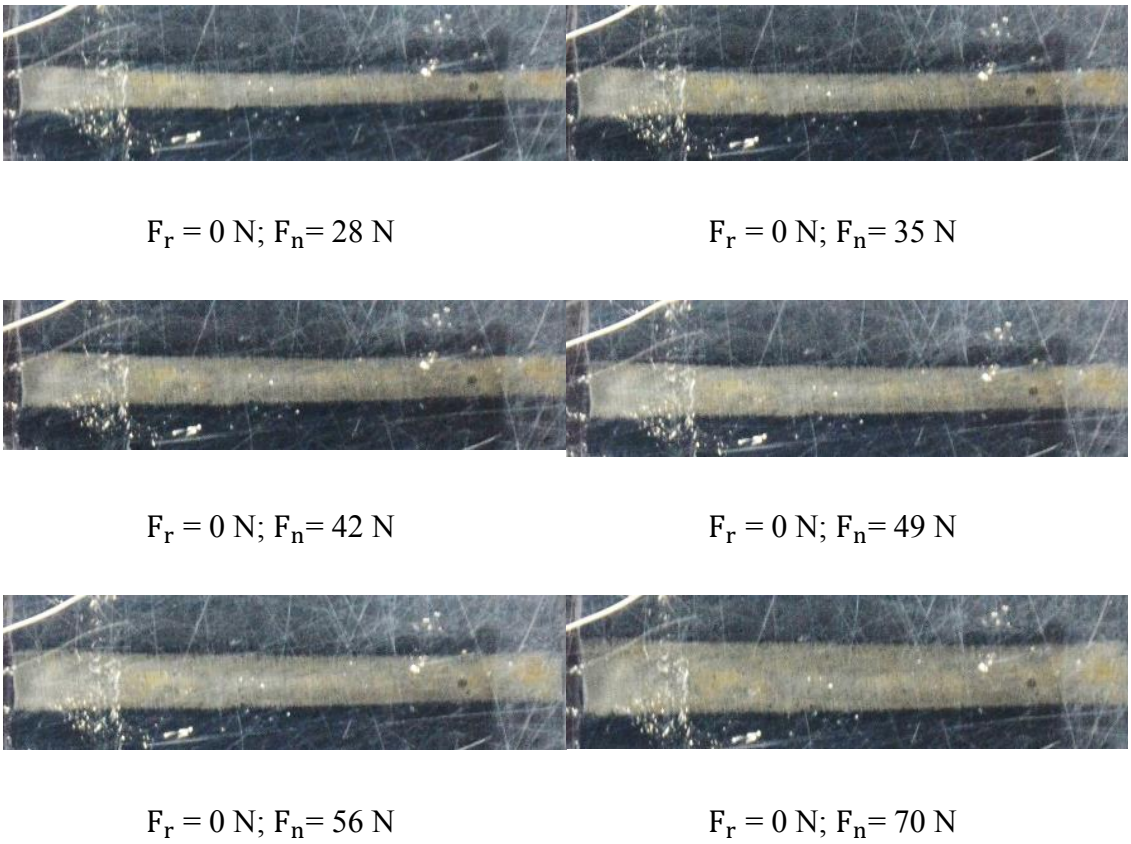

$F_r = 0$ N; $F_n = 28$ N

$F_r = 0$ N; $F_n = 35$ N

$F_r = 0$ N; $F_n = 42$ N

$F_r = 0$ N; $F_n = 49$ N

$F_r = 0$ N; $F_n = 56$ N

$F_r = 0$ N; $F_n = 70$ N

Figure 5.16: Photo of contact area depending on the normal force

The mean contact pressure is calculated by

$$\sigma = \frac{F_n}{A} \tag{5.5}$$

where F_n is the normal force and A the contact area.

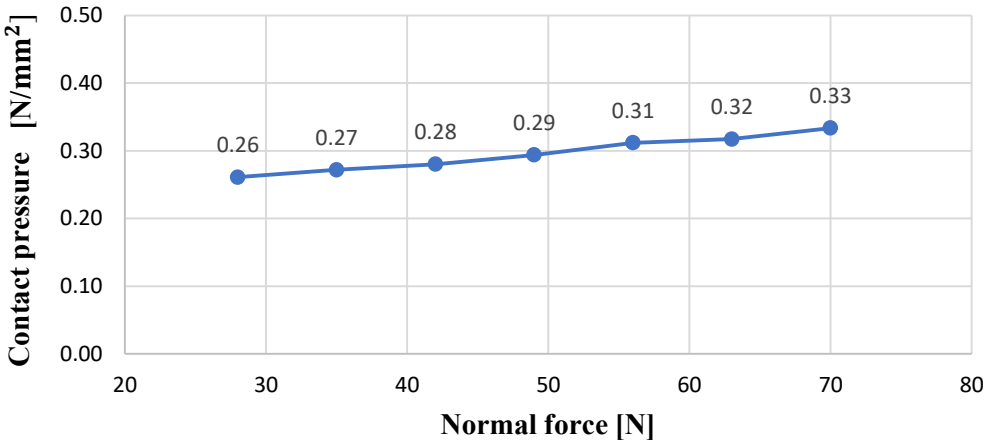

Figure 5.17: Effect of the normal force on the contact pressure with friction force F_r = 0 N

For geometries with a constant contact area, the contact pressure is linearly proportional to the normal force. When the contact area is not constant, the contact pressure is a function of normal force and contact area:

$$\sigma = f(F_{n,} A) \tag{5.6}$$

The contact pressure dependency on the normal force and the contact area is shown in Figure 5.17. It can be seen that with increasing normal force, the contact area increase and the contact pressure also increase. Thus, with increasing normal force, the contact area also increases, but the increase rate of the contact area is lower than the increased rate of the normal force. Therefore, the contact pressure increases with increasing normal force.

The contact area depends mainly on the normal force. The effect of the friction force on the contact area is small. With the change of the friction force, the contact area changes only a relatively small amount. In the experiments, the friction force increase from 0 to 48 N, the contact area varies only from 206 mm^2 to 221 mm^2, see Figure 5.18. This change is small.

If the normal force is constant (70 N) and the contact area changes small, the contact stress changes a small amount inversely to the contact area, see Figure 5.19.

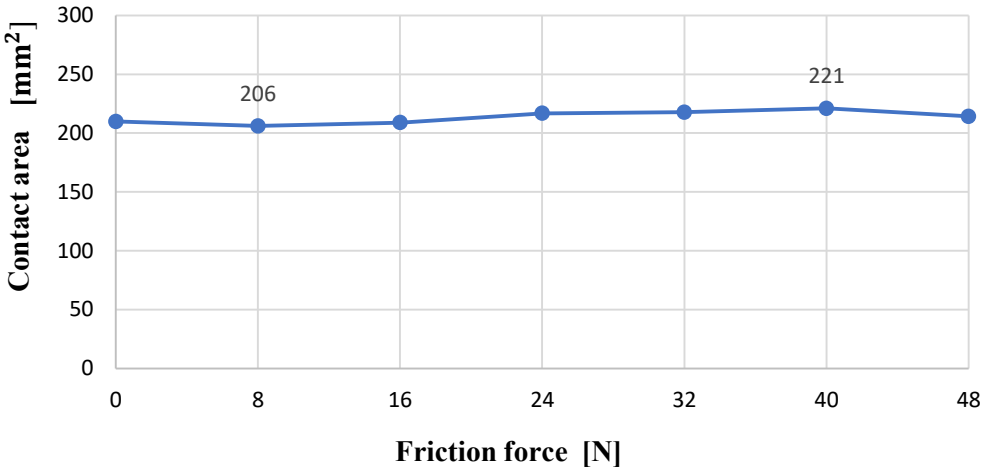

Figure 5.18: Effect of the friction force on the contact area, normal force F_n =70 N

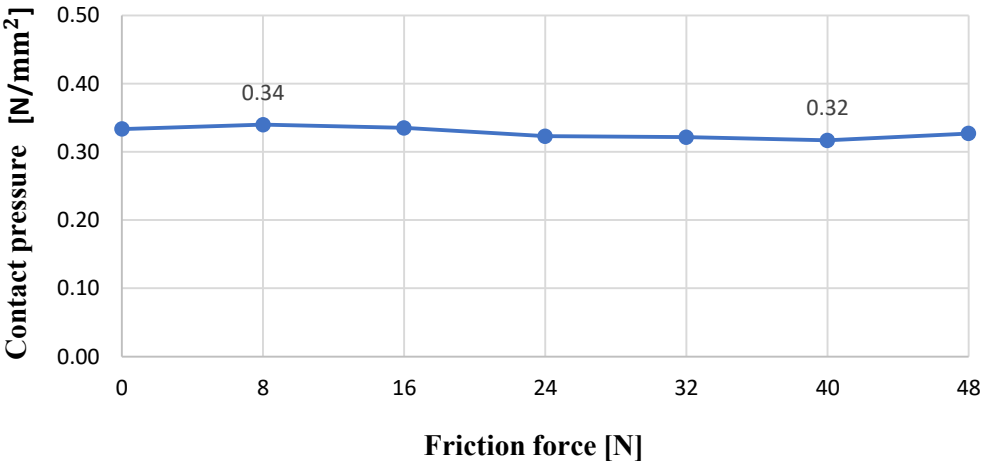

Figure 5.19: Effect of the friction force on the contact pressure, normal force F_n = 70 N

However, the shape and width of the contact area vary depending on the friction force. If the friction force increases, the contact area's width gets larger at the beginning and smaller at the end of the contact. The greater the friction, the lager is the difference in width of contact between the beginning position and the end position. This can be seen clearly in Figure 5.20. In fotos of contact area, friction force has direction from beginning to end of contact (from right side).

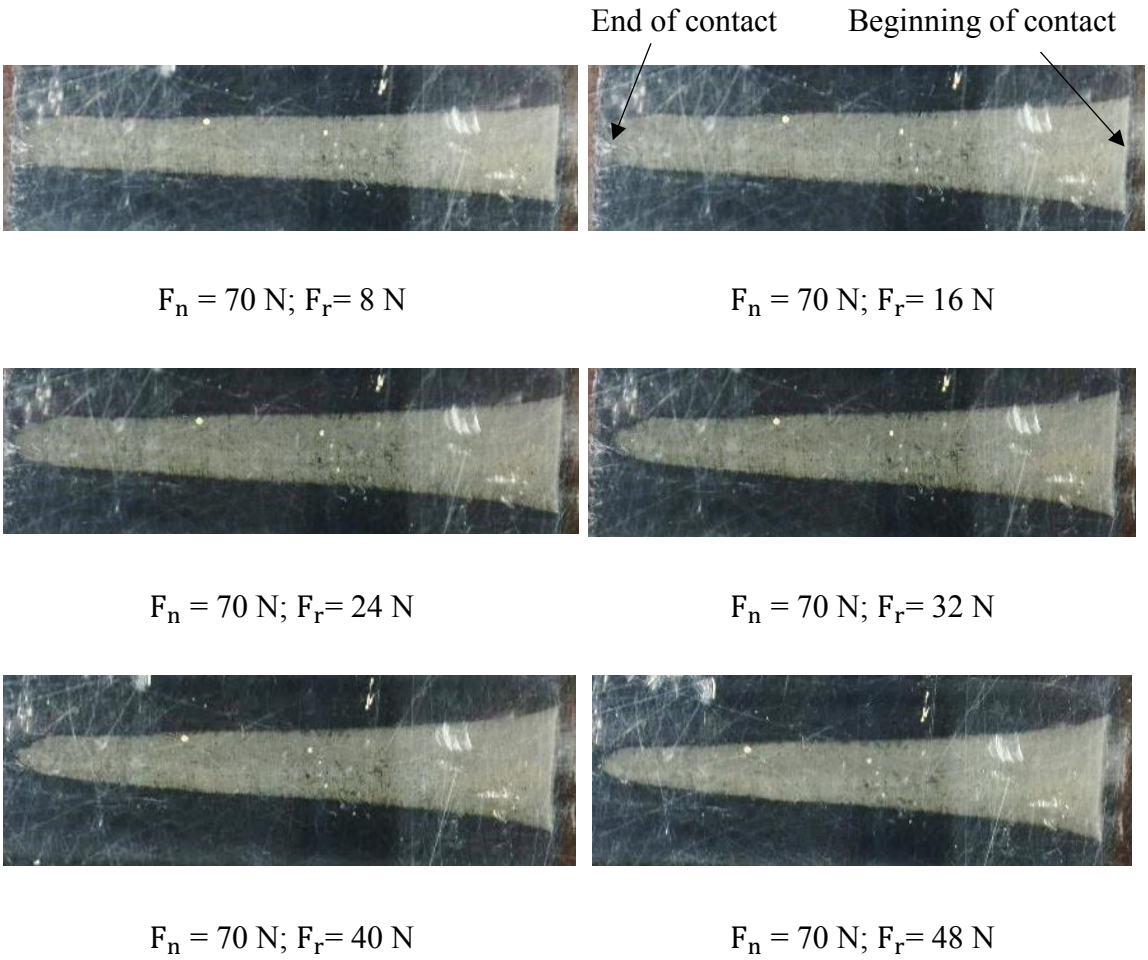

Figure 5.20: The contact area depending on the friction force

By analyzing images and graphs, it is generally recognized that the contact area's value varies depending on the normal force and is almost independent of friction force. However, the normal force and friction force also effect on deformations of the sample. The friction force does not change the contact area's value, but it changes the contact area's shape. The change of the contact area's shape is related to the pressure distribution on the contact surface and will be explained in section 6.3.3.

5.3 Summary

In this chapter, experiments are used to analyze the friction and wear properties of rubber seals under different contact environments, normal forces and sliding velocities. The deformation characteristics are also presented by changes in the contact area's shape and value for different applied forces.

In dry contact conditions:

With increasing normal force, the coefficient of friction between rubber seal and steel plate decreases. If the sliding velocity increases, the coefficient of friction increases.

The greater the normal force, the greater the amount of wear, and the higher the wear rate. If the sliding velocity increases, the amount of wear and wear rate increases. The wear rate decreases with increasing sliding distance.

In water and mud contact conditions:

Water and mud have the effect of significantly reducing the friction coefficient of the seal in contact with steel. The coefficient of friction between the rubber seal and steel plate is much smaller than in dry contact.

With increasing normal force, the coefficient of friction between the rubber seal and steel plate decreases. If the sliding velocity increases, the coefficient of friction decreases slightly.

Combined with the low coefficient of friction in water and mud, the amount of wear and wear rate of the seal is very small compared to dry contact. Comparing mud contact and water contact, the amount of wear and wear rate in wet contact conditions is smaller than in mud contact. If the sliding distance increases, wear rate decreases in both mud contact and wet contact.

The value of the contact area depends directly on the normal force. The friction force does not effect on the contact area, but it changes the shape of contact area.

CHAPTER 6

Simulation

6.1 Contact model

The geometry of the contact model

The simulation is performed on Hyperwork software. The contact model is drawn on SolidWorks software with the same parameters as the rubber seals and steel plate models, see Figure 3.2 and 3.9. The geometry of the contact model is built and imported into the Hyperwork software. The material is modelled linear elastic. The degrees of freedom of the rubber seals sample and the steel disc are limited in the motion binding them. The sample is attached to the holder in the experiment and can only move up and down vertically. In the model, there is a degree of freedom in the z-direction (DOF-03). The steel disc has a rotating motion that produces a relative sliding velocity between the two contact surfaces. The disc has a degree of freedom in the model that rotates around the z-axis (DOF-06), see Figure 6.1.

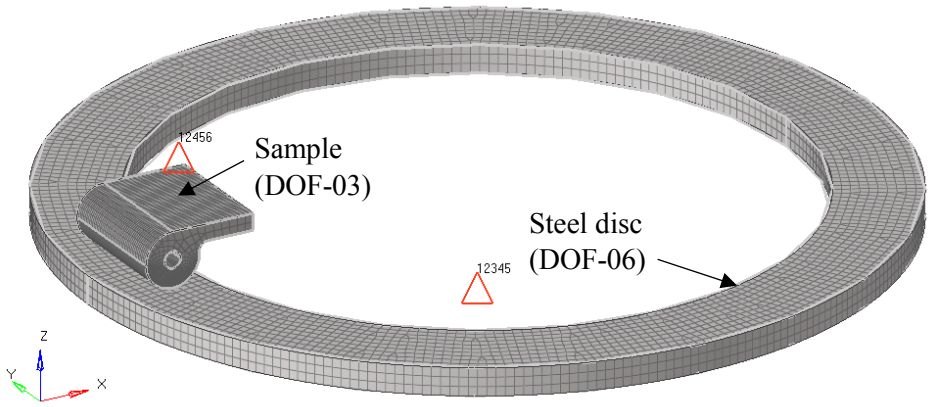

Figure 6.1: Geometry of the contact model

The input parameters of the model are shown in Table 3.6.

The different steps of the simulation process are:

- Import geometry of the contact model, see Figure 6.1

- Determine the finite element model mesh for the model. The element of the model are solid elements. Model mesh is different at other components and positions (rubber seals sample has 52394 nodes, 49950 elements and steel disc has 12100 nodes, 8355 elements). In the beginning, create a mesh using the fewest, reasonable number of elements and

analyze the model. Then recreate the mesh with a denser element distribution at the contact position, re-analyze it, and compare the results to those of the previous mesh, see Figure 6.2 a.

- Determine the contact surfaces

- Create load collectors and assign parameters

- The force application process follows two steps:

    Step 1: Assign the normal force to the sample elements

    Step 2: Assign rotation to disc elements

- Analysis of the finite element friction process.

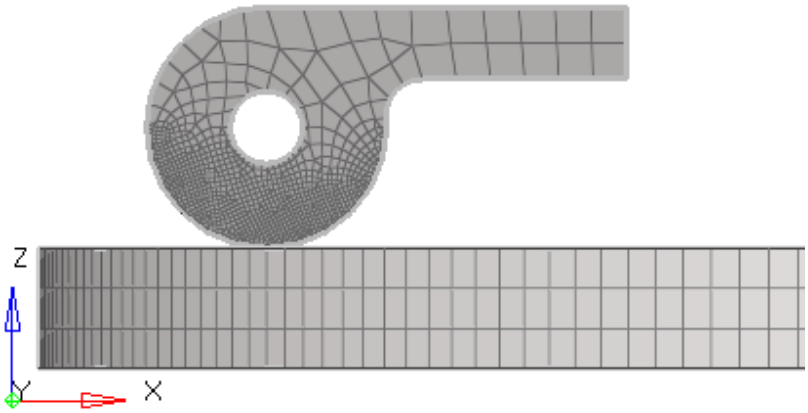

a) The rubber seals sample and steel disc

b) The model of long sample L_l = 480 mm

Figure 6.2: Finite element mesh of the model

Comparison between the short sample and long sample

The simulation model with a long sample L_l = 480 mm, see Figure 6.2 b, are simulated to see deformation tendency (via contact shape, contact area and contact pressure) compared to the experiment's sample (short sample L = 40 mm). The simulation results are presented in Section 6.2.

6.2 Results of simulation

6.2.1 Comparison of the long sample and the short sample

In the following the simulation model with short sample L = 40 mm is compared to long sample L_l = 480 mm.

The long sample L_l = 480 mm, D_s = 20 mm and d_s = 6 mm were used in contact simulation to see the deformation tendency of contact geometry and contact area compared to the short experiment's sample. The contact shape and contact area are shown in Figure 6.4 and Figure 6.5. The results are shown with line load F_n/L = 70 N / 40 mm =840 N/ 480 mm = 1.75 N/mm (short sample F_n = 70 N and long sample F_n = 840 N), friction force F_r= 0 and F_r=40 N.

The beginning, middle and the end of the contact responding to applied load were determined and shown in Figure 6.3

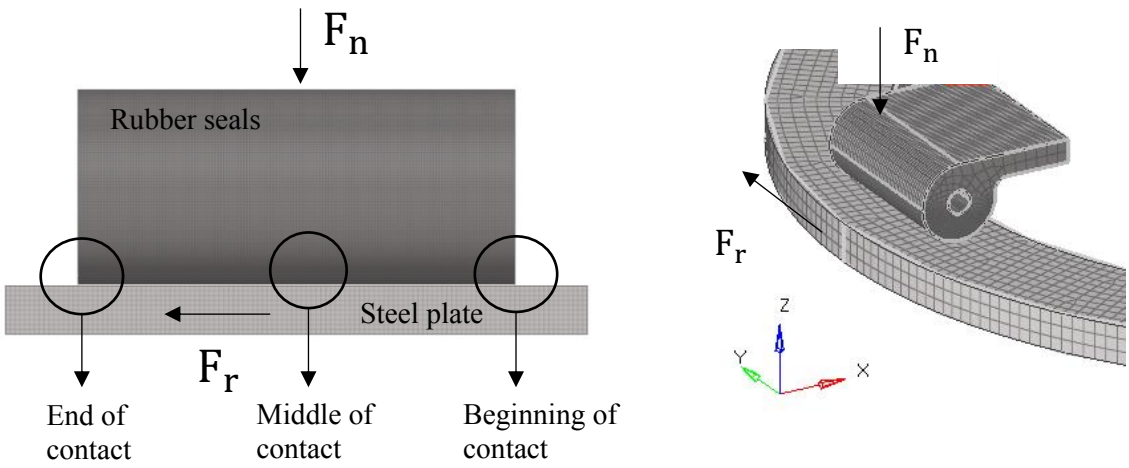

Figure 6.3: Direction of applied load and the contact

The contact area in the simulations is calculated and presented in Table 6.1. Figure 6.4 and 6.5 show that the contact area's geometry is the same for the long and short samples at the beginning and end positions. The ratio of the contact area to the length of the sample (A / L) of the long sample (L_l= 480 mm) and the short sample (L = 40 mm) and the contact area width at the middle position are not much different. (1.8% ÷ 3.9%).

Thus, it can be seen that the tendency to change the contact area depending on the friction force and normal force of the long and short samples is similar.

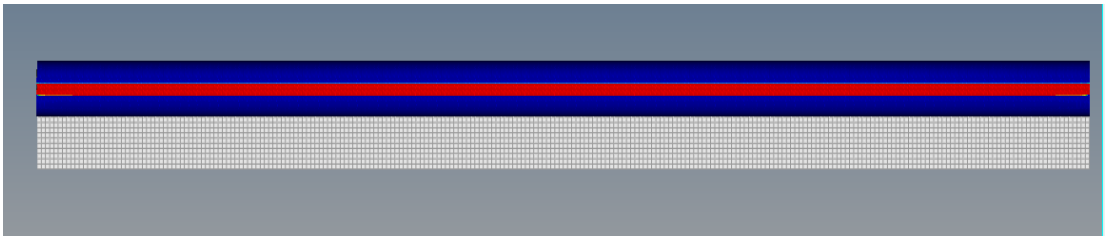

a)

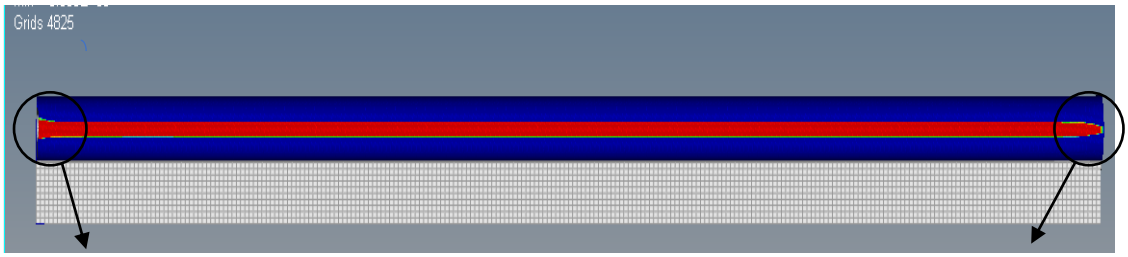

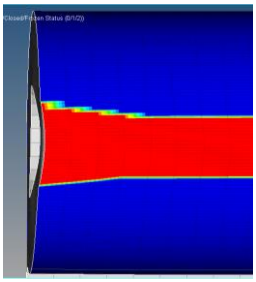

The beginning of contact sample

The end of contact sample

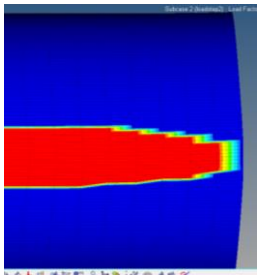

b)

Figure 6.4: a) Contact area of the long sample: a) normal force F_n =840 N, friction force F_r = 0; b) normal force F_n =840 N, friction force F_r = 40 N

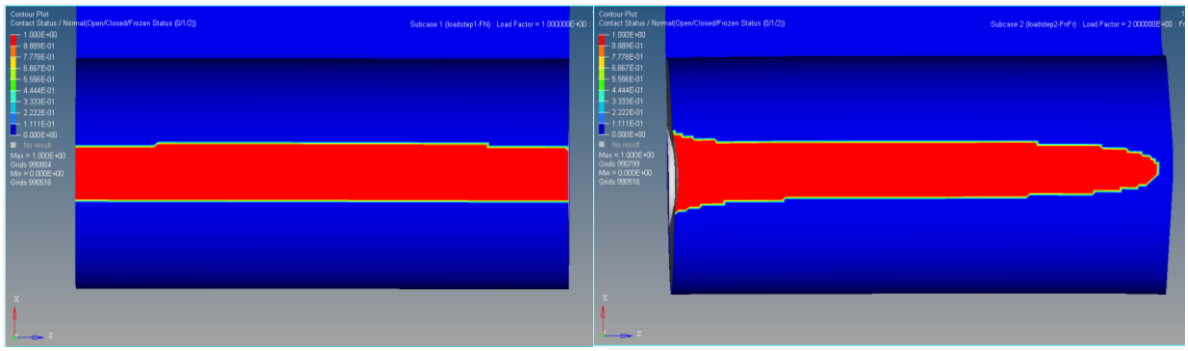

a) b)

Figure 6.5: Contact area of the short sample: a) normal force F_n =70 N, friction force F_r = 0; b) normal force F_n =70 N, friction force F_r = 40 N

The long and short samples have the same contact area geometry and the tendency to change is the same when having the same line load. Therefore, simulations and experiments are performed with samples of length L = 40 mm for the convenience of research and calculation.

Table 6.1: The contact area in the simulations

Type of sample	F_n/L =1.75 N/mm, F_r = 0 N			F_n/L =1.75 N/mm, F_r = 40 N		
	Contact area A [mm^2]	A/L [mm^2/m]	Width of contact area [mm]	Contact area A [mm^2]	A/L [mm^2/m]	Width of contact area [mm]
Short sample	206.2	5.16	5.14	201.9	5.05	5.03
Long sample	2380.4	4.96	4.96	2375.3	4.95	4.94

6.2.2 Contact area

The Hertzian contact problem between cylinder surfaces forms the basic foundation and is widely employed in the study of contact mechanics.

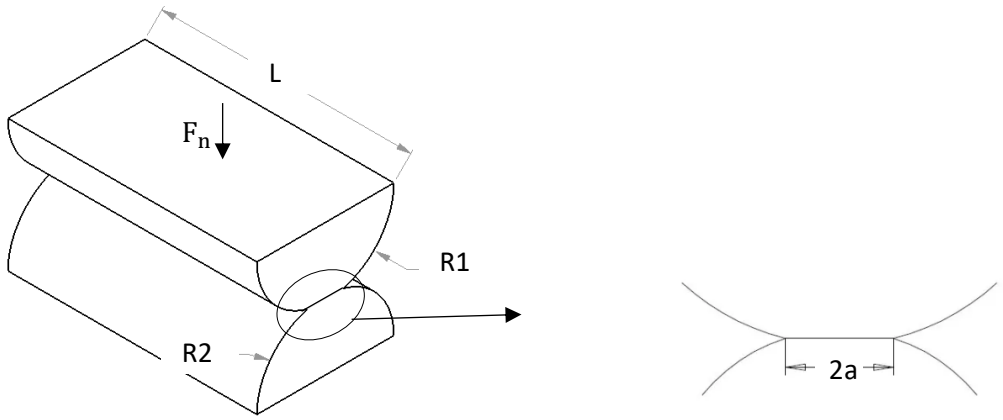

Figure 6.6: Contact between two cylinders

Contact area half-width a is given by:

$$a = 2\sqrt{\frac{F_n R}{\pi L E}} \tag{6.1}$$

where F_n is normal force and L is length of the sample. The relative curvature R and the equivalent elastic modulus of the contacting bodies E is defined by:

$$R = \left(\frac{1}{R_1} + \frac{1}{R_2}\right)^{-1} \quad (6.2); \qquad E = \left(\frac{1-\nu_1^2}{E_1} + \frac{1-\nu_2^2}{E_2}\right)^{-1} \tag{6.3}$$

where R_1, R_2 are radius, E_1, E_2 are the elastic modulus and ν_1, ν_2 the Poisson's ratios associated with each cylinder.

Thus, the contact area will change depending on the normal force for each pair of contacts with known dimensions and material properties.

Simulation of the contact

The contact area is simulated and calculated in two cases: First, friction force F_r = 0, normal force F_n changes with values of 18 N, 33 N, 57 N and 70 N, see Figure 6.7 a). Second, the normal force F_n = 70 N, friction force changes with values of 10 N, 19 N, 33 N and 40 N, see Figure 6.7 b). Contact area values of these cases are shown in Table 6.2.

If the normal force increases, the contact area's width increases, but the shape does not change much. If the friction force increases, the contact area's width is almost unchanged but mainly the shapes at the beginning and end positions change.

Table 6.2: Contact area values of different cases

F_r and F_n	Contact area [mm^2]	F_r and F_n [N]	Contact area [mm^2]
F_r = 0, F_n = 18 N	88,2	F_n = 70 N, F_r = 10 N	205.8
F_r = 0, F_n = 33 N	130,7	F_n = 70 N, F_r = 19 N	204.7
F_r = 0, F_n = 57 N	168.6	F_n = 70 N, F_r = 33 N	203.4
F_r = 0, F_n = 70 N	206.2	F_n = 70 N, F_r = 40 N	201.9

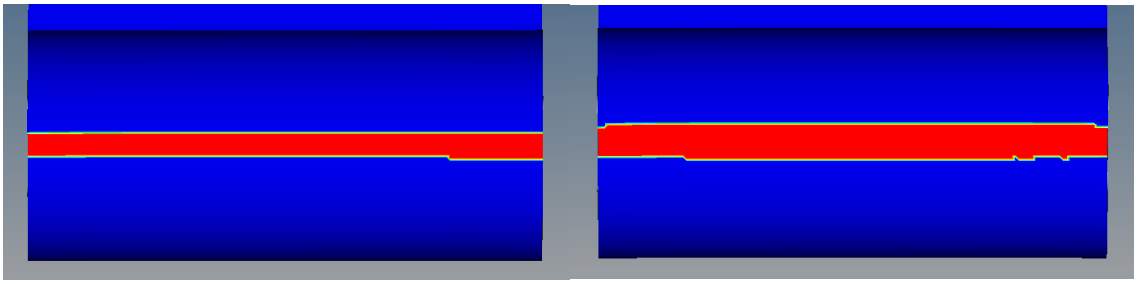

F_n = 18 N and F_r = 0 F_n = 33 N and F_r = 0

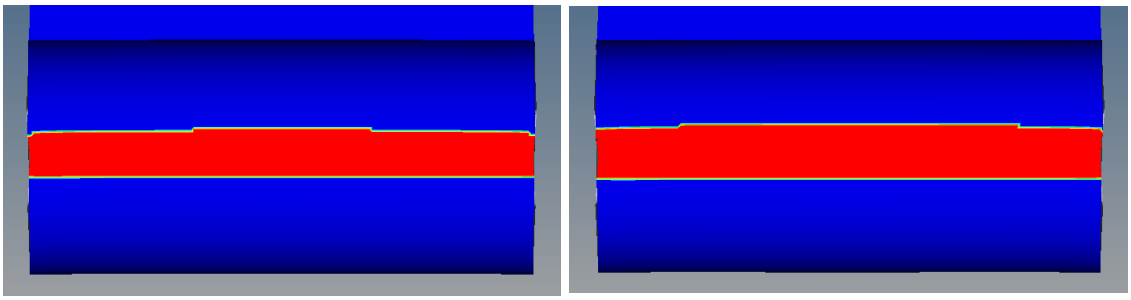

F_n = 57 N and F_r = 0 F_n = 70 N and F_r = 0

a) friction force F_r = 0 and various normal forces F_n

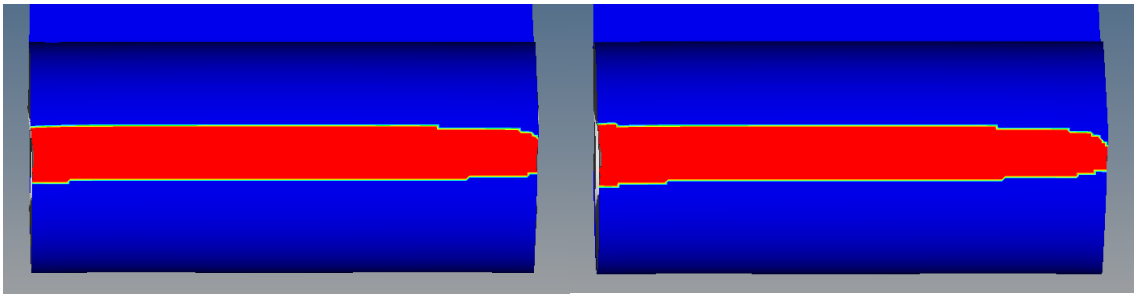

F_r = 10 N and F_n = 70 N F_r = 19 N and F_n = 70 N

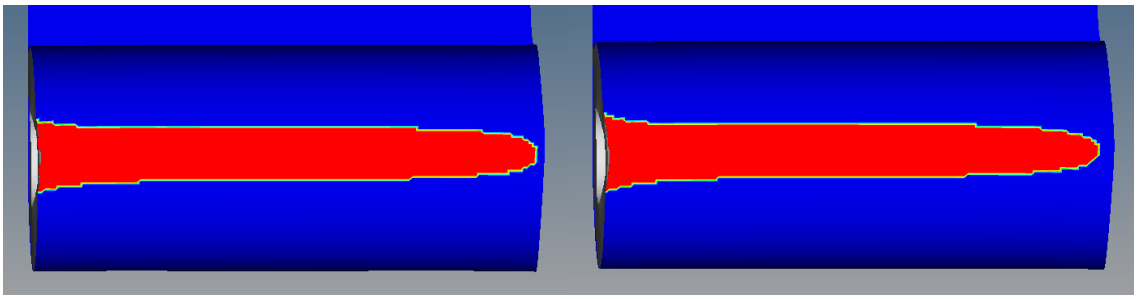

F_r = 33 N and F_n = 70 N F_r = 40 N and F_n = 70 N

b) normal force F_n = 70 N and various friction forces F_r

Figure 6.7: The contact area of simulation

Figure 6.8 shows the variation of the contact area according to normal force and friction force. The contact area varies in a non-linearly manner with the normal force. If the normal force is constant, the contact area value changes very small when the friction force changes. However, the geometry of the contact area changes with the friction force. The greater the friction force, the greater is the difference at the beginning and end positions.

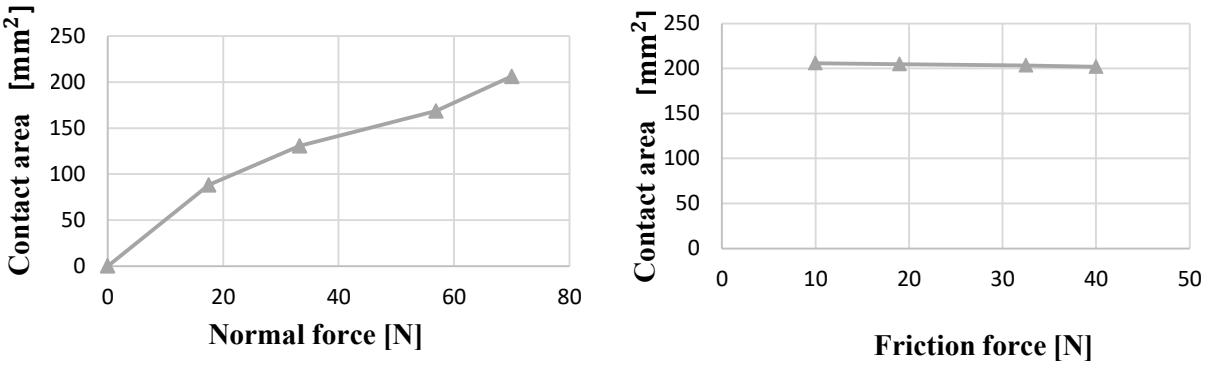

a) $F_r = 0$, F_n changed b) $F_n = 70$ N and F_r changed

Figure 6.8: Influence of normal force and friction force on the contact area

Comparison of experimental and simulated contact area results

The results of experimental and simulated contact areas are presented in Tables 5.6, 5.7 and 6.1. A comparison of the contact area between simulation and experiment is shown in Figure 6.9 and Figure 6.10.

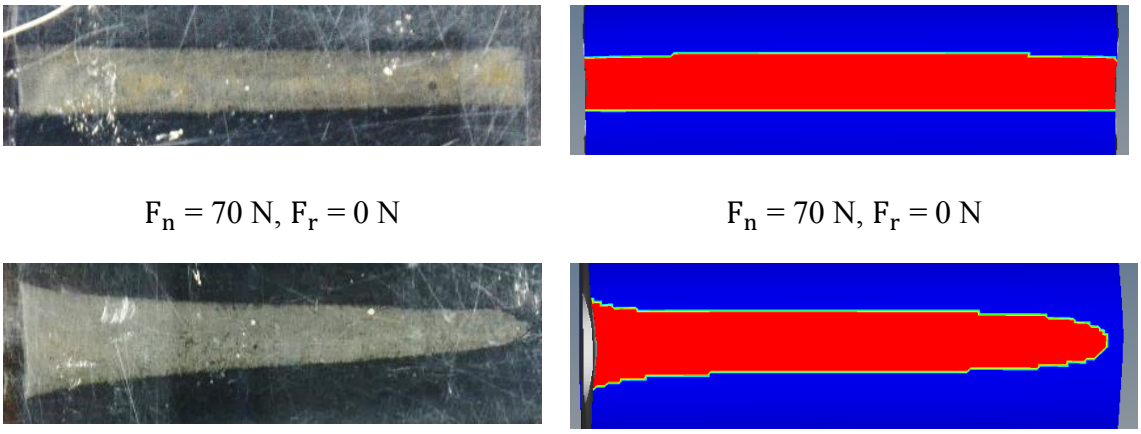

$F_n = 70$ N, $F_r = 0$ N $F_n = 70$ N, $F_r = 0$ N

$F_n = 70$ N, $F_r = 40$ N $F_n = 70$ N, $F_r = 40$ N

a) Results of experiments b) Results of simulations

Figure 6.9: Geometry of the contact area of simulation and experiment contact

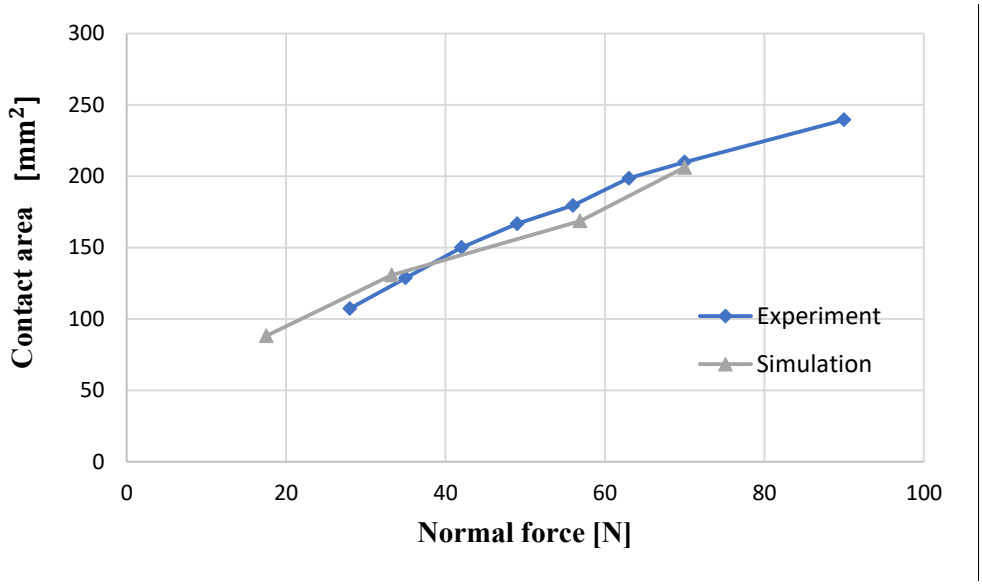

a)

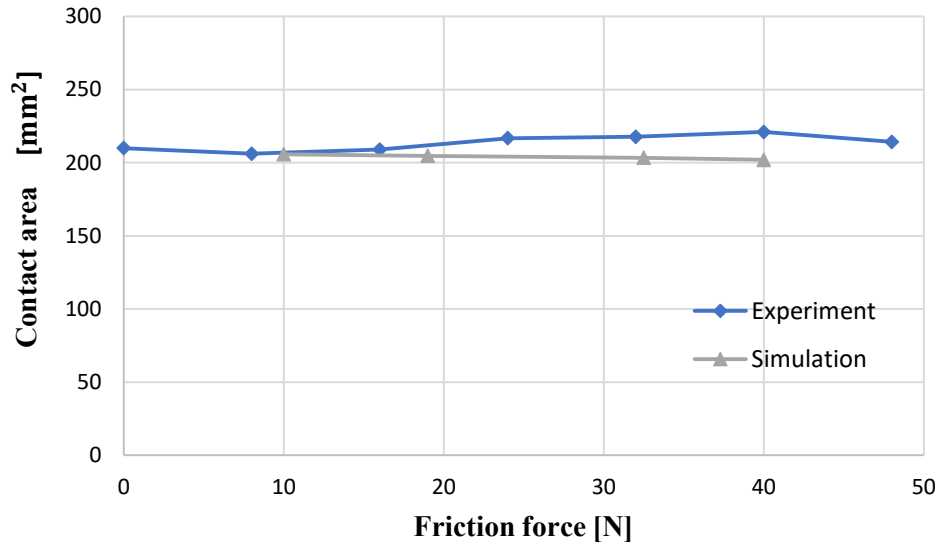

b)

Figure 6.10: Contact area of simulation and experiment: a) F_r = 0, F_n changed b) F_n = 70 N and F_r changed

The shape of the contact area between simulation and experiment behaves similarly when the applied force is changed. The contact area's values have only a small deviation (Fig 6.10 b) for F_n = 70 N and F_r = 40 N of maximum 8.6%. The maximum deviation of contact areas for F_r = 0 and F_n = 56 N (Fig 6.10 a) is 6.1%. This validates the simulation model.

6.2.3 Contact pressure

Results of simulated contact pressure along contact surface and cross-section are presented in Figures 6.11 and 6.12.

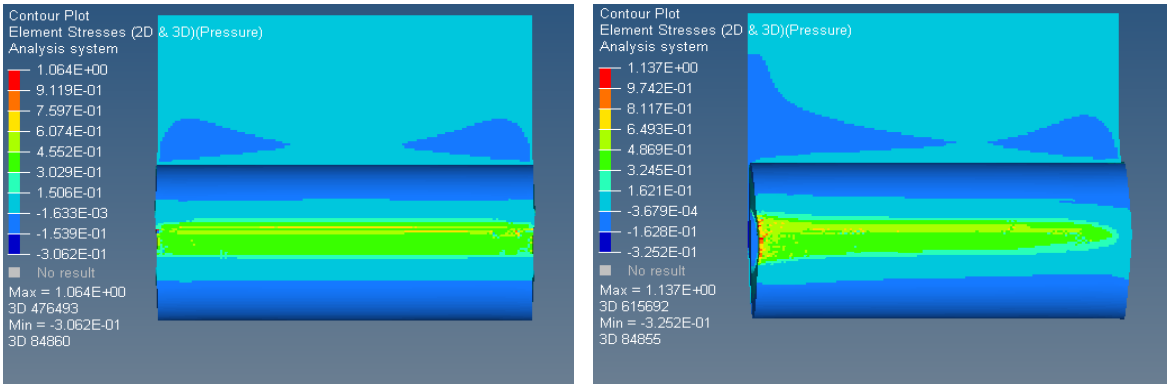

a) b)

Figure 6.11: Pressure distribution of the short sample: a) Normal force F_n =70 N, friction force F_r = 0; b) normal force F_n =70 N, friction force F_r = 40 N

In the longitudinal direction of the sample, the contact pressure is distributed according to the contact area**.**

According to the sample's cross-section, the pressure forces are greatest in the middle part of the contact area and gradually decrease to the sides. The internal pressure stresses also appear concentrated on the left and right edges of the sample's inside diameter. These are also two positions of large deformation under the effect of the normal force.

If the friction force is zero (Fig 6.12 a), the pressure difference between the ends and the middle of the sample is small. If friction force is applied (Fig 6.12 b), the pressure is concentrated mainly on the contact surface at the starting position of contact. At the end of the contact area, the pressure decreases. In the end, the internal pressure stresses increase at the point of contact between the sample and the sample clamp.

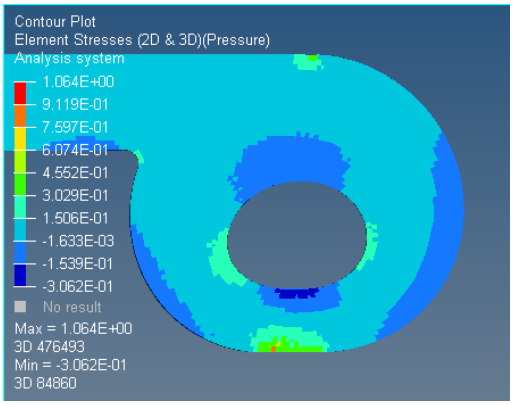

The end of the sample

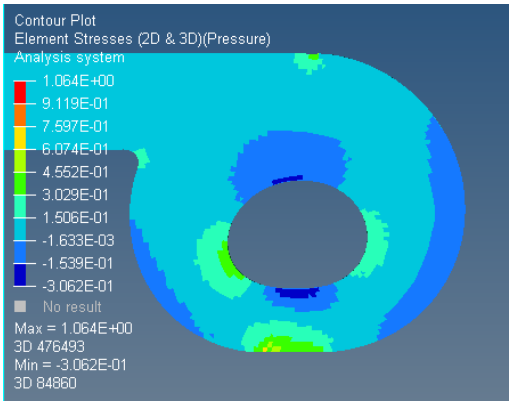

The middle of the sample

a)

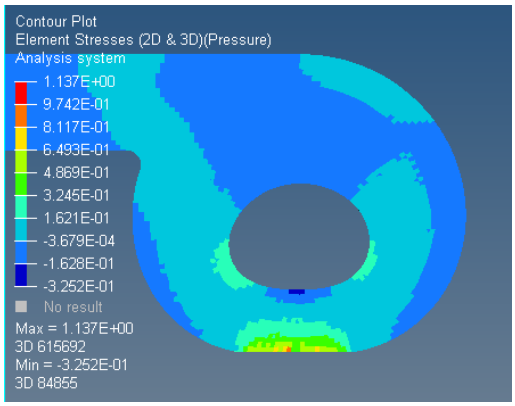

The beginning

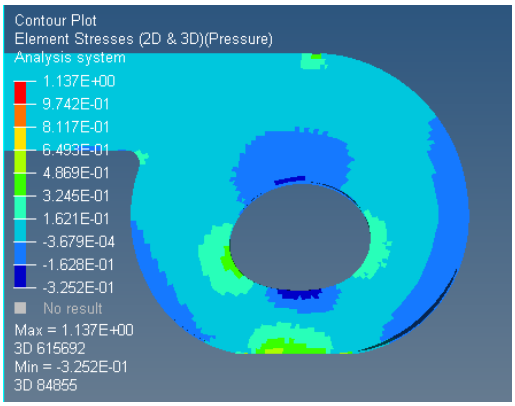

The middle

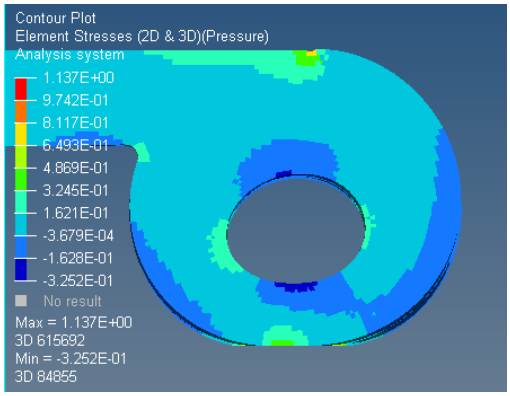

The end

b)

Figure 6.12: Pressure distribution on cross-section, a) normal force F_n =70 N, friction force F_r = 0; b) normal force F_n =70 N, friction force F_r = 40 N

6.3 Wear equation

In the research scope, wear properties are defined as a function depending on normal force, velocity, sliding distance and contact conditions [74]. The following equation shows the influence of parameters on the wear amount:

$$\Delta m = f(F_n, V, S, E_n) \tag{6.4}$$

where Δm is mass loss, F_n normal force, V velocity, S sliding distance and E_n contact condition.

6.3.1 Wear equation in dry contact

The experiment based equation is constructed from experimental data. The experimental data are presented in Table 6.3.

Table 6.3: Mass loss from the experiment in dry contact, Δm [g]

Sliding distance S [m]	Mass loss Δm [g]			
	V = 50 mm/s F_n = 45 N	V = 50 mm/s F_n = 95 N	V = 100 mm/s F_n = 45 N	V = 100 mm/s F_n = 95 N
60	0.027	0.031	0.060	0.116
120	0.043	0.061	0.112	0.218
180	0.066	0.084	0.163	0.280
240	0.087	0.113	0.203	0.328
300	0.111	0.137	0.237	0.376

Variation of sliding distance with constant normal force and velocity

The mass loss is a function depending on sliding distance and is calculated by follow equation

$$\Delta m = f(S) = k_s S^c \tag{6.5}$$

where k_s is the factor of wear depending on sliding velocity and c is the exponent.

The factors and exponents of equation 6.5 are calculated from experimental data and are shown in Table 6.4.

Table 6.4: Factor and exponents of equation (6.5)

Factor	V = 50 mm/s F_n = 45 N	V = 50 mm/s F_n = 95 N	V = 100 mm/s F_n = 45 N	V = 100 mm/s F_n = 95 N
k_s	0.000538	0.000737	0.00216	0.00766
c	0.932	0.917	0.825	0.686

When normal force and velocity are constant,

If velocity is 50 mm/s and normal force is 45 N, mass loss:

$$\Delta m = 0.000538\ S^{0.932} \tag{6.6}$$

If velocity is 50 mm/s and normal force is 95 N, mass loss:

$$\Delta m = 0.000737\ S^{0.917} \tag{6.7}$$

If velocity is 100 mm/s and normal force is 45 N, mass loss:

$$\Delta m = 0.00216\ S^{0.825} \tag{6.8}$$

If velocity is 100 mm/s and normal force is 95 N, mass loss:

$$\Delta m = 0.00766\ S^{0.686} \tag{6.9}$$

Table 6.5: The mass loss is calculated by experiment based equation (6.6 - 6.9), Δm [g]

Sliding distance S [m]	Mass loss Δm [g]			
	V = 50 mm/s F_n = 45 N	V = 50 mm/s F_n = 95 N	V = 100 mm/s F_n = 45 N	V = 100 mm/s F_n = 95 N
60	0.0244	0.0314	0.0633	0.1268
120	0.0465	0.0593	0.1121	0.2040
180	0.0679	0.0860	0.1566	0.2694
240	0.0887	0.1119	0.1986	0.3282
300	0.1093	0.1373	0.2387	0.3824

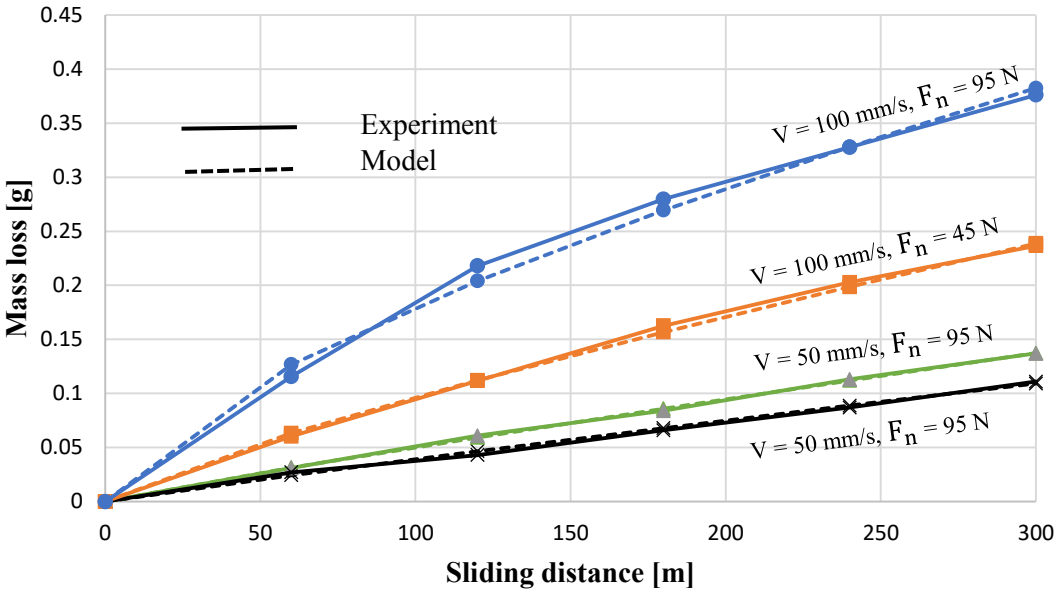

Figure 6.13: Model with the variable of sliding distance

The comparison of mass loss between experiment and modeling is shown in Figure 6.13. It is found that the experiment based formula's results are close to the experimental results when considering the sliding distance's effect on mass loss. For the different values of sliding velocity and normal force, the error is different. However, the errors are small.

Variation of normal force, velocity and sliding distance

The mass loss is a function depending on normal force, sliding velocity and sliding distance. The mass loss is calculated by follow equation [74].

$$\Delta m = f(F_n, V, S) = k_w F_n^a V^b S^c \quad (6.10)$$

where k_w is the factor of wear, F_n normal force, V velocity, S sliding velocity and a, b, c are exponents corresponding to F_n, V and S.

The factors are calculated from experimental data: $k_w = 3.38 * 10^{-7}$, a = 0.536, b = 1.46 and c = 0.84.

The mass loss is calculated follow equation

$$\Delta m = 3.38 * 10^{-7} F_n^{0.536} V^{1.46} S^{0.84} \quad (6.11)$$

Table 6.6. The mass loss is calculated by experiment based equation (6.11), Δm [g]

Sliding distance S [m]	Mass loss Δm [g]			
	V = 50 mm/s F_n = 45 N	V = 50 mm/s F_n = 95 N	V = 100 mm/s F_n = 45 N	V = 100 mm/s F_n = 95 N
60	0.0247	0.0368	0.0679	0.1014
120	0.0441	0.0659	0.1215	0.1814
180	0.0620	0.0926	0.1708	0.2550
240	0.0790	0.1179	0.2175	0.3247
300	0.0953	0.1422	0.2623	0.3916

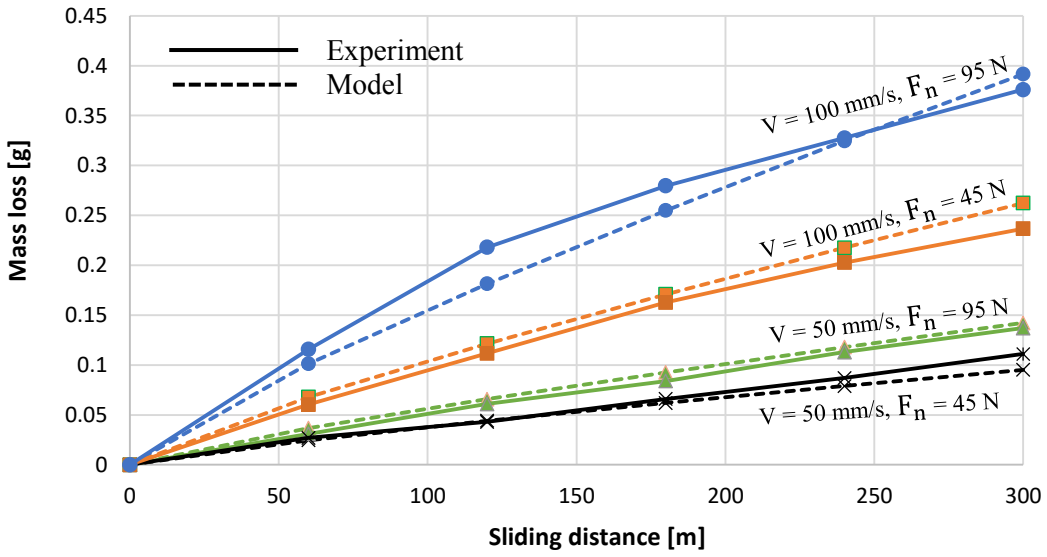

Figure 6.14: Model with the variable of normal force, velocity and sliding distance

Figure 6.14 compares the mass loss from the experiment and calculated from the experiment based formula (6.11) when considering the effects of all three factors, namely sliding velocity, normal force and sliding distance. For different sliding velocities and normal forces, the deviations are different. From the chart, it can be seen, that for the large value of sliding velocity (v = 100 mm/s), the difference between the experimental value and the calculated value is the largest. The difference between the experimental value and the value calculated according to the formula considering three influencing factors is larger than for the formula which only considers one influencing factor.

In dry contact, the coefficient of friction is higher than in mud and water contact, so the wear rate in dry contact is also higher. The wear tests were carried out in all three environments: Dry contact, mud contact and water contact to compare the mass loss. From the experimental results, the formula for calculating the amount of wear on mud contact and water contact is also determined and presented in sections 6.3.2 and 6.3.3.

6.3.2 Wear equation in mud contact

Normal force and velocity are constant, and only sliding distance is various. The mass loss is calculated following equation 6.5. The factors are calculated from experimental data, $k_s = 0.000012$ and $c = 0.938$:

$$\Delta m = k_s S^c = 0.000012\, S^{0.938} \quad . \tag{6.12}$$

Table 6.7: Mass loss from the experiment of three samples M15, M16, M17 in mud contact, Δm [g]

Sliding distance S [m]	Mass loss Δm [g] , V = 100 mm/s, F_n = 95 N		
	M15	M16	M17
0	0	0	0
8640	0.058	0.063	0.053
17280	0.112	0.115	0.119
25920	0.163	0.162	0.172
34560	0.215	0.205	0.227

Table 6.8: Mass loss calculated by experiment based equation (6.12), Δm [g]

Sliding distance S [m]	Mass loss Δm [g] , V = 100 mm/s, F_n = 95 N
0	0.000
8640	0.059
17280	0.113
25920	0.165
34560	0.217

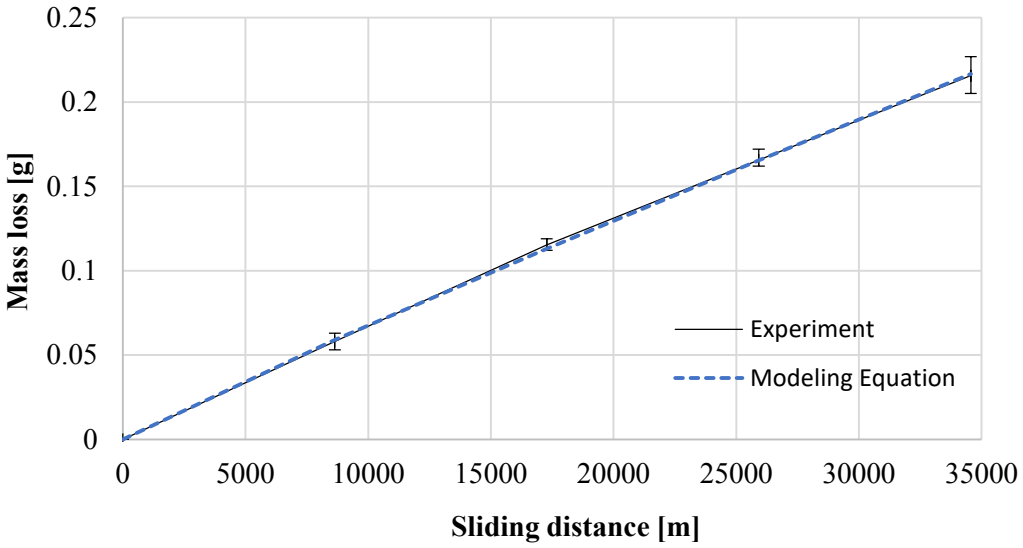

Figure 6.15: Model with the variable of sliding distance in mud contact

With a stable wear behavior in mud contact, the mass loss of different samples is insignificant different. Figure 6.15 shows that the difference between the mass loss from the experimental and the equation is insignificant.

6.3.3 Wear equation in water contact

Table 6.9: Mass loss from the experiment in water contact, Δm [g]

Sliding distance S [m]	Mass loss Δm [g] , V = 100 mm/s, F_n = 95 N		
	M18	M19	M42
0	0	0	0
8640	0.025	0.027	0.017
17280	0.044	0.052	0.037
25920	0.069	0.073	0.056
34560	0.095	0.091	0.083

Normal force and velocity are constant, and only sliding distance is various. The mass loss is calculated with equation (6.5). The factors are calculated from experimental data, k_s = 0.000002 and c =1.0067:

$$\Delta m = k_s S^c = 0.000002\, S^{1.0067} \quad . \tag{6.13}$$

Table 6.10: Mass loss is calculated by experimental equation (6.13), Δm [g]

Sliding distance S [m]	Mass loss Δm [g] , V = 100 mm/s, F_n = 95 N
0	0
8640	0.022
17280	0.045
25920	0.067
34560	0.090

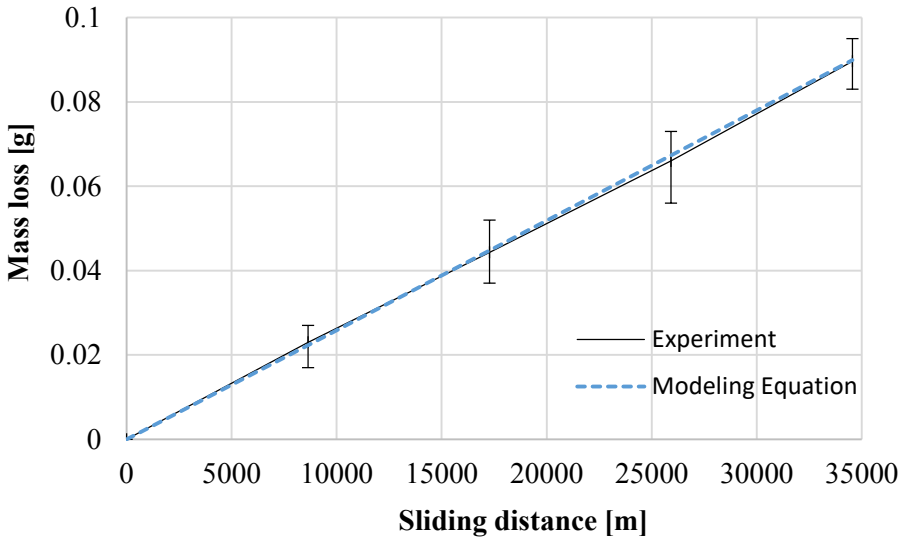

Figure 6.16: Model with the variable of sliding distance in water contact

The mass loss of different samples in water contact are more different than in mud contact. For the same sliding distance, the mass loss in water contact is smaller than in mud contact. The mass loss from the equation is between the values from experimental. The difference between the mass loss from the experimental and the equation is small.

6.4 Summary

In this chapter, the contact process between rubber gaskets and steel is simulated with software. The simulation results show that the pressure change and the contact area depend on the applied force.

The contact area's value depends directly on the normal force but depends very little on the friction force. Friction forces affect the change in the shape of a contact area and contact pressure distribution.

The pressure is greatest in the middle part of the contact area and gradually decreases to the sides.

The internal pressure stresses also appear concentrated on the left and right edges of the sample's inside diameter. These are also two positions of large deformation under the effect of the normal force.

If the friction force is zero, the pressure difference between the ends and the middle of the sample is not much.

If friction force is applied, the pressure is concentrated mainly on the contact surface at the starting position of contact. At the end of the contact area, the pressure decreases. Further, the internal pressure stresses also appear at the point of contact between the sample and the sample clamp.

The formula for calculating the amount of wear in different contact conditions is also built based on the experimental data.

In dry contact, the wear equation is built in dependency of the normal force, velocity and sliding distance. In mud and water contact, the wear equation is built when the sliding distance is varied.

The mass loss in dry contact is much more than both in mud and water contact, see Figure 6.17. Influence of water is smaller than mud on wear. Figure 6.17 also shows that the difference between the mass loss from the experimental and the equation is small.

Simulation results and experiment based formulas can be used to calculate and predict the tendency to change some seal properties under different exposure conditions, especially when it is difficult to do experiments.

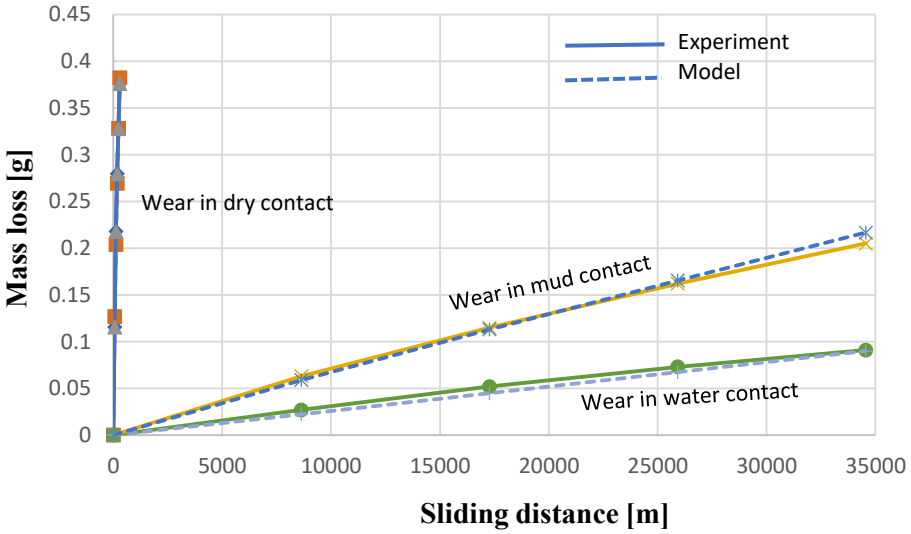

Figure 6.17: Comparision of wear for dry, mud and water contact with F_n = 95 N and V = 100 mm/s

CHAPTER 7

Conclusions and Recommendations

7.1 Summary and conclusion

The theoretical modeling and experimental investigations of friction in rubber-metal contact have been presented in the previous chapters. The main conclusions of the research are summarized in this section.

Experimental investigation with the rubber block

Experimental investigation of frictional properties of the contact between rubber sample and steel plate was performed under different contact conditions (dry contact, wet contact, mud contact), different geometry of sample (half-cylinder, half-sphere), different contact direction (sliding direction axial and sliding direction lateral), different fillet radius, contact angle and rubber material with different sliding velocity and normal force. The dependency of friction coefficient on parameters was determined.

In dry contact, the lateral cylindrical sample has a higher coefficient of friction than the axial cylindrical sample. In the mud contact and water contact, the friction coefficient of the lateral cylindrical sample is smaller than the friction coefficient of the axial cylindrical sample. The friction coefficient of the spherical sample is smaller than the friction coefficient of the cylindrical sample in both dry and wet contact.

The friction coefficients of samples with fillet radius (R = 1 mm and R = 2 mm) and with contact angles (θ_c = 105 °, 120 ° and 135 °) are smaller than the sample´s friction coefficient without fillet radius (R = 0 mm) and contact angles (θ_c = 90 °).

When sliding velocity increases, the friction coefficient decreases in water contact and increases in dry contact. In mud contact, sliding velocity is nearly not effecting on the friction coefficient. The influence of normal force on the friction coefficient is small. But the contact condition is one of the parameters that affect a lot on the friction coefficient. The friction coefficient in mud and water contact is much smaller

than in dry contact. The friction coefficient of different sample materials is different. The friction coefficient of the EPDM rubber is smaller than NR rubber.

Experimental investigation with a hydraulic seal

The friction and wear properties of hydraulic rubber seals under different contact environments, normal forces and sliding velocities were investigated. The deformation characteristics are also expressed through changes in the shape and value of the contact area when changing the applied force.

In dry contact, the friction coefficient decreases if the normal force increases. But the friction coefficient increases if sliding velocity increases. The mass loss in dry contact is much higher than in mud and water contact. With the large sliding velocity and normal force, the mass loss is higher and the wear rate is higher. The wear rate decreases if the sliding distance increases.

The friction coefficient in mud and water contact is much smaller than in dry contact. If the sliding velocity and normal force increase, the coefficient of friction decreases. The mass loss and wear rate in water contact is smaller than in mud contact. If the sliding distance increases, wear rate decreases both in mud and water contact.

The value of the contact area depends directly on the normal force and depends very little on the friction force. But the friction forces affect the shape of a contact area and contact pressure distribution.

Simulation and wear experimental-based equation

The simulation of the contact process between rubber seals and steel plate show that the contact pressure and contact area depend on the applied force. The influence of applied load on the contact area is the same between simulation and experiment. The pressure is concentrated mainly on the contact surface. In addition, stress focus at the left and right edges of the sample's inside diameter. If friction force is applied, the contact pressure and contact area are different between the beginning and the end of the contact.

A formula for calculating the wear in different contact conditions was also built based on the experimental data. In dry contact, the wear equation was built in dependency of the normal force, velocity and sliding distance. In mud and water

contact, the wear equation was built when the sliding distance was varied. The mass loss calculated from the wear equation is close to the experiment.

Simulation and experiment results can be used to calculate and predict the tendency to change some seals properties under different exposure conditions. Applying the results to optimize the designs is possible, improving the life and working efficiency of the hydraulic rubber seals for each application condition.

The main new research results are:

- Identification of influences on friction and wear.
- The large influence of water and mud on friction and much more on wear.
- Friction force influences contact pressure and contact shape.
- Approximation of the influence on wear by an experimental-based analytical formula.

7.2 Recommendations

Although the condition of the experiment is close to the application, the simulation results are in good agreement with experimental results; it is necessary to improve the condition of the experiment. It is recommended that further research should be focused on:

- The contact condition can be a mixture of water, mud and other things (leaves, hyacinth, grass, trash,..).
- Experiment with larger water-hydraulic seals.
- Simulation of the wear process of hydraulic rubber seals.

References

[1] I. V. Kragelsky, V. V. Alisin, Tribology - Lubrication, Friction, and Wear, *Professional Engineering Publishing* (2001).

[2] F. P. Bowden, *The friction and lubrication of solids*. Oxford: Clarendon Pr. (1986).

[3] I. G. Goryacheva, *Contact Mechanics in Tribology*. Springer Netherlands (1998).

[4] G. Fleischer, *Verschleiß und Zuverlässigkeit*. Berlin: Verlag Technik (1980).

[5] P. L Menezes, M. Nosonovsky, S. P. Ingole, S. V. Kailas, M. R. Lovell, *Tribology for Scientists and Engineers*. Springer New York (2013).

[6] J. S McFarlane, D. Tabor, Relation between friction and adhesion, *Proceedings of the Royal Society of London. Series A, Mathematical and Physical Science*, Vol. 202, Issue 1069, 244-253. (1950).

[7] S. Bahadur, Friction of Polymers. In: Wang Q.J., Chung YW. (eds) *Encyclopedia of Tribology*. Springer, Boston, MA (2013).

[8] R. Stribeck, Die Wesentlichen Eigenschaften der Gleit- und Rollenlager, *Z. Verein. Deut. Ing.* 46, 38, 1341-1348 (1902) .

[9] K. Grosch, The relation between the friction and visco-elastic properties of rubber, *Proc. R. Soc. London A* 274, 21-39 (1963).

[10] M. Barquins, A.D. Roberts: "Rubber friction variation with rate and temperature: some new observations" *J. Phys. D 19*, 547 (1986).

[11] H. Czichos, K. H. Habig, Tribologische Systeme. In: *Tribologie-Handbuch*, 8-18. Vieweg+Teubner (2010).

[12] I. Hutchings, M. Gee, E. Santner, Friction and Wear. In: *Springer Handbook of Materials Measurement Methods*, 685-710. Springer Berlin Heidelberg (2006).

[13] V. L. Popov, Contact Mechanics and Friction, *Physical Principles and Applications*. Berlin Heidelberg: Springer Berlin Heidelberg (2010).

[14] E. Rabinowicz, A. Mutis, Effect of abrasive particle size on wear. In: *Wear,* 8, No. 5, pp. 381-390 (1965).

[15] R. G. Bayer, Fundamentals of Wear Failures. In: *ASM Handbook Volume*, 901-905 (2002).

[16] H.Czichos, *Tribologie-Handbuch. Tribometrie, Tribomaterialien, Tribotechnik*. Wiesbaden: Vieweg + Teubner (2010).

[17] A. Misra, I. Finnie, A classification of three-body abrasive wear and design of a new tester. In: *Wear,* 60, No. 1, pp. 111-121 (1980).

[18] T. Mang, K. Bobzin, T. Bartels, *Industrial Tribology: Tribosystems, Friction, Wear and Surface Engineering, Lubrication*. Wiley-VCH (2011).

[19] P. L. Menezes, M. Nosonovsky, S. P. Ingole, S. V. Kailas, M. R. Lovell, *Tribology for Scientists and Engineers*. Springer New York (2013).

[20] B. N. J. Persson, *Sliding friction*: *Physical Principles and Applications*, Springer Verlag, Berlin, Heidelberg, N.Y. (1998).

[21] A. D. Roberts, Lubrication studies of smooth rubber contacts", *The physics of tire traction – Theory and experiment* 179 (1974).

[22] Y. T. Doan, *Experimental Investigation and Wear Simulation of Three-Body Abrasion*, (2014).

[23] A. N. J. Stevenson, I. M. Hutchings, Development of the dry sand/rubber wheel abrasion test. In: *Wear,* 195, No. 1–2, pp. 232-240 (1996).

[24] N. B. Dube, I. M. Hutchings, Influence of particle fracture in the high stress and low-stress abrasive wear of steel. In: *Wear,* 233–235, No. 0, pp. 246-256 (1999).

[25] M. A. Chowdhury, M. K. Khalil, D. M. Nuruzzaman, M. L. Rahaman, The effect of sliding speed and normal load on friction and wear property of Aluminum. In: *International Journal of Mechanical & Mechatronics Engineering IJMME-IJENS,* 11, No. 01 (2011).

[26] Y. T. Doan, K. M. de Payrebrune, M. Kröger, Experimental investigation of three-body abrasive wear with high pressure. In: *GACM Colloquium on Computational Mechanics*. Dresden, Germany (2011).

[27] Y. T. Doan, K. M. de Payrebrune, M. Kröger, Experimental investigation of friction characteristics on three-body abrasion with low applied loads. In: *Tribologie-Fachtagung* 9/1–9/8. Göttingen, Germany (2012).

[28] M. K. A. Hamid, G. W. Stachowiak, S. Syahrullail, Effects of hard particles on friction coefficients and particle embedment in brake system during hard braking. In: *AIP Conference Proceedings,* 1440, No. 1, pp. 905-913 (2012).

[29] G. P. Ostermeyer, Friction and wear of brake systems, Reibung und Verschleiß in Bremssystemen. In: *Forschung im Ingenieurwesen*, 267 – 272 (2001).

[30] E. Berger, *Friction modeling for dynamic system simulation*. Appl. Mech. Rev. 55, 535–577 (2002).

[31] J. H. Dieterich, *Time-dependent friction and the mechanics of stick-slip*. Pure Appl. Geophys. 116, 790–806 (1978).

[32] B. N. J. Persson, *Sliding friction: physical principles and applications*, 2nd edition. Springer, Berlin (2000).

[33] J. Williams, *Engineering tribology*. Oxford University Press, Oxford (1994).

[34] T. Qing, T. Shao, S. Wen, *Micro-friction and adhesion measurements for Si wafer and TiB2 thin film*. Tsinghua Sci. Technol. 12, 261–268 (2007).

[35] Q. Li, T. E. Tullis, D. Goldsby, R. W. Carpick, Frictional aging from interfacial bonding and the origins of rate and state friction. *Nature* 480, 233–236 (2011).

[36] H. Hirabayashi, Y. Kato, H. Ishiwata, "Excessive Abrasion of Mechanical Seals Caused by Salt Solutions," *Proceedings of the Third International Conference on Fluid Sealing*, BHRA, pp. B1-1–B1-15 (1967).

[37] A. Golubiev, V. Gordeev, Investigation of Wear Mechanical Seals in Liquids Containing Abrasive Particles, *Proceedings of the 7th International Conference on Fluid Sealing*, Paper B3, pp. B3-23–B3-32 (1965).

[38] R. Verma, S. Tiwari, V. Gehlot, An Investigation of Abrasive Wear in Rubber Material, *International Journal of Advanced Mechanical Engineering*, ISSN 2250-3234 Volume 4, Number 6, pp. 681-686, (2014).

[39] J. Wu, C. Zhang, Y. Wang & B. Su, Wear Predicted Model of Tread Rubber Based on Experimental and Numerical Method, *The Society for Experimental Mechanics*, (2017).

[40] H. Hertz, *Miscellaneous Papers*, Macmillan, London, 146 (1896).

[41] J. Greenwood, J. B. P. Williamson, Contact of nominally flat surfaces, *Proc. R. Soc. London A* 295, 300 (1966).

[42] F. P Bowden, D. Tabor, *The friction and lubrication of solids*. Oxford University Press, Oxford (1964).

[43] D. Tabor, Tribology - the last 25 years a personal view. *Tribol. Int*. 28, 7–10 (1995).

[44] N. S. Tambe, B. Bhushan, Identifying materials with low friction and adhesion for nanotechnology applications. *Appl. Phys. Lett*. 86, 061906 (2005).

[45] L. Heim, J. Blum, M. Preuss, H. Butt, Adhesion and friction forces between spherical micrometer-sized particles. *Phys. Rev. Lett.* 83, 3328–3331 (1999).

[46] R. Holm, *Electric contacts handbook*. Springer-Verlag, Berlin (1958).

[47] E. Diaconescu, M. Glovnea, Visualization and measurement of contact area by reflectivity. *ASME. J. Tribol.* 128, 915–917 (2006).

[48] A. Ovcharenko, G. Halperin, G. Verberne, I. Etsion, In situ investigation of the contact area in elastic-plastic spherical contact during loading - unloading. *Tribol. Lett.* 25, 153–160 (2007).

[49] B. A. Krick, J. R. Vail, B. N. Persson, W. G. Sawyer, Optical in situ micro tribometer for analysis of real contact area for contact mechanics, adhesion, and sliding experiments. *Tribol. Lett.* 45, 185–194 (2012).

[50] I. Serre, M. Bonnett, R. P. Duval, Modelling an abrasive experiment by the boundary element method, *Comptes Rendus de l'Académie des Sciences Paris* Série II b 329: 803-808 (2001).

[51] N. Fillot, I. Iordanoff, Y. Berthier, Simulation of Wear Through Mass Balance in a Dry Contact, *ASME Journal of Tribology* 127: 230-237 (2005).

[52] P. Moldenhauer, M. Kröger, Simulation and Experimental Investigations of the Dynamic Interaction between Tyre Tread Block and Road. In: *Elastomere Friction*, 165-200. Springer Berlin Heidelberg (2010).

[53] G. P. Ostermeyer, M. Müller, Dynamic interaction of friction and surface topography in brake systems. In: *Tribology International,* 39, No. 5, pp. 370-380 (2006).

[54] G. Ostermeyer, On the dynamics of the friction coefficient. In: *Wear,* 254, No. 9, pp. 852-858 (2003).

[55] C. Ludwig, *Analytische, numerische und experimentelle Untersuchungen zum chemisch-mechanischen Polieren von Siliziumwafern*. III, 174 S. Freiberg: Techn. Univ. Bergakademie (2013).

[56] C. Ludwig, M. Kuna, An Analytical Approach to Determine the Pressure Distribution During Chemical Mechanical Polishing. In: *Journal of Electronic Materials,* 41, No. 9, pp. 2606-2612 (2012).

[57] P. Pödra, S. Andersson, Simulating sliding wear with finite element method, *Tribology International* 32: 71–81, doi:10.1016/S0301-679X(99)00012-2 (1999).

[58] J. F. Archard, Contact and rubbing of flat surface, *J Applied Physics*. 24: 981–988 (1953).

[59] A. Söderberg, S. Andersson, Simulation of Wear and Contact Pressure Distribution at the Pad-to-Rotor Interface in a Disc Brake Using General Purpose Finite Element Analysis Software, *Wear*, 267: 2243-2251 (2009).

[60] M. A. Ashraf, B. Sobhi-Najafabadi, Ö. Göl, D. Sugumar, Numerical Simulation of Sliding Wear for a Polymer-Polymer Sliding Contact in an Automotive Application, *International Journal of Advanced Manufacturing Technology*, 41: 1118-1129 (2009).

[61] L. Kónya, K. Váradi, Wear simulation of a polymer–steel sliding pair considering temperature- and time-dependent material properties In: K. Friedrich, A. K. Schlarb editors. *Tribology of Polymeric Nanocomposites*, *Tribology and Interface Engineering Series*, Volume 55, pp. 130-145 (2008).

[62] A. Le Gal, *Investigation and Modelling of Rubber Stationary Friction on Rough Surfaces*, (2007).

[63] V. L. Popov, *Contact Mechanics and Friction Physical Principles and Applications*, Springer-Verlag Berlin Heidelberg (2010).

[64] D. M. Nuruzzaman, M. A. Chowdhury, Effect of Normal Load and Sliding Velocity on Friction Coefficient of Aluminum Sliding Against Different Pin Materials, *American Journal of Materials Science* (2012).

[65] J. F. Archard, *Wear Theory and Mechanisms, Wear Control Handbook*, M. B. Peterson and W.O. Winer, eds., ASME, New York, pp. 35-80 (1980).

[66] B. N. J. Persson, A. I. Volokitin, Theory of rubber friction: Nonstationary sliding, *Physical Review B, Volume 65*, 134106 (2002).

[67] B. N. J. Persson, U. Tartaglino, O. Albohr and E. Tosatti, Rubber friction on wet and dry road surfaces: the sealing effect, *Phys. Rev. B 71*, 035428 (2005), 035428 (2005).

[68] D. M. Nuruzzaman, M. A. Chowdhury, *Friction and Wear of Polymer and Composites*, Chapter 14, (2012).

[69] D. Tabor, Friction and Wear – Developments Over the Last 50 Years, Keynote Address, *Proc. International Conf. Tribology – Friction, Lubrication and Wear*, 50 Years on, Lon-don, Inst. Mech. Eng., pp. 157-172 (1987).

[70] K. C. Ludema, *Friction, Wear, Lubrication, A Textbook in Tribology*, CRC Press, London (1996).

[71] B. Bhushan, *Principle and Applications of Tribology*, John Wiley & Sons, Inc., New York (1999).

[72] A. A. Alazemi, A. Ghosh, F. Sadeghi, L. Stacke, Experimental Investigation of the Correlation Between Adhesion and Friction Forces, *Springer Science + Business Media New York* (2016).

[73] H.Pihtili and N.Tosun, Effect of load and speed on the wear behavior of woven glass fabrics and aramid fibre-reinforced composites, *Wear*, 252 (2002) 979-984.

[74] S.K. Rhee, Wear of metal-reinforced phenolic resins, *Wear*, 18 (1971), p. 471.